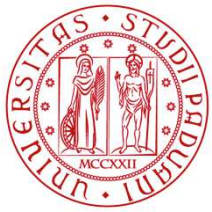

UNIVERSITÀ
DEGLI STUDI
DI PADOVA

Head Office:
Università degli Studi di Padova
Department of Molecular Medicine

Ph.D. COURSE IN: Molecular Medicine
CURRICULUM: Regenerative Medicine
SERIES XXX

# STUDYING AUTOPHAGY-RELATED GENES IN ZEBRAFISH, A CRISPR/Cas9-BASED APPROACH

**Coordinator:** Ch.mo Prof. Stefano Piccolo
**Supervisor**: Ch.ma Prof. Luisa Dalla Valle
**Co-Supervisor**: Ch.mo Prof. Paolo Bonaldo

**Ph.D. student** : Giacomo Meneghetti

**INDEX**

# RIASSUNTO

L'autofagia è un processo catabolico evolutivamente conservato in cui la cellula degrada e ricicla, mediante i lisosomi, proteine e organelli non più funzionanti, per mantenere l'omeostasi cellulare. Questo processo svolge un ruolo chiave durante lo sviluppo, la normale fisiologia della cellula e la sopravvivenza in mancanza di nutrienti, ma anche in diverse patologie umane come malattie infiammatorie e neurodegenerative, distrofie congenite, e sviluppo tumorale.

L'autofagia si compone di una cascata di passaggi finemente regolati che coinvolgono un insieme specifico di proteine. Due di queste, Ambra1 ed Epg5, sono state l'oggetto della mia tesi di dottorato. La proteina Ambra1 è un regolatore positivo dell'autofagia Beclin 1 (BECN1) dipendente, ma è anche coinvolta in processi quali apoptosi, proliferazione cellulare e sviluppo, grazie alla sua capacità di legare altre proteine regolatrici. Epg5 (*Ectopic P-granule protein 5*) è invece necessaria nella fase finale del processo autofagico per la fusione degli autofagosomi con gli endosomi tardivi e i lisosomi. Nell'uomo, mutazioni recessive di questo gene sono state associate a un raro disturbo multisistemico, la sindrome di Vici, principalmente caratterizzata da agenesi del corpo calloso, ipopigmentazione oculocutanea, immunodeficienza variabile, cardiomiopatie e miopatie del muscolo scheletrico, e ridotta attività autofagica.

In questa tesi descrivo la generazione, validazione e caratterizzazione di tre linee mutanti di zebrafish ottenute mediante la tecnica di mutagenesi mirata CRISPR/Cas9, per studiare le funzioni delle proteine autofagiche Epg5, Ambra1a e Ambra1b. Inoltre, sempre nello zebrafish, ho anche validato la specificità degli oligo morfolino per i geni paraloghi *ambra1a* e *ambra1b,* utilizzando la linea mutante *ambra1a*$^{-/-}$. Ho inoltre analizzato il coinvolgimento di questi geni paraloghi nello sviluppo del cuore.

Nel **primo capitolo** è descritta la preparazione e caratterizzazione delle linee mutanti per *epg5*, generate per ottenere un modello di studio per la sindrome di Vici o per altre malattie correlate all'autofagia. Nello zebrafish i trascritti di *epg5* sono presenti come eredità materna nei primi stadi dello sviluppo, suggerendo un loro possibile ruolo nello sviluppo dello zebrafish. Sono state generate due linee mutanti, con delezioni rispettivamente di 13 e di 20 nucleotidi nel primo esone codificante, che portano, in entrambi i casi, alla formazione di codoni di stop prematuri. Una completa caratterizzazione della linea è stata condotta solo su quella che presenta la delezione più lunga. Nei mutanti è stato confermato il blocco del processo autofagico, sia in condizioni basali che di digiuno, grazie ad esperimenti di western blotting e analisi sia di birifrangenza che ultrastrutturali del muscolo delle larve. Tutti gli approcci sperimentali

hanno mostrato come i mutanti *epg5*$^{-/-}$ presentino un marcato accumulo di autofagosomi non degradati e una riduzione delle fibre muscolari in seguito al digiuno. Un possibile ritardo nello sviluppo dell'intestino è stato messo in evidenza dall'analisi delle cellule mucipare caliciformi e da una riduzione nel tasso di crescita osservato negli stadi larvali della linea mutante. Nonostante questo, i mutanti *epg5*$^{-/-}$ si sviluppano normalmente e raggiungono la maturità sessuale privi di un fenotipo evidente. Tuttavia, dopo 8-10 mesi i mutanti presentano una riduzione della fertilità, confermata dalla presenza di soli ovociti primari nell'ovario e di alterazioni nella morfologia dei testicoli, una diminuita motilità e una riduzione delle dimensioni dei muscoli nel tronco. In accordo con la sindrome di Vici, gli adulti presentano inoltre una dilatazione del cuore e riduzione dello spessore del miocardio compatto.

Per analizzare il flusso autofagico, sono state generate delle linee *epg5*$^{-/-}$ in background transgenico per *lc3*, *rab7*, *rab5* e *lamp1*. Gli spot fluorescenti Lc3-II (che evidenziano gli autofagosomi), Lamp1 (che evidenziano i lisosomi maturi), come anche quelli Rab7 (negli endosomi tardivi e lisosomi) si accumulano nelle larve *epg5*$^{-/-}$, confermando come il silenziamento di Epg5 porti ad un blocco del flusso autofagico.

Il **secondo capitolo** descrive la generazione di linee zebrafish mutanti per i geni paraloghi *ambra1a* e *ambra1b*. A differenza dei risultati ottenuti con i corrispondenti ATG-morpholino, gli embrioni mutanti *ambra1a*$^{-/-}$ e *ambra1b*$^{-/-}$ non mostrano difetti evidenti durante lo sviluppo. Un aumento della trascrizione del gene *ambra1b* nei mutanti *ambra1a*$^{-/-}$ suggerisce un possibile effetto compensatorio tra i due geni paraloghi. Inoltre, i mutanti *ambra1a*$^{-/-}$ non presentano alterazioni del fenotipo quando iniettati con *ambra1a*-MO, mentre evidenziano un fenotipo abbastanza severo dopo knockdown con *ambra1b*-MO.

La completa assenza di femmine adulte nella linea mutante *ambra1b*$^{-/-}$ suggerisce che Ambra1b possa avere un ruolo critico nella determinazione sessuale e/o nello sviluppo e differenziamento dell'ovario. Inoltre, nonostante i mutanti *ambra1a*$^{-/-}$ e *ambra1b*$^{-/-}$ siano singolarmente vitali, non è stato possibile ottenere la linea doppia mutante, poiché i pesci con entrambe le mutazioni non sopravvivono oltre lo stadio larvale.

Il **terzo capitolo** descrive l'analisi degli effetti del *knockdown* con i morfolini *ambra1a*-ATG e *ambra1b*-ATG sullo sviluppo cardiaco. Lavori precedenti avevano infatti mostrato il coinvolgimento di queste proteine nello sviluppo del cuore. Entrambi i trascritti di *ambra1* sono presenti nella regione del cuore di embrioni a due giorni dalla fecondazione. Il silenziamento delle due proteine mediante ATG-morfolino modifica in modo evidente lo sviluppo del cuore che risulta più piccolo, di forma allungata e con edema pericardico. La microiniezione di morfolino che agisce sul processo di *splicing*

(SPLIC-MO) non determina alcun fenotipo cardiaco, indicando come in questo processo siano fondamentali i messaggeri materni.

Le analisi condotte hanno anche messo in evidenza come il silenziamento di entrambe le forme di *ambra1* interferisca con la lateralizzazione del cuore. Il fenotipo cardiaco dei morfanti viene recuperato con successo mediante co-iniezione con il messaggero *AMBRA1* umano, risultato che sottolinea la conservazione delle funzioni di questa proteina durante l'evoluzione.

Infine, essendo stato suggerito in topi e ratti un ruolo per la defosforilazione mediata da PP2A (*Protein Phosphatase 2*) nella morfogenesi cardiaca e sapendo che questa proteina interagisce con AMBRA1 per controllare la proliferazione cellulare, sono stati condotti esperimenti di recupero del fenotipo con il messaggero umano di *AMBRA1* mutato nel sito di legame per PP2A (*hAMBRA1*$^{PXP}$).

È interessante notare come questo messaggero non sia in grado di recuperare il fenotipo cardiaco allo stesso modo della co-iniezione con mRNA non mutato suggerendo quindi che il ruolo rivestito dalle proteine Ambra1 nello sviluppo del cuore, sia, almeno in parte, legato all'interazione con la proteina fosfatasi PP2A.

## SUMMARY

Autophagy is an evolutionarily conserved catabolic process in which a cell degrades and recycles, through the lysosomes, long-lived proteins and dismantles organelles in order to maintain cellular homeostasis. This process plays a central role during embryo development, normal physiology and survival during starvation. It is also involved in several human disorders like inflammatory and neurodegenerative diseases, congenital dystrophies, oncogenesis and cancer progression.

Autophagy consists of a cascade of steps that are finely regulated and employ a specific subset of proteins two of which, Ambra1 and Epg5, have been the targets of my thesis. Ambra1 is a central positive regulator of the Beclin 1 (BECN1) dependent autophagic process and it is also involved in other cellular processes such as apoptosis, cell proliferation, development and cancer, thanks its capability of binding to other regulatory proteins. Epg5 (ectopic P-granules autophagy protein 5) is required for fusion of autophagosomes with late endosomes and lysosomes. Human recessive mutations of the EPG5 gene have been associated to a rare multisystem disorder called Vici syndrome, mainly characterized by agenesis of the corpus callosum, hypopigmentation, variable immunodeficiency, cardio- and skeletal myopathy and decreased autophagy activity.

In this thesis are described the generation, validation and characterization of three zebrafish mutant lines obtained by CRIPR/Cas9 targeted mutagenesis in order to study the autophagic proteins Epg5, Ambra1a and Ambra1b. Moreover, I have validated the specificity of *ambra1a*- and *ambra1b*-morpholinos using the Ambra1a mutant line and analysed the involvement of these proteins on heart development by means of these knockdown approach.

**In chapter I,** it is described the generation and characterization of the *epg5* zebrafish mutant line, in order to obtain a model for autophagy-related Vici syndrome or autophagy-related diseases. In zebrafish *epg5* transcripts were present as maternal mRNA in early stages of development, suggesting a potential role of this protein during embryogenesis. Two *epg5* mutant lines were produced, characterized respectively by a deletion of 20 and 13 nucleotides in the first coding exon of the gene. This led, in both cases, to the generation of premature stop codons. Characterization was mainly performed using the -20 nt line. Dysfunctional autophagy was confirmed in the epg5 mutant line, by western blotting experiments, by birefringence and ultrastructural analyses of skeletal muscle, both in fed and starved conditions. All experimental approaches showed that *epg5*$^{-/-}$ mutants display a marked accumulation of degradation-

defective autolysosomes and reduction of muscular fibres after starvation. A possible delay in intestinal development was also suggested by goblet cells analysis and by a reduced growth rate during larval stages. *epg5*$^{-/-}$ mutants display a normal development and reach sexual maturity without exhibiting a clear phenotype. However, after 8-10 months, homozygous mutants show fertility reduction, confirmed by the presence in the ovary of only primary oocytes, alteration in testis morphology together with an impaired motility and muscle thickness reduction. Moreover, in agreement with Vici syndrome, adult mutants present dilated heart and reduction of the compact myocardium.

To analyse the autophagy flux in *epg5*$^{-/-}$, mutant lines were generated in *lc3*, *rab7*, *rab5* and *lamp1* transgenic backgrounds. Lc3-II puncta (labelling autophagosomes), Lamp1 (labelling mature lysosomes), as well as Rab7 (labelling late endosomes and lysosomes) fluorescence signals were accumulated in muscle of *epg5*$^{-/-}$ larvae confirming that silencing of Epg5 resulted in block of the autophagic flux.

In **chapter II** it is described the generation of zebrafish mutant lines for the two zebrafish paralogous genes, *ambra1a* and *ambra1b*. Differently from results obtained with the corresponding ATG-morpholinos, *ambra1a*$^{-/-}$ and *ambra1b*$^{-/-}$ mutant embryos do not display developmental defects. Up-regulation of *ambra1b* transcripts in *ambra1a*$^{-/-}$ mutants suggests that there might be a potential compensatory effect of the paralogous genes. Moreover, *ambra1a*$^{-/-}$ mutants are weakly sensitive to *ambra1a*-MO but suffer greatly *ambra1b*-MO knockdown. Lack of adult female in *ambra1b*$^{-/-}$ line suggests that Ambra1b plays a critical role in zebrafish sex determination and/or ovarian differentiation and development. Although both *ambra1a* and *ambra1b* mutants are viable, generation of a stable double Ambra1 mutant line was not possible as double mutant do not survive after larval stages.

In **chapter III** It is described the analysis of *ambra1a* and *ambra1b* knockdown effects on cardiac development by means of validated *ambra1a* and *ambra1b* ATG-morpholinos, since a previous work showed an involvement of these proteins in this process and both zebrafish *ambra1* transcripts are present in the heart region of 2-dpf embryos. Silencing of the two proteins affects heart morphogenesis, resulting in a small, string-like heart with pericardial edema. Treatment with SPLIC-MOs does not result in a clear cardiac phenotype, underlining the importance of maternally supplied *ambra1* transcripts. ATG-MOs microinjection on a zebrafish transgenic line with green fluorescent heart and WMISH of *pitx2c* transcripts revealed defects on cardiac looping, indicating that Ambra1 silencing interferes on heart laterality. The cardiac phenotypes were rescued by co-injection of MOs with human *AMBRA1* mRNA, pointing to the conservation of Ambra1 functions during evolution.

Finally, as it has been suggested a role for Protein phosphatase 2 (PP2A)-mediated dephosphorization in cardiac morphogenesis and development in mouse and rat, and this protein interacts with AMBRA1 to control cell proliferation, co-injection of MOs with *hAMBRA1* mRNA and with a messenger mutated in the PP2A binding sites (*hAMBRA1*$^{PXP}$ mRNA) was used to analyze their rescue effectiveness on heart. Interestingly, co-injections of Ambra1-ATG-MOs with *hAMBRA1*$^{PXP}$ was not able to rescue the cardiac phenotypes as *hAMBRA1* mRNA and treatment of zebrafish embryos with the specific inhibitor of PP2A, cantharidin, resulted in similar developmental cardiac defects. These results suggest a possible role of Ambra1 proteins in heart development, likely involving the interaction with the PP2A phosphatase.

# INTRODUCTION

## AUTOPHAGY

Autophagy is an evolutionary conserved catabolic process involved in the lysosome-mediated degradation of damaged organelles, protein aggregates, long-lived proteins and intracellular pathogens (Boya *et al*., 2013). Under basal conditions, cellular events regulated by the autophagy-related signaling network are the quality controls that maintain cellular homeostasis. Moreover, under different stress stimuli, ranging from starvation to DNA damage, autophagy is a key pro-survival response, permitting adaptation to different stress conditions (Abada and Elazar, 2014; Boya *et al*., 2013; Choi *et al*., 2013).

Autophagy has a role not only during embryonic development (Levine and Klionsky, 2004; Cecconi and Levine, 2008), like in heart morphogenesis and nervous system development (Lee *et al*., 2014; Amber *et al*., 2013), but also in aging process (Rubinsztein *et al*., 2011). In human, failure to remove aggregates of damaged toxic proteins could lead to several disorders such as inflammatory and neurodegenerative pathologies including Huntington's disease, Parkinson's disease, amyotrophic lateral sclerosis and Alzheimer's disease (Rubinsztein *et al*., 2007; Levine and Kroemer, 2008). Moreover, in some congenital muscular dystrophies, defective activation of the autophagic machinery causes accumulation of dysfunctional mitochondria, leading to the damage and the subsequent loss of muscle fibers (Grumati *et al*., 2010). Autophagy has also been identified as an anti-oncogenic process in early stages of cancer progression (Mizushima *et al*., 2008). On the contrary, in later stages of tumorigenesis, autophagy could provide a survival strategy to cancer cells under nutrient depletion, chemotherapy or irradiation, acting in a pro-oncogenic way (Mowers *et al*., 2017).

Three main types of autophagy have been identified, depending on the way cargo is delivered to the lysosomes: macroautophagy, usually referred as "autophagy", chaperone-mediated autophagy (CMA) and microautophagy. All these subtypes work with different cellular mechanisms and play distinctive functions (Fig. 1) (García-Arencibia *et al*., 2010). The chaperone-mediated form of autophagy, until now reported only in mammals, is a very selective form in which a cytosolic chaperones complex binds proteins containing the CMA targeting motif KFERQ. The complex then directly contacts lysosomes through Lamp2 receptors and this interaction drives substrate translocation into lysosome with the subsequent degradation (Kaushik and Cuervo, 2012).

In the microautophagy process, the substrate that has to be degraded is engulfed directly by lysosomes by means of membrane invagination (Li *et al*., 2012).

In macroautophagy (hereafter "autophagy"), the most common type of the autophagic process, cytoplasm components, including misfolded proteins or damaged organelles, are isolated in a double membrane vesicle called autophagosome (Yang and Klionsky, 2010). This structure fuses with lysosomes and in the last step autolysosomes degrade itself thanks to lysosomal enzymes and to the acidification of the compartment. This process can be subdivided into different steps: autophagy induction, membrane nucleation and elongation leading to autophagosome formation, trafficking and autophagosome fusion with lysosome, and finally, degradation of the cargo followed by transport of the resulting small molecules back to the cytosol. Each step is regulated by a specific pool of genes that include AuTophaGy-related (Atg) identified in yeast (Klionsky, 2014).

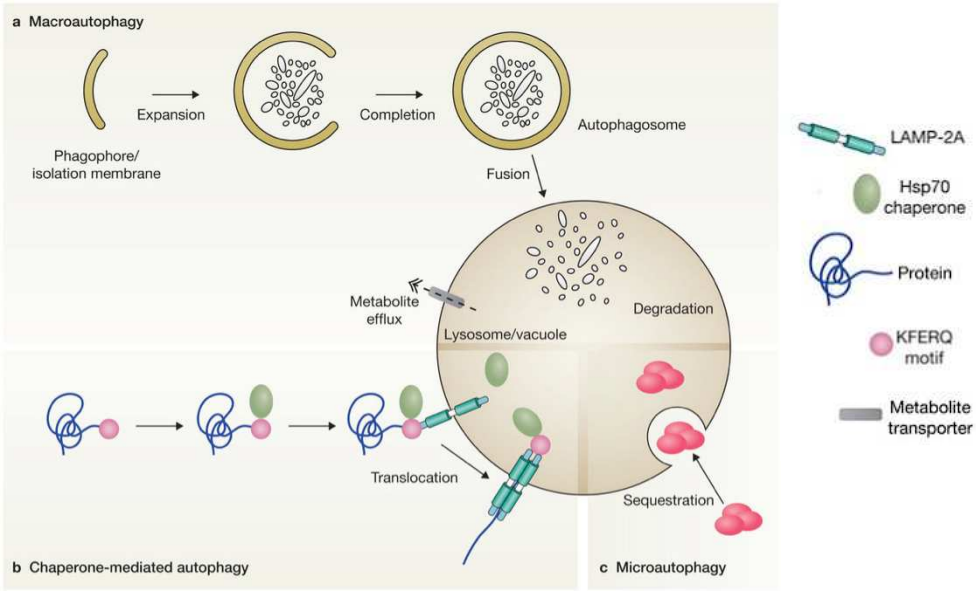


**Fig. 1.** Schematic illustration of the three main types of autophagy in mammalian cells: macroautophagy (a), microautophagy (c) and chaperone-mediated autophagy (b). Figure modified from Boya *el al*., 2013.

## The autophagy process

mTOR (mammalian target of rapamycin), a serine/threonine kinase protein, works as a master regulator of cellular process, such as cell growth, proliferation and autophagy, forming two different complexes, mTORC1 and mTORC2, with different functions. The first complex, in presence of growth factor signaling or nutrients, inhibits autophagy through phosphorylation of autophagy related proteins like ULK1, ATG13, AMBRA1 and ATG14L and promote anabolic metabolism (Kim and Guand, 2015). The second complex, mTORC2 is instead involved in regulation of autophagy in the skeletal muscles, through a

pathway that involved FoxO3 and its specific serin-threonine kinase AKT (Mammucari *et al*., 2007). Under stress conditions or nutrient depletion, mTOR is inactivated, resulting in the dephosphorization of ULK proteins, and mTOR dissociation from the initiation complex ULK1/2, that includes UNC51-like autophagy activating kinase 1 (ULK), autophagy-related protein 13 (ATG13), FAK family kinase interacting protein of 200 kDa (FIP200) and ATG101 (Kaur & Debnath, 2015). Activated ULK1/2 complex recruits, a multiprotein complex called nucleation complex, to the autophagosome nucleating site, named phagophore (autophagosome precursor, also defined as the pre-autophagosomal structure) assembly sites (PAS) (Stanley *et al.*, 2014). The nucleation complex is provided of Class III phosphatidylinositol 3-kinase (PI3K) activity and contains Beclin 1 (BECN1), the class III phosphoinositol-3-kinase Vps34 (Vacuolar protein sorting 34), phosphoinositide-3-kinase regulatory subunit 4 (PI3KR4 or VPS15), ultraviolet radiation associated (UVRAG) and ATG14L (Galluzzi *et al*., 2017). Vps34 catalyzes the synthesis of a crucial component for the elongating phagophore, the phosphatidylinositol-3-phosphate (PI3P) and the progression of autophagy (Russell *et al*. 2013). The PI3P regulates the localization of other ATG proteins to the PAS and promotes the formation of specific structures of the ER called omegasomes because of thier Ω-like form (Fig. 2)(Mizushima e Komatsu, 2011).

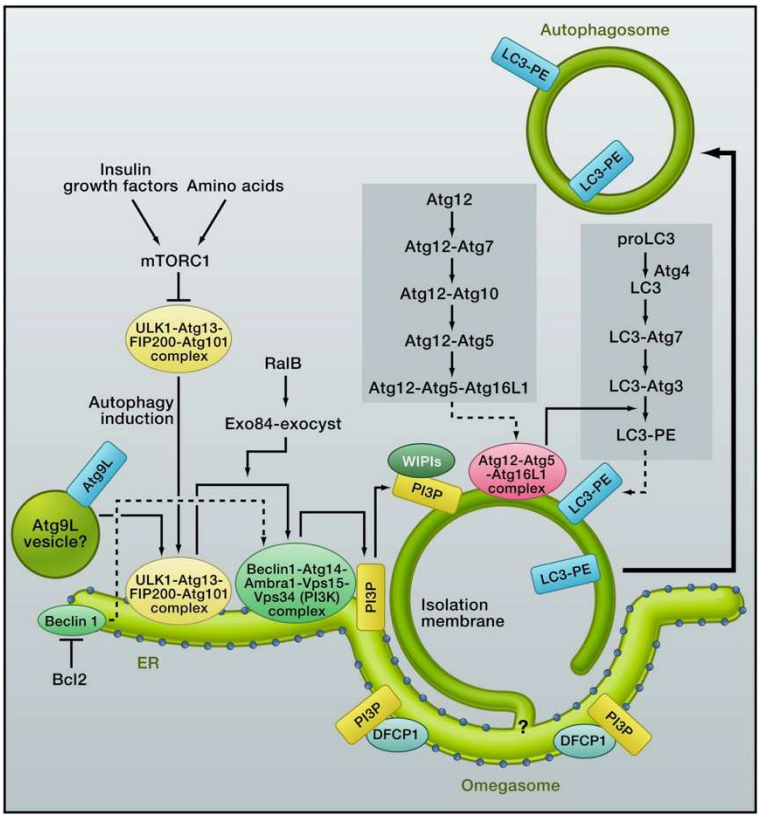


**Fig. 2.** Formation of the autophagosome and role of Atg proteins in mammals. Mizushima e Komatsu, 2011.

The elongation of the membrane from the omegasome requires two ubiquitin-like conjugation systems. The first, ATG12-ATG5-ATG16L is essential for the formation of the PAS (Ravikumar *et al*., 2009). The second ubiquitin-like system catalyzes the chemical modification of the soluble protein ATG8 (LC3 in mammals). The cytosolic LC3 is first cleaved by cysteine protease ATG4 and then, by the activity of ATG7 and ATG3, conjugated with phosphatidylethanolamine to form LC3-phosphatidylethanolamine (PE) or simply LC3-II (Weidberg *et al*., 2011). LC3-II level is linked to the number of mature autophagosome, where this protein remains until the fusion with lysosome and, for this reason, can be used as an excellent marker of autophagy (Klionsky *et al*., 2008). However, an impaired autophagic flux can also determine an increase of this marker.

Mature autophagosomes are transported along microtubules by dynein proteins to the lysosomal rich perinuclear region (Ravikumar *et al.* 2005). Before they merge with a lysosome, the autophagosome can also fuse with a late endosome, forming an amphisome. Autophagosome-lysosome fusion is regulated by proteins that are shared with the endocytic pathway, in particular the soluble N-ethylmaleimide-sensitive fusion attachment protein receptors (SNAREs) proteins and Rab proteins. Lysosome hydrolases catalyze the autophagosome content degradation into basic molecules that are then transported back to the cytoplasm to be recycled for anabolic reaction (Fader *et al.,* 2009; Furuta *et al.,* 2010).

**AMBRA1**

One of the main regulators of the autophagy process is AMBRA1 (activating molecule in Beclin1-regulated autophagy) (Fimia *et al*., 2007), a large intrinsically disordered protein (IDP) of approximately 1300 amino acids containing three repeats of a WD40 domain. Moreover, the intrinsic disorder of Ambra1 makes it a scaffold-molecule able to coordinate other intracellular processes beside autophagy (Mei *et al*., 2014; Peng *et al*., 2013). A great number of partners of AMBRA1 have been identified, linking the protein to different functions, from autophagy to apoptosis and cell proliferation (Fimia *et al.,* 2013; Cianfanelli *et al*., 2015a; Cianfanelli *et al.,* 2015b).

On basal conditions, AMBRA1, Beclin-1, and Vps34 are bound to the dynein light chains (DLC1 and DLC2) of the dynein motor complex (Di Bartolomeo *et al*., 2010). Moreover, the inactive state of this protein is maintained also by AMBRA1 phosphorylation at serine residue 52, a reaction that prevents the ULK1 ubiquitination (Nazio *et al*., 2013). Upon autophagy induction, activated ULK1 complex can phosphorylate AMBRA1 thus determining its release from dynein and its translocation, together with Beclin-1 and Vps34 to ER, to the autophagosomes nucleation site. At the same time AMBRA1 regulates activity and stability of ULK1. The two proteins thus interact reciprocally, pointing to a wider role of AMBRA1 in supporting autophagy. Regarding the molecular mechanism, in the early stages after autophagy induction AMBRA1 stabilize ULK1 promoting a Lys-63-linked ubiquitination, an essential reaction for the self-association of ULK1. The reaction is mediated by TRAF6 (TNF receptor associated factor 6), an E3 ligase. Ambra1 helps to regulate the autophagy flux by increasing the signaling capability of ULK1 in a positive feedback loop (Nazio *et al.,* 2013).

Part of the cellular pool of AMBRA1 is normally linked to Bcl2 and thus localized to mitochondria (Strapazzon *et al.,* 2011). The release of AMBRA1 from Bcl-2 occurs when the apoptotic process is activated, forming the crosstalk between the two cellular processes (Fimia *et al*., 2013). It is shown that AMBRA1 proteolysis at the amino acid residue D482 is then required to direct the cell towards the dead program instead of the autophagic process (Pagliarini *et al*., 2012). AMBRA1 interacts also with Parkin protein in mitochondria, activating a specific and selective type of autophagy, mitophagy, essential to remove damaged mitochondria from the cell (Van Humbeeck *et al*., 2011).

Research on AMBRA1 functions was mainly performed with human cell lines and the mouse model where the protein was first identified in 2007 (Fimia et al., 2007). In this model, Ambra1 is expressed at high level in brain compartments, such as the hippocampus, the cerebellum, and the striatum (Di Bartolomeo *et al*., 2010). Consistent

with these expression data, AMBRA1 knockout demonstrated that the protein is essential for the proper nervous system development during embryogenesis as its silencing resulted on early embryonic lethality, neural tube development abnormalities, uncontrolled cell proliferation and excessive cell death (Fig. 3)(Fimia *et al*., 2007).

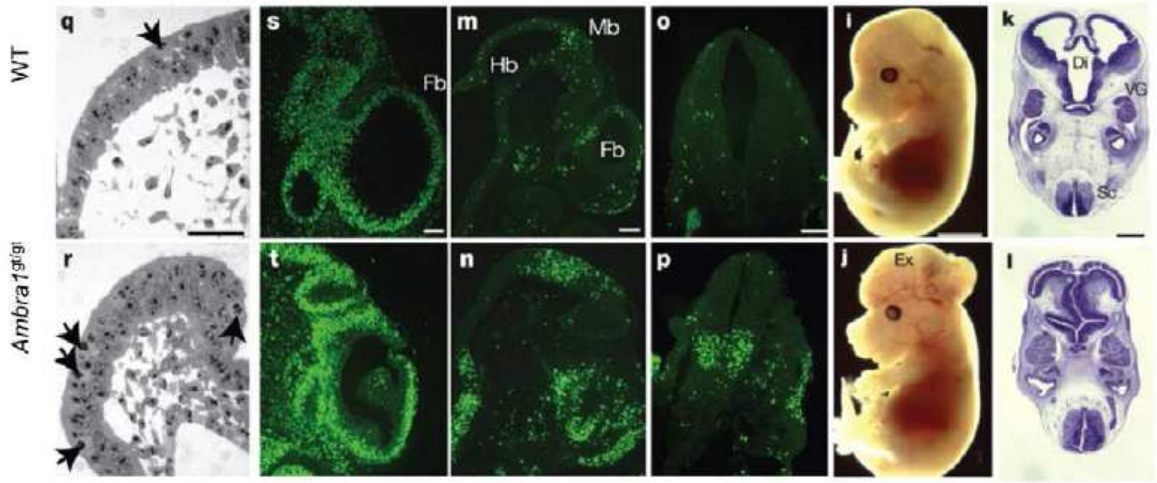


**Fig. 3.** Neural tube defects in Ambra1 mutant embryos. Analysis of cell proliferation in wild-type (q, s) and Ambra1gt/gt (r, t) embryos on transverse sections of E8.5 cephalic neural folds in prospective hindbrain region (mitoses, arrows in q, r) and on sagittal sections of E10.5 forebrain (BrdU uptake, s, t). TUNEL (TdTmediated dUTP nick end labelling) staining of E10.5 brain (m, n) and E9.5 spinal cord (o, p) in wild-type (m, o) and Ambra1gt/gt (n, p) embryo sections. E14.5 wild-type (i) and Ambra1gt/gt (j) embryos are characterized by prominent exencephaly. Histological analysis of E12.5 wild-type (k) and Ambra1gt/gt (l) embryos on cross-section show the absence of a normal ventricular system, the extensive overgrowth of the proliferative neuroepithelium in the diencephalon (Di) and spinal cord (Sc), and the enlarged fifth ganglia (VG) in the Ambra1gt/gt embryo. Scale bars: c, g, h, k, 500 mm; d, 1 mm; e, 150 mm; i, 2 mm; m, s, 400 mm; o, 78mm; and q, 50mm. Figures as well as figure legends were taken from Fimia *et al*., 2007.

In the zebrafish model, due to a genome duplication event during teleost evolution, two paralogous genes encode for Ambra1 proteins, named *ambra1a* and *ambra1b* (Benato *et al*., 2013). Transcripts of both genes are deposited as maternal RNAs in the oocytes and are then replaced by zygotic mRNAs. After 24 hours post fertilization (hpf), *ambra1a* and *ambra1b* mRNA are mainly localized in the head, as in mouse. Using morpholino knockdown to block translation (ATG-MOs) severe embryonic defects occurs, mainly in the neural tube, heart and skeletal muscles as well as impairment of the autophagic process and apoptosis increase. Treatment with splice-blocking morpholino (SPLIC-MOs) leads to less severe developmental defects, underlining the importance of maternally supplied *ambra1* transcripts (Fig. 4)(Benato *et al*., 2013). In addition, both proteins are required for the correct morphogenesis of skeletal muscle and for locomotor activity (Fig. 4) (Skobo *et al.*, 2014). The presence of specific phenotypes, as the more severe brain-related phenotypes in *ambra1a* morphants,

suggests the possible acquisition of specific functions by the two paralogous genes through evolution (Benato *et al*., 2013). Successfully rescued of morphant phenotypes by co-injection of morpholinos with human *AMBRA1* mRNA, suggests also the evolutionary conservation of AMBRA1 functions (Skobo *et al*., 2014).

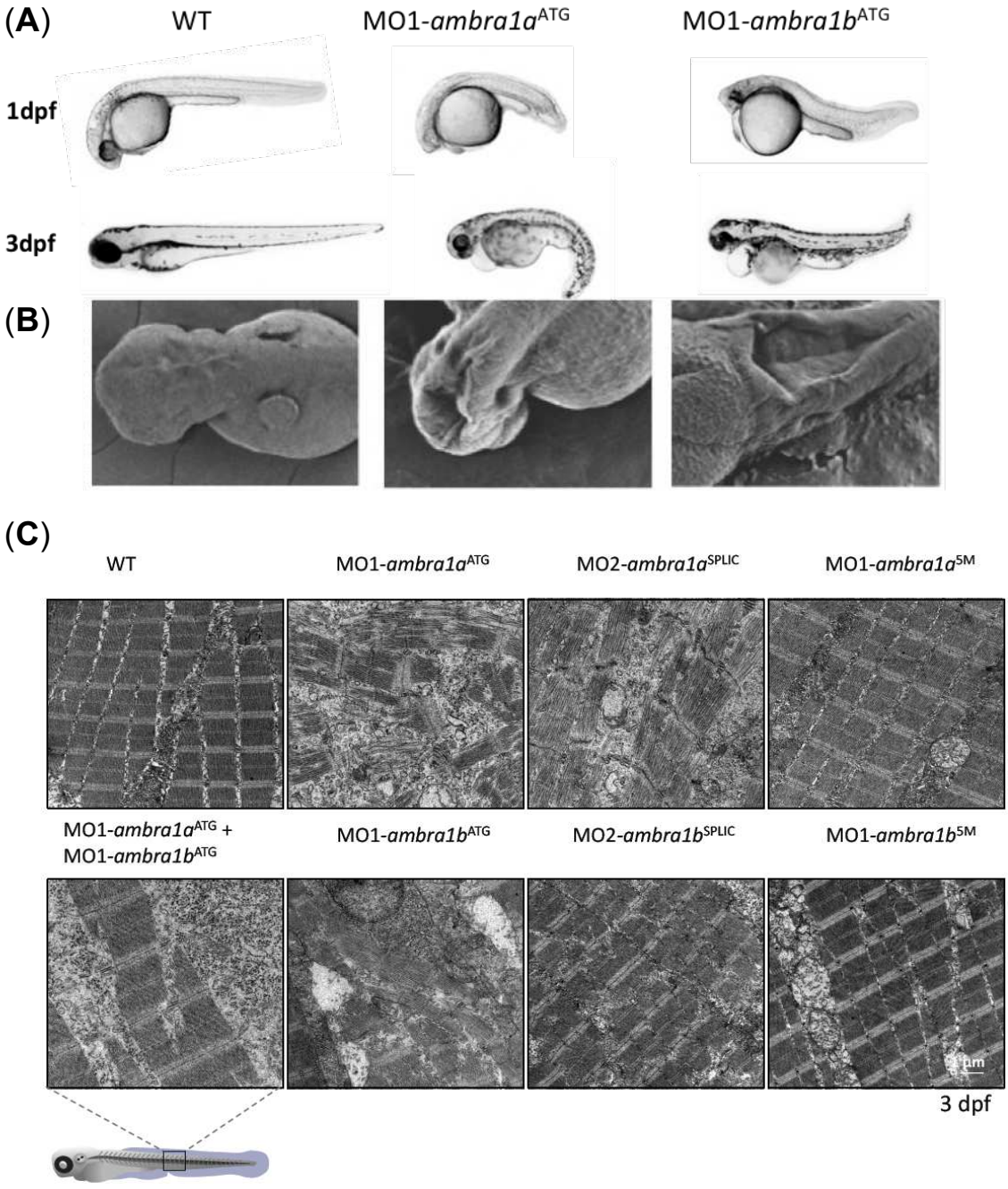


**Fig. 4.** (a) Curved shape and pericardial edema of *ambra1* morphants observed by light microscopy images at 1 dpf and 3 dpf, image of lateral view, anterior to the left. (b) Lacking in the closure of the neural tube observed at SEM (scanning electron microscope) at 2 dpf, images of dorsal view, anterior to the left. (c) Representative electron micrographs of longitudinal sections of 3 dpf WT and *ambra1* ATG/splice-morphants. Ambra1 depleted muscles show a number of ultrastructural defects, with small patches of disorganized myofibers and mitochondria scattered throughout the cytoplasm. Modified from Benato *et al*., 2013 and Skobo *et al*., 2014.

Regarding the role of AMBRA1 in various diseases, the protein is linked to various human disorders, mainly linked to the nervous system. This protein has been associated with schizophrenia (Rietschel *et al*., 2012) by a genetic variation in a limited region of chromosome 11. Moreover, studies that correlate behavioral aspects to a genetic approach demonstrated a link between AMBRA1 and impulsivity (Heinrich *et al*., 2013). Recently, a deeper analysis of mice heterozygote mutants for *Ambra1* gene revealed an autism-like phenotype in adult and pup females in which social interactions are compromised and female mice show the tendency to exhibit repetitive behaviors with impaired cognitive flexibility (Dere *et al.,* 2014).

Recently, a link between Ambra1 and cell proliferation was demonstrated by Cianfanelli and co-worker (2015c). The protein contains two protein phosphatase PP2A interaction regions, (termed PXP motifs) that allow interaction of the dephosphorylated form of AMBRA1 with the catalytic subunit of PP2A (PP2Ac). The AMBRA1-PP2Ac complex destabilizes the proto-oncogene c-Myc, leading to an overall reduction of its pro-proliferative activity.

Consistently with this, Ambra1 haploinsufficiency is linked to susceptibility to cancer as also demonstrated with Ambra1$^{+/gt}$ heterozygous mice that are three times more affected by tumors in lungs, liver, and kidney than wild-type (Cianfanelli *et al.,* 2015c). Accordingly, nonsense and frame-shift mutations of the AMBRA1 gene have also been linked with cancer in human (Cianfanelli *et al.,* 2015c).

**EPG5**

Epg5 (ectopic P-granules autophagy protein 5) was first identified, together with other three new proteins named Epg2, Epg3 and Epg4, in the nematode *C. elegans* as a protein involved in the degradation of germline P granule components in somatic cells during embryogenesis (Tian *et al*., 2010).

In mammals Epg5, together with the homologs of Epg3 and Epg4 (respectively VMP1 and EI24), was demonstrated to be essential for starvation-induced autophagy (Tian *et al.,* 2010) and required for fusion of autophagosomes with late endosomes and lysosomes, a late step of the autophagic process (Tian *et al.*, 2010).

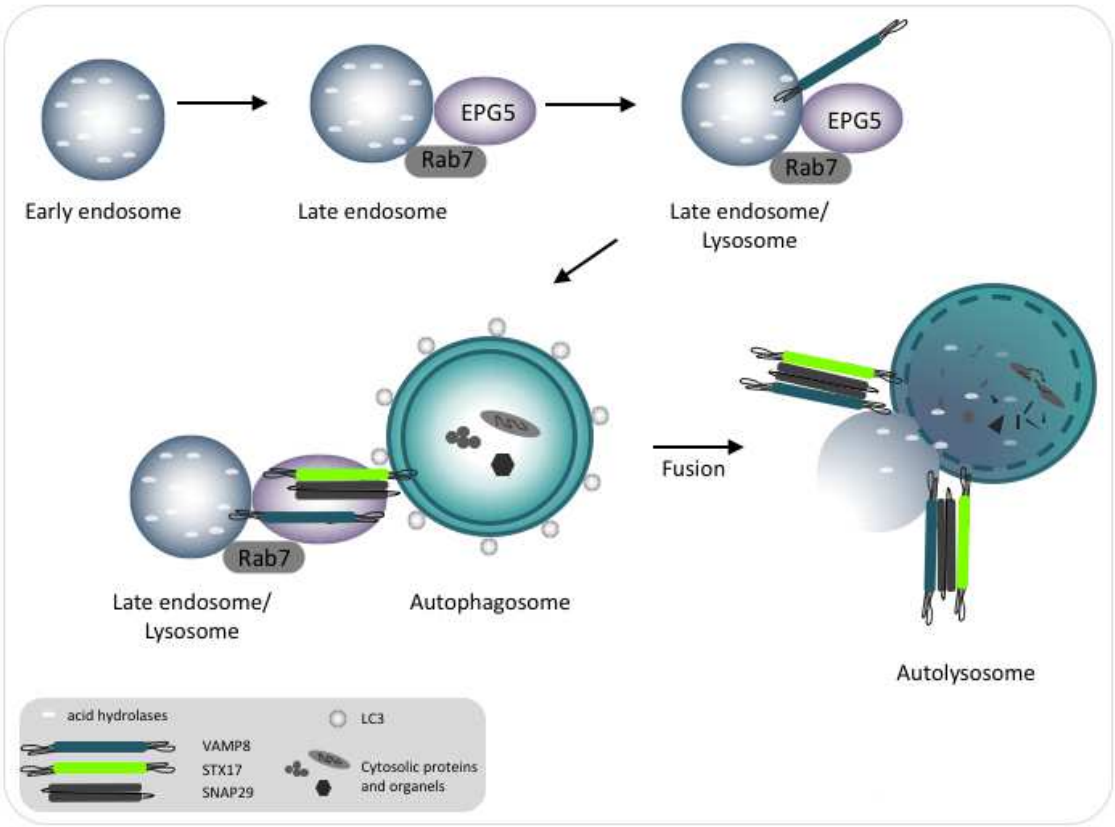


**Fig. 5.** Schematic representation of the EPG5 mechanism. This protein is a Rab7 effector responsible for the fusion specificity of autophagosomes with late endosomes/lysosomes. EPG5 stabilizes the formation of trans-SNARE complexes required for autophagosome fusion with lysosome, by interaction with Rab7 and VAMP7/8 on lysosome and LC3 on autophagosome. Figure by https://tatyscientificillustrations.com/ based on Wang *et al*., 2016.

Analysis of Epg5 molecular functions revealed that is essential for the correct association and stabilization of SNARE complexes. Indeed, this protein interacts with Rab7 and VAMP-8 on late endosomes/lysosomes and with Lc3 and STX17–SNAP29 complexes on

autophagosomes, promoting the fusion specificity between these vesicles (Fig. 5)(Wang *et al*., 2016).

In humans the *EPG5* gene, initially named KIAA1632, was identified within a search for genes mutated in breast cancer tissues (Sjöblom *et al*., 2006). The gene consists of 44 exons, with the longest transcript encoding a protein of 2.579 amino acids. *EPG5* is mainly expressed in central nervous system (CNS), skeletal and cardiac muscle, thymus, immune cells, lung and kidney (Hamala *et al*., 2007). Recessive mutations of the *EPG5* gene have been associated with a rare multisystem human disorder called Vici syndrome, mainly characterized by agenesis of the corpus callosum, variable immunodeficiency, cardio- and skeletal myopathy and decreased autophagic activity (Cullup *et al.,* 2013). The disease results in marked reduced life expectancy with death occurring early in childhood due mainly to severe infection and heart failure (Ebrahimi-Fakhari *et al*., 2016). This syndrome represents the first multisystem disorder directly associated with mutations in an autophagy-related gene (Cullup *et al*., 2013). The so far identified *EPG5* mutations are distributed all along the gene (Cullup *et al*., 2013; Ehmke *et al*., 2014).

The mice *epg5* knockout model grows normally and reach sexual maturity, but progressively develop neuronal damages, myofibril atrophy associated with behavioural and motor abnormalities and premature death at 10-12 months (Zhao *et al*., 2013). Although the mice model present feature of the Vici syndrome, it has also been described as a model for amyotrophic lateral sclerosis (Zhao *et al*., 2013b) and for retinitis pigmentosa (Miao *et al*., 2016) which could make them useful for studying the molecular mechanism of these pathologies.

The Epg5 absence in mice led to impaired autophagosome maturation and endosome trafficking (Zhao *et al.,* 2013). This characteristic is in agreement with the autophagic phenotype of the *C. elegance* KO model, that shows also a non-specific fusion between autophagosomes and early autophagic vesicles, suggesting a role of Epg5 in the fusion specificity (Wang *et al.,* 2016). Epg5 functions have also been analysed in *Oryzias latipes*, a teleost fish model, commonly named medaka. In this model, Epg5 KO results in sperm production impairment due to the failure of germ plasm and mitochondria clearance during the process of germ cell specification and during spermatogenesis (Herpin *et al*., 2015).

## ZEBRAFISH MODEL ORGANISM

*Danio rerio* (Zebrafish) is a small tropical freshwater teleost that belongs to the *Cyprinidae* family. Its natural habitat consists of rivers, ponds, and waterways near paddies. It is diffused in South-East Asia and principally in India, Pakistan, Buthan and Nepal (Dahm and Geisler, 2006). Nowadays it is exported all around the world for genetics, developmental biology, and toxicology studies. Due to its several advantages, it has been widely used in research in the last decades.

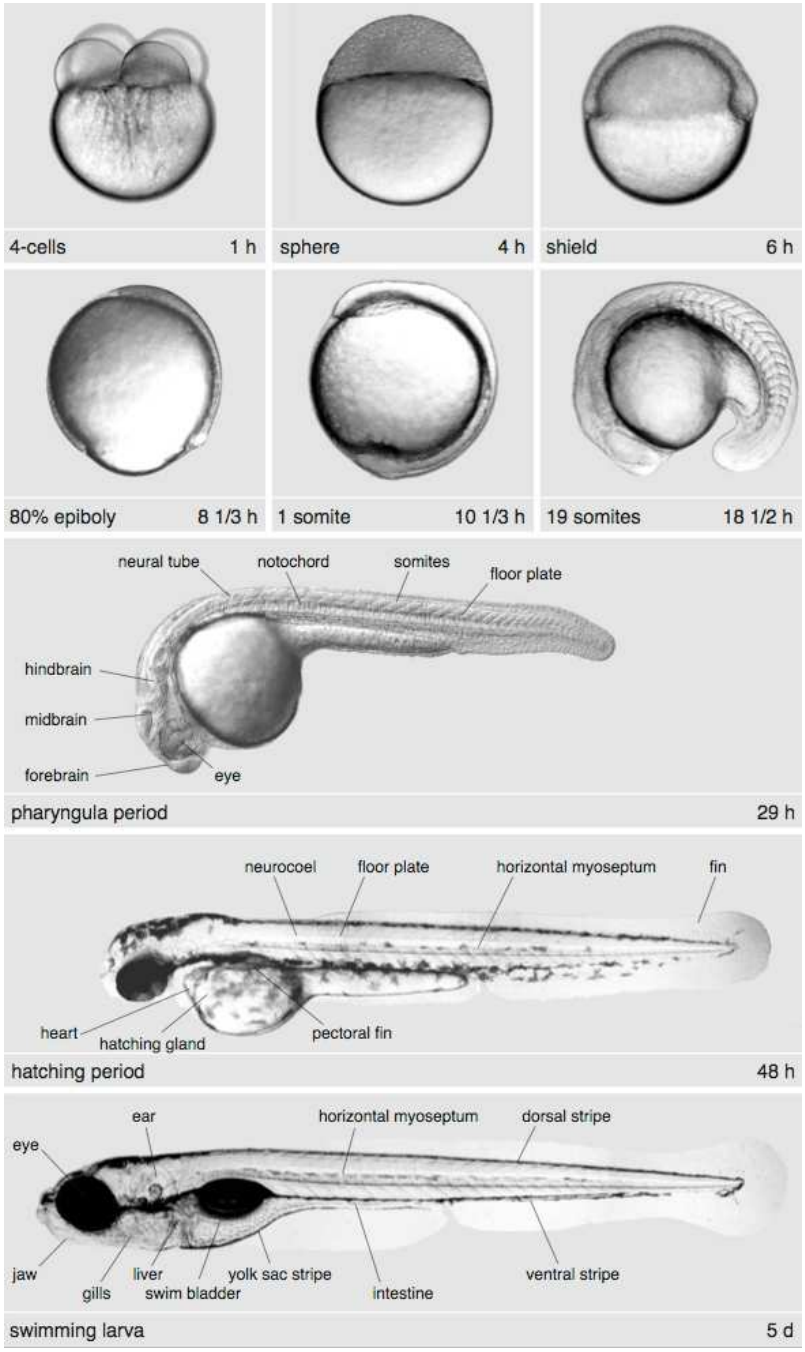


**Fig. 6.** Stages of zebrafish development from 0 hpf to 5 dpf. Haffter *et al*., 1996.

This fish is small in size, between 4 and 6 cm. Zebrafish can be maintained and bred in captivity in a reproducible and cost-effective way. Males and females display a clear sex dimorphism that makes recognition easy by the operators. Males are thinner and their abdomen region is gold-reddish, while females are light-silver coloured and present a larger abdominal region, for the ovary presence (Nasiadka and Clark, 2012). Embryos are transparent and small in size and this, together with the external fertilization, make them suitable for microinjection, drug treatments and *in vivo* imaging using various fluorescent transgenic lines. Zebrafish have a fast development, giving that the first division occurs after 45 minutes at 28,5°C from the fertilization, gastrulation occurs within 10 hours post fertilization (hpf) and by 24 hpf the body axes have already been established allowing to distinguish eyes, somites, the vascular system and an organized nervous system. After 5-6 days post fertilization (dpf), organogenesis is complete and embryos have already developed into swimming and feeding larvae (Fig. 6). At 30 dpf the sexual determination takes place whereas at 3-4 months they reach sexual maturity (Kimmel *et al*., 1995; Dahm and Geisler, 2006; Vacaru *et al*., 2014).

**Genetics tools in zebrafish**

Despite the evolutionary distance between human and zebrafish, genes and molecular mechanisms of the embryonic development and physiology are highly conserved, a comparison with the human genome reveal that 70% of human genes have an orthologue in zebrafish (Howe *et al.,* 2013). These genetic features together with the presence of similarity in organ structures organization and physiology with mammals, make zebrafish useful in research as an animal model for several human diseases including muscular dystrophies, neurodegenerative disease (like Alzheimer and Parkinson), cancer, diabetes and cardiovascular disease (Ingham, 2009; Tavares and Santos Lopes, 2013).

The approaches to obtain a genetic model are two:

- Forward genetics. It is based on the screening of mutants that show a phenotype, randomly generated with chemical compounds (N-ethyl-N- nitrosourea ENU), retroviruses or transposons. This approach was the most used in the past 20 years, but it is not target-specific and the analysis to identify the mutated region is time- and money-consuming. Furthermore, as the Teleost underwent genome duplication (Meyer and Van de Peer, 2005), many genes are present as paralogous genes and can exert a functional compensation between them, making more difficult the analysis of the phenotype (Walker e Streisinger 1983; Kimmel 1993; Driever *et al*., 1996).

- Reverse genetics. This approach was adopted after the sequencing of the zebrafish genome and it is based on site-directed mutagenesis obtained with different techniques and the subsequent analysis of the phenotypic consequences. In zebrafish reverse genetics can be performed both using gene knock-down and knock-out approaches. Targeting both paralogous genes can solve the problem of redundancy in the zebrafish genome.

## MORPHOLINO GENE KNOCKDOWN

Knockdown agents are antisense short nucleotide strands that bind sense RNA to silence gene expression. There are three main types of knockdown agents:

- S-DNAs (phosphorothioate-linked DNAs), that uses the enzyme RNase H to cut the RNA target sequence (Summerton, 2007). The percentage of success is low as only 20% of targets are successfully silenced.
- siRNAs (short interfering RNAs), are constituted by synthetic double-stranded RNA molecules with length between 20-25 base pairs. These molecules block the expression of the selected genes by degrading mRNA after transcription and preventing translation according to the RNA interference (RNAi) pathway (Saxena et al., 2013; Zeng et al., 2003). About 50% are functional in zebrafish.
- Morpholinos (MOs) that make a steric obstruction inhibiting translation (ATG-MO) or splicing (splice-MO) of the target gene (Summerton e Weller 1997). They are more stable and reproducible if used with the appropriate controls.

In zebrafish, the most used approach is morpholino, which is a synthetic molecule typically 20-25 bases in length, produced by Gene Tools (http://www.gene-tools.com). This molecule is a nucleic acid analogue that target sequences of RNA by complementary base-pairing. Compared to a nucleic acid molecule, morpholino have a morpholine-ring (6C) instead of a ribose or deoxyribose molecule (5C). Nucleotides are then linked together by a phosphorodiamidate bridge that substitute the natural phosphate group. These two modifications lead to a strong resistance of these molecules to nucleases and thus make these knockdown agents more stable than the others (Summerton e Weller, 1997). The translation blocking morpholinos are designed to be complementary to a region between the 5'-CAP and the first 25 nucleotides after the first methionine codon (ATG). Thanks to this feature, they sterically prevent the recognition of ribosome and block protein translation (Summerton, 1999). Besides translation-blocking MOs there are splice-blocking morpholinos. These molecules are designed to be complementary to a splice acceptor-donor site in pre-mRNA. In this case the morpholinos produce a steric block at the intron-exon or exon-intron boundary that prevent the activity of the splicing apparatus and interfere with maturation of pre-mRNA in the nucleus (Fig. 7). The advantage of these MOs is that the resulting exon loss or intron retention can be detected easily by quantitative RT-PCR analysis of morphant RNA (Sazani *et al*., 2001, Draper *et al*., 2001). However, these MOs cannot block translation of maternal mRNAs present in the embryos as these are mature mRNA.

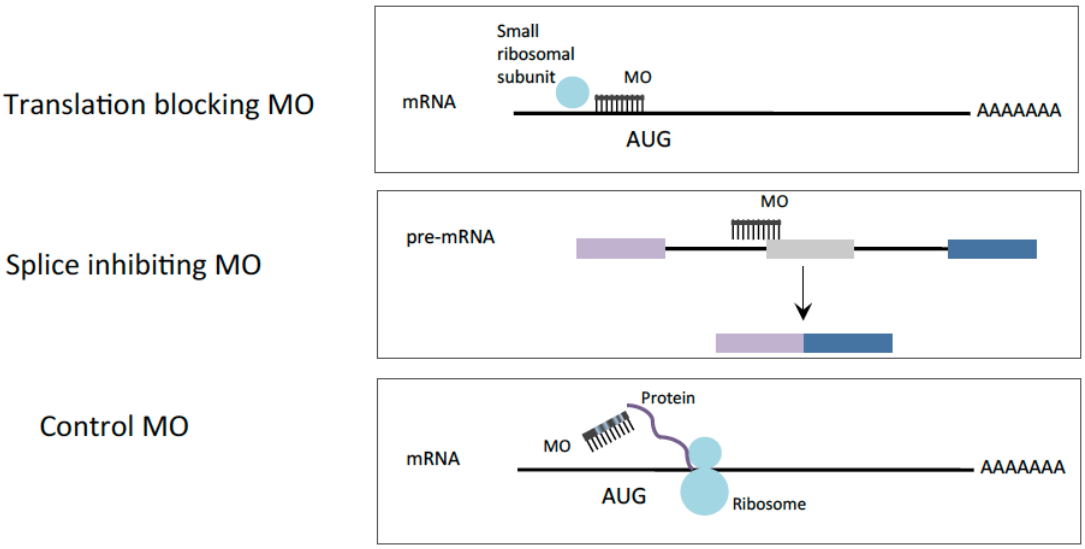


**Fig. 7.** Schematic representation of ATG-MO, Splice-MO and control Mismatch-MO. https://tatyscientificillustrations.com/

The MO is widely used in zebrafish to study the functions of genes by knockdown. Technically MO agents are microinjected in fertilized eggs at the stage of one/two cells. The resulting embryos showing a phenotype caused by MOs are called morphants (Nasevicius e Ekker, 2000). To verify the specificity of morphant phenotypes this experimental approach requires specific controls since MOs can be toxic, causing apoptosis in the nervous system, and/or can produce off-target effects driven by their similarity to other sequences in the genome. The controls required for a reliable MO knockdown experiment are:

- Designing two morpholinos, complementary to different portions of the target transcript (this should produce the same phenotypic effects).
- Utilizing a mismatch MO that differs for 4-5 bases from the specific MO and thus cannot bind the target transcript. This MO should not produce a morphant phenotype.
- Performing a rescue experiment in which MOs are co-injected with a mRNA encoding the target protein which should restore, in a good percentage of embryos, the normal phenotype. To prevent the block of the injected mRNA by MOs, the messanger can derive from another organism or the transcript should be modified in the region recognized by the MO (Eisen e Smith, 2008).
- When the antibody is available, verify by Western Blotting analysis the effective reduction of the protein translation (Heasman, 2002).

- Identifying the appropriate dose in a null background, if a knockout mutant for the target gene is available. Increasing dosages of the MO should injected on the mutant to identify the first concentration causing a phenotype as the limit dosage to prevent off-target effects (Stainier *et al*., 2015).

**CRISPR-CAS9 BASED KNOCKOUT**

In the last 10 years, knockout in zebrafish was totally revolutionized thanks to novel powerful gene targeting strategies, named sequence-specific nucleases like TALENs and CRISPR-Cas9 system that are based on induced mutations and have already been successfully applied to zebrafish (Hwang *et al*., 2013; Chang *et al*., 2013; Cade *et al.,* 2012). These new tools have expanded, in zebrafish and many other model animals, the genome editing possibilities.

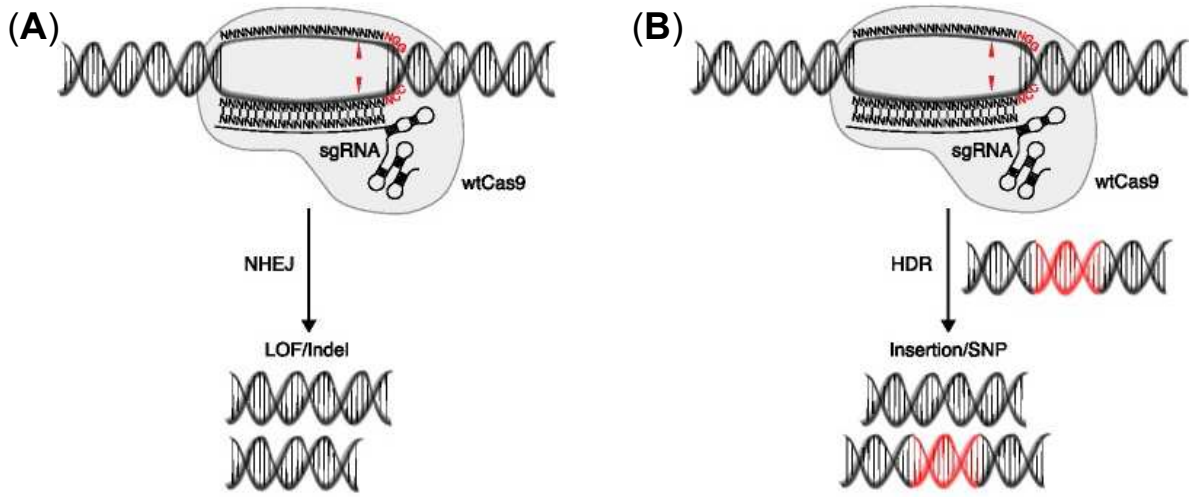


**Fig. 8.** CRISPR/Cas9 mechanism of action. (A) Knockout approaches generate null alleles by means of indel mutations incurred by erroneous repair of DNA double-strand breaks by nonhomologous end joining (*NHEJ*). **(**B**)** To introduce defined mutations endogenous homology-directed repair (*HDR*) mechanism exploit donor DNA templates. Modified from Graham and Root (2015).

The CRISPR-Cas9 technology is based on an adaptive immunity mechanism of archaea and bacteria, which prevent themselves from viruses or plasmid infections. The CRISPR (Clustered Regularly Interspaced Shorts Palindromic Repeats) loci are present in the genome of these groups and are responsible for the acquired immunity. The CRISPR locus is organized in patterns composed of palindromic repeats alternate with the protospacer regions, containing the fragment of foreign DNA. This locus is normally located near the nuclease Cas protein locus (Haft *et al.*, 2005). Invading DNA from viruses or plasmids is cut into small fragments by the Cas nucleases and then inserted between the short repeats. If the viruses attack a second time, the CRISPR array are then transcribed into crRNA (CRISPR RNA) to guide the nuclease Cas proteins to invasive DNA resulting in its cleavage and degradation (Marraffini e Sontheimer, 2010, Van der Oost *et al*., 2014). Thus, this process allows the formation of an adaptive sequence-specific immunity.

There are three main types of CRISPR-Cas system: type I that use helicase-nuclease Cas proteins, type II that use Cas9 nuclease and type III that use Cas10 protein, which is still not well characterized (Makarova *et al.*, 2015).
The system used in genetic engineering involves the type II nuclease Cas9, which need a particular sequence near the Protospacer, called PAM (Protospacer Adjacent Motif) and composed by 3 nucleotides downstream the target sequence, indispensable for the cleavage. The Cas9 nuclease has two regions of interaction: the first interacts with the guide-RNA for the positioning whereas the second recognizes the PAM sequence and exerts the exonuclease activity (Van der Oost *et al*., 2014). In this system the guide crRNA has to be processed by an RNase III starting from a duplex composed by the pre-crRNA and a tracrRNA (trans-encoded CRISPR RNA). When the crRNA is mature is called sgRNA (single guide-RNA) (Barrangou e Marraffini, 2014).
The most used Cas9 derives from *Streptococcus pyogenes*, and recognises the specific PAM sequence "NGG", from 5' to 3'. To maximize the transport into the nucleus and the efficiency of the mutagenesis the Cas9 mRNA and the translate protein contains a Nuclear Localization Sequence (Jao *et al.,* 2013).
The Cas9 results in a double filament break upstream the PAM sequence that will then repaired by the endogenous mechanisms of repair in two principal ways:

- NHEJ (Non-Homologous End Joining): leads to random in-del mutations and it is the more common repair mechanism.
- HDR (Homology-Directed Repair): more difficult to achieve, it needs an exogenous template to direct the filling of the gaps (Ran *et al*., 2013)(Fig. 8).

Nowadays this second mechanism, together with other tools of homologous recombination that use Cas9 breaking, are the new frontiers for the gene knock-in in zebrafish, a technique that is going to be widely used in the future (Albadri *et al*., 2017).

**Morpholino vs CRISPR-Cas9**

It was recently reported by Kok and collaborators (2015) that, in a pool of more than 80 mutated genes, approximately only the 20% of mutant phenotypes resemble the corresponding morphants. This result pointed out the problem of an over-interpretation of antisense morpholino data, underlining the possibility of a high off-target effect rate in MOs based studies (Kok *et al*., 2015).
Moreover, in a recent work, Rossi and co-workers (2015) showed that generally mutants present a lower severe phenotype compared to those of morphants knocked down for the same gene. However, a transcriptomic analysis revealed the up-regulation of a set of genes in mutants but not in morphants, thus suggesting the activation of a

compensatory pathways able to rescue the phenotypes of deleterious mutations. The same was not observed using translational or transcriptional knockdown (Rossi *et al*., 2015). From these works it seems that for the study of gene functions there is not a right approach, but it is necessary a case-to-case evaluation to identify the best strategy, that could be the simultaneous use of both approaches.

Both CRISPR-Cas9 and morpholino can result in off-target effects and, because of this, both approach must be used with the appropriate controls. Probably, to study the effect on early development, the fastest and most phenotypically outstanding tool could be the morpholino approach. However, MOs off-target effects can be extensive at high doses. The generation of the mutant line allows the scientist to titrate the MO in a null genetic background (where the additional phenotype is surely due to the off-target effects) to identify the appropriate dose for the injection (Strainier *et al*., 2015).

**REFERENCES**

**Abada A. and Elazar Z. 2014.** Getting ready for building: signaling and autophagosome biogenesis. EMBO Rep. 15, 839-852.

**Albadri S., Del Bene F., Revenu C. 2017.** Genome editing using CRISPR/Cas9-based knock-in approaches in zebrafish. Methods. May 15;121-122:77-85.

**Barrangou R., Marraffini L.A. 2014.** CRISPR-Cas systems: Prokaryotes upgrade to adaptive immunity. Mol Cell. Apr 24;54(2):234-44.

**Benato F., Skobo T., Gioacchini G., Moro I., Ciccosanti F., *et al.,* 2013.** Ambra1 knockdown in zebrafish leads to incomplete development due to severe defects in organogenesis. Autophagy. Apr;9(4):476-95.

**Boya P., Reggiori F. and Codogno P. 2013.** Emerging regulation and functions of autophagy. Nat. Cell Biol. 15, 713-720.

**Cade L., Reyon D., Hwang W.Y., Tsai S.Q., Patel S., *et al.,* 2012.** Highly efficient generation of heritable zebrafish gene mutations using homo- and heterodimeric TALENs. Nucleic Acids Res. 40(16): 8001–8010.

**Cecconi F., Levine B. 2008.** The role of autophagy in mammalian development: cell makeover rather than cell death. Dev Cell. 15, 344–357.

**Chang N., Sun C., Gao L., Zhu D., Xu X., *et al*., 2013.** Genome editing with RNA-guided Cas9 nuclease in Zebrafish embryos. Cell Res. Apr; 23(4): 465–472.

**Choi A.M., Ryter S.W., and Levine B. 2013.** Autophagy in human health and disease. N. Engl. J. Med. (2013). 368, 651-662.

**Cianfanelli V., De Zio D., Di Bartolomeo S., Nazio F., Strappazzon F., Cecconi F. 2015b.** Ambra1 at a glance. J Cell Sci 128: 2003-2008.

**Cianfanelli V., Nazio F., Cecconi F. 2015a.** Connecting autophagy: AMBRA1 and its network of regulation. Mol Cell Oncol. Jan-Mar; 2(1): e970059.

**Cianfanelli, V., Fuoco, C., Lorente, M., Salazar, M., Quondamatteo, F., et al. 2015c.** AMBRA1 links autophagy to cell proliferation and tumorigenesis by promoting c-Myc dephosphorylation and degradation. Nat. Cell Biol. 17, 20-30.

**Cullup T., Kho A.L., Dionisi-Vici C., Brandmeier B., Smith F., *et al*., 2013.** Recessive mutations in EPG5 cause Vici syndrome, a multisystem disorder with defective autophagy. Nat. Genet. 45, 83-87.

**Dahm R. and Geisler R. 2006.** Learning from small fry: the zebrafish as a genetic model organism for aquaculture fish species. Marine Biotechnology, 2006. 8: 329-45.

**Dere E., Dahm L., Lu D., Hammerschmidt K., Ju A., *et al.,* 2014.** Heterozygous ambra1 deficiency in mice: a genetic trait with autism-like behavior restricted to the female gender. Front. Behav. Neurosci. 8, 181.

**Di Bartolomeo S., Corazzari M., Nazio F., Oliverio S., Lisi G., *et al.,* 2010.** The dynamic interaction of AMBRA1 with the dynein motor complex regulates mammalian autophagy. J. Cell Biol. 191, 155-168.

**Draper B.W., Morcos P.A., Kimmel C.B. 2001.** Inhibition of Zebrafish fgf8 Pre-mRNA Splicing With Morpholino Oligos: A Quantifiable Method for Gene Knockdown. Genesis. 30, 154– 156.

**Driever W., Solnica-Krezel L., Schier A.F., Neuhauss S.C., Malicki J., *et al.*, 1996.** A genetic screen for mutations affecting embryogenesis in zebrafish. Development. 123, 37-46.

**Ebrahimi-Fakhari D., Saffari A., Wahlster L., Lu J., Byrne S., *et al.,* 2016.** Congenital disorders of autophagy: an emerging novel class of inborn errors of neuro-metabolism. Brain. Feb;139(Pt 2):317-37.

**Ehmke N., Parvaneh N., Krawitz P., Ashrafi M.R., Karimi P., *et al.*, 2014**. First description of a patient with Vici syndrome due to a mutation affecting the penultimate exon of EPG5 and review of the literature. Am J Med Genet A. Dec; 164A(12):3170-5.

**Eisen J.S., Smith J.C. 2008.** Controlling morpholino experiments: don't stop making Antisense. Development 135, 1735–1743.

**Fader C.M., Sánchez D.G., Mestre M.B., Colombo M.I. 2009.** TI-VAMP/VAMP7 and VAMP3/cellubrevin: two v-SNARE proteins involved in specific steps of the autophagy/multivesicular body pathways. Biochim Biophys Acta. Dec;1793(12):1901-16.

**Fimia G.M., Corazzari M., Antonioli M., Piacentini M. 2013.** Ambra1 at the crossroad between autophagy and cell death. Oncogene. 32, 3311–3318.

**Fimia G.M., Stoykova A., Romagnoli A., Giunta L., Di Bartolomeo S., *et al.,* 2007.** Ambra1 regulates autophagy and development of the nervous system. Nature. 2007. 447, 1121-1125.

**Furuta N., Yoshimori T., Amano A. 2010.** Mediatory molecules that fuse autophagosomes and lysosomes. Autophagy. Apr;6(3):417-8.

**Galluzzi L., Baehrecke E.H., Ballabio A., Boya P., Bravo-San Pedro J.M., *et al.,* 2017.** Molecular definitions of autophagy and related processes. EMBO J. 2017 Jul 3;36(13):1811-1836.

**García-Arencibia M., Hochfeld W.E., Toh P.P.C. 2010.** Autophagy, a guardian against neurodegeneration. Semin Cell Dev Biol. 21, 691–8.

**Graham D.B. and Root D.E. 2015.** Resources for the design of CRISPR gene editing experiments. Genome Biol 16:260.

**Grumati P, Coletto L, Sabatelli P, Cescon M, Angelin A, *et al*., 2010.** Autophagy is defective in collagen VI muscular dystrophies, and its reactivation rescues myofiber degeneration. Nature Medicine 16, 1313–1320.

**Haft D.H., Selengut J., Mongodin E.F., Nelson K.E. 2005.** A guild of 45 CRISPR-associated (Cas) protein families and multiple CRISPR/Cas subtypes exist in prokaryotic genomes. PLoS Comput Biol. Nov;1(6):e60.

**Halama N., Grauling-Halama S.A., Beder A., Jager D. 2007.** Comparative integromics on the breast cancer-associated gene KIAA1632: clues to cancer antigen domain. Int. J. Oncology. 31: 205-210.

**Hale A.N., Ledbetter D.J., Gawriluk T.R. and Rucker E.B. 2013.** Autophagy, Regulation and role in development. Autophagy. Vol. 9 , Iss. 7. 951-972.

**Heasman J. 2002.** Morpholino oligos: making sense of antisense? Dev Biol. Mar 15;243(2):209-14.

**Heinrich A., Nees F., Lourdusamy A., Tzschoppe J., Meier S., *et al.,* 2013.** From gene to brain to behavior: schizophrenia-associated variation in AMBRA1 alters impulsivity-related traits. IMAGEN consortium. Eur. J. Neurosci. 38, 2941-2945.

**Herpin A., Englberger E., Zehner M.,Wacker R., Gessler M., *et al*., 2015.** Defective autophagy through epg5 mutation results in failure to reduce germ plasm and mitochondria. FASEB. J. 29, 4145–4161.

**Howe K., Clark M.D., Torroja C.F., Torrance J, Berthelot C, *et al.,* 2013.** The zebrafish reference genome sequence and its relationship to the human genome. Nature. Apr 25; 496(7446): 498–503.

**Hwang W.Y., Fu Y., Reyon D., Maeder M.L., Tsai S.Q*., et al.,* 2013.** Efficient In Vivo Genome Editing Using RNA-Guided Nucleases. Nat Biotechnol. Mar; 31(3): 227–229.

**Ingham P.W. 2009.** The power of the zebrafish for disease analysis. Human Molecular Genetics. 18: R107-R112.

**Jao L.E., Wente S.R., Chen W. 2013.** Efficient multiplex biallelic zebrafish genome editing using a CRISPR nuclease system. Proc Natl Acad Sci U S A. Aug 20;110(34):13904-9.

**Kaur J. and Debnath J. 2015.** Autophagy at the crossroads of catabolism and anabolism. 2015. Nature Reviews Molecular Cell Biology 16, 461–472.

**Kaushik S. and Cuervo A.M. 2012.** Chaperone-mediated autophagy: a unique way to enter the lysosome world. Trends Cell Biol. 22, 407–417.

**Kim Y.C. and Guan K.L. 2015.** mTOR: a pharmacologic target for autophagy regulation J. Clin. Invest.;125(1):25-32.

**Kimmel C.B. 1993.** Patterning the brain of the zebrafish embryo. Annu Rev Neurosci, 16, 707-732.

**Kimmel C.B., Ballard W.W., Kimmel S.R., Ullmann B., Schilling T.F. 1995.** Stages of embryonic development in the zebrafish. Developmental Dynamics. 203: 253–310.

**Klionsky D.J. 2014.** Citing recent declines in the discovery of new ATG genes, some scientists now suggest that the end of autophagy research may be within sight. Autophagy.;10(5):715–716.

**Klionsky D.J., Abeliovich H., Agostinis P., Agrawal D.K., Aliev G. *et al*. 2008.** Guidelines for the use and interpretation of assays for monitoring autophagy in higher eukaryotes. Autophagy 4, 151–175.

**Kok F.O., Shin M., Ni C.W., Gupta A., Grosse A.S., *et al.* 2015.** Reverse genetic screening reveals poor correlation between morpholino-induced and mutant phenotypes in zebrafish. Dev Cell. Jan 12;32(1):97-108.

**Lee E., Koo Y., Ng A., Wei Y., Luby-Phelps K., *et al.* 2014.** Autophagy is essential for cardiac morphogenesis during vertebrate development. Autophagy Apr;10(4):572-87.

**Levine B. and Klionsky D.J. 2004.** Development by self-digestion: Molecular mechanisms and biological functions of autophagy. Dev Cell 6: 463–477.

**Levine B. and Kroemer G. 2008.** Autophagy in the pathogenesis of disease. Cell 132: 27-42.

**Li W.W., Li J., Bao J.K. 2012.** Microautophagy: Lesser-known self-eating. Cell Mol Life Sci 69, 1125–1136.

**Makarova K.S., Wolf Y.I., Alkhnbashi O.S., Costa F., Shah S.A., *et al*. 2015.** An updated evolutionary classification of CRISPR-Cas systems. Nat Rev Microbiol 13:722–36.

**Mammucari C., Milan G., Romanello V., Masiero E., Rudolf R., *et al*. 2007.** FoxO3 controls autophagy in skeletal muscle in vivo. Cell Metab 6, 458–71.

**Marraffini L.A. and Sontheimer E.J. 2010.** CRISPR interference: RNA-directed adaptive immunity in bacteria and archaea. Nat Rev Genet Mar;11(3):181-90.

**Mei, Y., Su M., Soni, G., Salem, S., Colbert, C. L. and Sinha, S. C. 2014.** Intrinsically disordered regions in autophagy proteins. Proteins 82, 565-578.

**Meyer A., Van de Peer Y. 2005**. From 2R to 3R: evidence for a fish-specific genome duplication (FSGD). Bioessays 27(9): 937-45.

**Miao G., Zhao Y.G., Zhao H., Ji C., Sun H., *et al*. 2016.** Mice deficient in the Vici syndrome gene Epg5 exhibit features of retinitis pigmentosa. Autophagy Dec;12(12):2263-2270. Epub 2016 Oct 7.

**Mizushima N. and Komatsu M. 2011.** Autophagy: renovation of cells and tissues. Cell. 2011.147, 728–741.

**Mizushima N., Levine B., Cuervo A.M., Klionsky D.J. 2008.** Autophagy fights disease through cellular self-digestion. Nature 451, 1069–1075.

**Mowers E.E., Sharifi M.N. and Macleod K.F. 2017.** Autophagy in cancer metastasis. Oncogene 36, 1619–1630.

**Nasevicius A. and Ekker S.C. 2000.** Effective targeted gene knockdown' in zebrafish. Nat Genet. 2000 26, 216–20.

**Nasiadka, A. and Clark, M.D. 2012.** Zebrafish breeding in the laboratory environment. ILAR Journal. 2012, 53: 161-168.

**Nazio, F., Strappazzon, F., Antonioli, M., Bielli, P., Cianfanelli, V., *et al*. 2013.** mTOR inhibits autophagy by controlling ULK1 ubiquitylation, self-association and function through AMBRA1 and TRAF6. Nat. Cell Biol 15, 406-416.

**Pagliarini, V., Wirawan, E., Romagnoli, A., Ciccosanti, F., Lisi, G., *et al.* 2012.** Proteolysis of Ambra1 during apoptosis has a role in the inhibition of the autophagic pro-survival response. Cell Death Differ 19, 1495-1504.

**Peng Z., Xue B., Kurgan L., Uversky V. N. 2013.** Resilience of death: intrinsic disorder in proteins involved in the programmed cell death. Cell Death Differ 20, 1257-1267.

**Ran F.A., Hsu P.D., Wright J., Agarwala V., Scott D.A., *et al.,* 2015.** Resources for the design of CRISPR gene editing experiments. Genome Biol. 16: 260.

**Ravikumar B, Acevedo-Arozena A, Imarisio S, Berger Z, Vacher C, *et al*. 2005.** Dynein mutations impair autophagic clearance of aggregate-prone proteins. Nat Genet Jul;37(7):771-6.

**Ravikumar B., Futter M., Jahreiss L., Korolchuk V.I., Lichtenberg M., *et al*. 2009.** Mammalian macroautophagy at a glance. J Cell Sci 122, 1707–11.

**Rietschel, M., Mattheisen, M., Degenhardt, F., Mühleisen, T. W., Kirsch, P., *et al*. 2012.** Association between genetic variation in a region on chromosome 11 and schizophrenia in large samples from Europe. Mol. Psychiatry 17, 906-917.

**Rossi A., Kontarakis Z., Gerri C., Nolte H., Hölper S., *et al*., 2015.** Genetic compensation induced by deleterious mutations but not gene knockdowns. Nature Aug 13;524(7564):230-3.

**Rubinsztein D.C. 2005.** Dynein mutations impair autophagic clearance of aggregate-prone proteins. Nat Genet Jul;37(7):771-6.

**Rubinsztein D.C., Mariño G., Kroemer G. 2011.** Autophagy and aging. Cell 146, 682-695.

**Russell R.C., Tian Y., Yuan H., Park H.W., Chang Y.Y., *et al*. 2013.** Guan KL. ULK1 induces autophagy by phosphorylating Beclin-1 and activating VPS34 lipid kinase. Nat Cell Biol Jul;15(7):741-50.

**Saxena S, Kesharwani RK, Singh V, Singh S. 2013.** Designing of putative siRNA against geminiviral suppressors of RNAi to develop geminivirus-resistant papaya crop. Int J Bioinform Res Appl 9(1):3-12.

**Sazani P., Kang S.K., Maier M.A., Wie C., Dillman J., *et al*. 2001.** Nuclear antisense effects of neutral, anionic and cationic oligonucleotide analogs. Nucl. Acids Res 29, 3965–3974.

**Sjoblom T., Jones S., Wood L.D., Parsons D.W., Lin J., *et al*. 2006.** The consensus coding sequences of human breast and colorectal cancers. Science 314, 268–274.

**Skobo T., Benato F., Grumati P., Meneghetti G., Cianfanelli V., *et al*. 2014.** Zebrafish ambra1a and ambra1b knockdown impairs skeletal muscle development. PLoS ONE 9, e99210.

**Stainier D.Y., Kontarakis Z., Rossi A. 2015.** Making sense of anti-sense data. Dev Cell Jan 12;32(1):7-8.

**Stanley R.E., Ragusa M.J., Hurley J.H. 2014.** The beginning of the end: How scaffolds nucleate autophagosome biogenesis. Trends Cell Biol Jan; 24(1): 10.1016

**Strappazzon F., Vietri-Rudan M., Campello S., Nazio F., Florenzano F., *et al*. 2011.** Mitochondrial BCL-2 inhibits AMBRA1-induced autophagy. EMBO J 30, 1195-1208.

**Summerton J. 1999.** Morpholino antisense oligomers: the case for an RNase H-independent structural type. Biochim Biophys Acta Dec 10;1489(1):141-58.

**Summerton J. 2007.** Mopholino, siRNA, and S-DNA compared: impact of structure and mechanism of action on off-target effects and sequence specifity. Med Chem 7, 651–660.

**Summerton J. and Weller D. 1997.** Morpholino antisense oligomers: design, preparation, and properties. Antisense Nucleic Acid Drug Dev Jun;7(3):187-95.

**Tavares B., Santos Lopes S. 2013.** The importance of zebrafish in biomedical research. Acta Medica Portuguesa 26: 583-592.

**Tian Y., Li Z., Hu W., Ren H., Tian E., Zhao Y., *et al*. 2010.** C. elegans screen identifies autophagy genes specific to multicellular organisms. Cell Jun 11;141(6):1042-55.

**Vacaru A.M., Unlu G., Spitzner M., Mione M., Knapik E.W., Sadler, K.C. 2014.** In vivo cell biology in zebrafish - providing insights into vertebrate development and disease. Journal of Cell Science 127: 485-495.

**Van der Oost J., Westra E.R., Jackson R.N., Wiedenheft B. 2014.** Unravelling the structural and mechanistic basis of CRISPR-Cas systems. Nat Rev Microbiol Jul;12(7):479-92.

**Van Humbeeck C., Cornelissen T., Hofkens H., Mandemakers W., Gevaert K., *et al.* 2011.** Parkin interacts with Ambra1 to induce mitophagy. J. Neurosci 31, 10249-10261.

**Walker C. and Streisinger G. 1983.** Induction of Mutations by gamma-Rays in Pregonial Germ Cells of Zebrafish Embryos. Gen 103, 125-136.

**Wang Z., Miao G., Xue X., Guo X., Yuan C*. et al.* 2016.** The Vici Syndrome Protein EPG5 Is a Rab7 Effector that Determines the Fusion Specificity of Autophagosomes with Late Endosomes/Lysosomes. Mol Cell Sep 1;63(5):781-95.

**Weidberg H., Shpilka T., Shvets E., Abada A., Shimron F., Elazar Z. 2011.** LC3 and GATE-16 N termini mediate membrane fusion processes required for autophagosome biogenesis. Dev Cell Apr 19;20(4):444-54.

**Yang Z. and Klionsky D.J. 2010.** Eaten alive: A history of macroautophagy. Nat Cell Biol. 2010. 12, 814–822.

**Zeng Y., Yi R., Cullen B.R. 2003.** MicroRNAs and small interfering RNAs can inhibit mRNA expression by similar mechanisms. Proc Natl Acad Sci U S A Aug 19;100(17):9779-84.

**Zhao H., Zhao Y.G., Wang X., Xu L., Miao L., *et al.* 2013.** Mice deficient in Epg5 exhibit selective neuronal vulnerability to degeneration. J Cell Biol Mar 18;200(6):731-41. doi: 10.1083/jcb.201211014.

**Zhao Y.G., Zhao H., Sun H., Zhang H. 2013b.** Role of Epg5 in selective neurodegeneration and Vici syndrome. Autophagy Aug;9(8):1258-62. doi: 10.4161/auto.24856.

# The *epg5* knockout zebrafish line: a model to study Vici syndrome

**Advanced draft**

**ABSTRACT**

EPG5 protein is a Rab7 effector involved in fusion specificity between autophagosomes and late endosomes/lysosomes during autophagy. Mutations in the human EPG5 gene cause a rare and severe multisystem disorder called Vici syndrome. In this work, we show that zebrafish *epg5*$^{-/-}$ mutants from both heterozygous and incrossed homozygous matings show a normal development and reach sexual maturity without any evident phenotype. In agreement with the dysfunctional autophagy of Vici syndrome, western blot analysis shows a higher level of Lc3-II autophagy markers in mutant larvae with respect to wild type (WT) controls. Moreover, in response to starvation *epg5*$^{-/-}$ larvae display higher accoumulation of Lc3-II with respect to WT, together with a significant reduction of birefringence of the skeletal muscle. Accordingly, muscle ultrastructural analysis revealed accumulation of degradation-defective autolysosomes in starved mutants, together with a clear reduction of muscular fibers. Before one year of age, *epg5*$^{-/-}$ mutants display impaired motility and muscle thinning, confirmed by accumulation of non-degradative autophagic vacuoles. Furthermore, at this same age *epg5*$^{-/-}$ fish show morphological alterations in gonads and heart revealed by histological analysis. These results suggest that the zebrafish *epg5* mutants represent a good model of Epg5-related disorders and will provide a new tool for studying the contribution of Epg5 on the Vici syndrome development and progression as well as for high-throughput autophagy-related drugs screening.

Chapter 1

## INTRODUCTION

Epg5 (ectopic P-granules autophagy protein 5), has been initially identified, together with other three new proteins, Epg2, Epg3 and Epg4, in the nematode *C. elegans* as a protein involved in the degradation of germline P granule components in somatic cells during embryogenesis (Tian *et al*., 2010).

All Epg proteins are involved in starvation-induced autophagy, an evolutionary conserved catabolic process in which a cell degrades and recycles, through the lysosomes, long-lived proteins and dismantles damaged organelles in order to maintain cellular homeostasis. This process, which consists of a cascade of finely regulated steps and employs a specific subset of proteins, plays a central role also during embryonic development, cellular differentiation, normal physiology, survival during starvation and ageing (Levine, 2004; Cecconi, 2008). In particular, Epg5 was found to be required for the fusion of autophagosomes with late endosomes and lysosomes, a late step of the autophagy process (Tian *et al*., 2010).

More recently, the analysis of Epg5 molecular functions revealed its interaction with Rab7 and VAMP-8 on late endosomes/lysosomes and with Lc3 and STX17–SNAP29 complexes on autophagosomes. Its tethering activity allows assembly and stabilization of SNARE complexes and promotes the fusion specificity (Wang *et al.*, 2016).

In humans, *EPG5* gene (18q12.3) was initially named *KIAA1632* and identified among a group of genes found to be mutated in breast cancer tissues (Sjöblom *et al.*, 2006). This gene consists of 44 exons, with the longest transcript, between those reported on Ensemble (Flicek *et al.*, 2014), encoding a protein of 2,579 amino acids (Halama *et al.*, 2007). *EPG5* gene is mainly expressed in central nervous system (CNS), skeletal and cardiac muscle, thymus, immune cells, lung and kidney (Halama *et al.*, 2007).

Human recessive mutations of the *EPG5* gene have been associated to a rare multisystem disorder, called Vici syndrome (OMIM 242840), mainly characterized by agenesis of the corpus callosum, hypopigmentation, variable immunodeficiency, cardio- and skeletal myopathy and decreased autophagy activity (Cullup *et al.*, 2013). The disease determines a markedly reduced life expectancy with death occurring in infancy or early childhood. The main causes of mortality are represented by recurrent and severe infections and/or progressive heart failure (Ebrahimi-Fakhari *et al.*, 2015).

This syndrome represents the first multisystem disorder identifield to be directly associated with mutations in an autophagy-related gene (Cullup *et al.*, 2013). *EPG5* mutations are distributed along the whole coding sequence (Cullup *et al.*, 2013; Ehmke *et al.*, 2014). The majority of these are *null* mutations predicted to produce truncated

EPG5 proteins with variable length; missense mutations are present in very low number of cases (Byrne *et al.*, 2016). However, at least one of the latter was found to produce also multiple misspliced mRNA isoforms that give rise to truncated EPG5 proteins (Kane *et al.*, 2017).

To study Epg5 functions a Epg5 *null* mouse model was recently generated (Zhao *et al.*, 2013a). The *epg5* KO mice grow normally into sexually mature adults, but progressively develop neuronal damages, myofiber atrophy associated to behavioural and motor abnormalities, resulting in death between 10-12 months of age (Zhao *et al.*, 2013a, b). Although this model resembles several features linked to Vici syndrome, other features of the disease such as hypopigmentation, facial dysmorphism and cataract, are absent (Zhao *et al.*, 2013a).

Moreover, Epg5-deficient mice show key characteristics of amyotrophic lateral sclerosis (Zhao *et al.*, 2013b) and retinitis pigmentosa (Miao *et al.*, 2016) and thus they could be used to study the molecular mechanisms of these pathologies. Like in *C. elegans*, Epg5 loss of function in mice led to impaired autophagosome maturation and endosome trafficking (Zhao *et al.*, 2013a). The last function seems not be present on cells from Vici syndrome patients and thus, Hori and co-workers (2017) propose that the function of EPG5 could be limited to autophagosome-lysosome fusion.

Finally, medaka Epg5 KO model shows that the silencing of this gene not only impairs the autophagic flux but also spermatogenesis, due to failure of germ plasm and mitochondria clearance during the process of germ cell specification and also in the adult gonads (Herpin *et al.*, 2015).

In the present study, we describe the generation and characterization of a zebrafish *epg5* mutant line by means of targeted CRISPR/Cas9 mutagenesis. The resulting *epg5* mutants represent, to our knowledge, the first model to study Epg5-related disorders by means of a stable zebrafish line and will provide a new tool for studying the contribution of this protein on the Vici syndrome development and progression from embryonic stages to adult. Moreover, this model will be useful for high-throughput drugs screening.

## METHODS

### Zebrafish maintenance and care

Wild type and mutant zebrafish were staged and maintained according to standard procedures (Kimmel *et al.*, 1995; Westerfield, 1995). Embryos were obtained by natural mating and raised at 28.5°C in Petri dishes containing fish water (50X: 25 g Instant Ocean, 39.25 g $CaSO_4$ and 5 g $NaHCO_3$ for 1 l) and kept in a 12:12 light-dark (LD) cycle. For screening and *in vivo* imaging, embryos and larvae were anesthetized with 0.04% tricaine (Sigma-Aldrich, E10521). Non-mutant embryos or larvae indicated by *WT* or *epg5*$^{+/+}$correspond to samples deriving from different or from the same eggs batches of *epg5*$^{-/-}$ respectively.

During experiments with transgenic lines having a heat shock promoter, mutant transgenic larvae were collected and heat shocked by placing in 42°C fish water and then incubating for 60-min at 37°C. Fish were then placed back at 28.5°C, whereas images were taken 12 hours after the heat shock.

All husbandry and experimental procedures complied with European Legislation for the Protection of Animals used for Scientific Purposes (Directive 2010/63/EU) and were previously authorized by the University of Padua, Body for the Protection of Animals (OPBA-Project Number 568/2016).

### Generation of the *epg5* mutant lines

*epg5* mutant zebrafish were generated using the CRISPR/Cas9-mediated genome editing. Briefly, the e-crisp design software (available at: https://e-crisp.org) was used to design the gene-specific guide RNA (sgRNA) to target *epg5* gene on exon 3 (sequence submitted to EMBL). *epg5* target sequence is listed in Supplemental S-Table 1. BLAST analysis of the target sequences revealed no specific binding with other genes. sgRNA was generated according to previously described methods (Gagnon *et al*., 2014) and *in vitro* transcribed using MEGAshortscript T7 kit (Life Technologies, AM1354). Cas9 mRNA was transcribed from linearized pCS2-nls-zCas9-nls plasmid (Addgene, Plasmid #47929) using mMessage Machine SP6 kit (Life Technologies, AM1340).

Fertilized eggs were injected with 1 nl of a solution containing 400 ng/µl Cas9 mRNA and 50 ng/µl gRNA. Genomic DNA was extracted from 5-dpf larvae from individually injected eggs to verify the presence of mutations and confirm the activity of the guide RNA. Injected embryos were raised to adulthood and F0 founders selected by genotyping (see below). Embryos collected from the outcrosses between these F0 founders and WT were raised and genotyped to confirm germline transmission of the mutation (F1 generation).

Heterozygous mutants were breed with WT and the resulting heterozygous (F2 generation) were selected and crossed, to obtain two lines of homozygous mutant embryos (F3 generation).

**Genomic DNA extraction from embryos/larvae and fin clips**

Genomic DNA was extracted from single larvae euthanized with a lethal dose of tricaine (MS222) using the HotSHOT protocol (Meeker *et al.*, 2007). For fin clips DNA extraction, adult fish were anesthetized with tricaine and biopsies from the caudal fin were removed with a sharp blade. The specimens were then treated with the same protocol.

**Genotyping *epg5*$^{-/-}$ mutants**

Mutations in F0 were detected using heteroduplex mobility assay (HMA). In this case, genomic fragments at the target sites were amplified by PCR with 5x HOT FIREPol® Blend Master Mix (Solis BioDyne, 04-25-00125) and the locus-specific primers (*epg5*-F2 and *epg5*-R3) listed in Supplemental Table 1 that gave rise to a 265 bp fragment on WT samples.

PCR conditions were as follows: 15 min at 95°C, 35 cycles at 95°C for 20 s, 60°C for 30 s and 72°C for 30 s. The resultant PCR amplicons were electrophoresed on a 15% polyacrylamide gel (Life Technologies, NP0323PK2). For verification, PCR products from fish harbouring indel mutations were subjected to sequencing. Poly Peak Parser software (http://yosttools.genetics.utah.edu/PolyPeakParser/) was used for identification and sequence characterization of heterozygous mutant carriers generated by genome editing.

The same primers used for F0 HMA were utilised for screening of heterozygous and homozygous fish. PCR products were resolved with Gel Red-stained 3% agarose low EEO gel (Fisher BioReagents, BP160-500) to identify *epg5*$^{+/+}$, *epg5*$^{+/-}$ and *epg5*$^{-/-}$ samples.

**Generation of mutant epg5 transgenic zebrafish lines**

The *epg5*$^{-/-}$ mutant line was crossed with the following transgenic zebrafish lines:

Tg(mnx1:GFP) (formerly hb9:GFP) (Flanagan-Steet *et al.*, 2005), Tg(h2afx:EGFP-Rab5c)$^{mw5}$ and Tg(h2afx:EGFP-Rab7)$^{mw7}$ (Clark *et al.*, 2011), Tg(hsp:Lamp1-RFP) and Tg(hsp:RFP-LC3), generated by Prof. Enrico Moro using the plasmids provided by Prof. Michel Bagnar of the Duke University Medical Center in Durham (Ellis *et al.*, 2013).

**RNA isolation and quantitative real time reverse transcription PCR (qRT-PCR)**

For expression analysis, total RNA was extracted from pools of 15 larvae with TRIzol reagent (Thermo Fisher Scientific, 15596026). RNA samples were treated with *DNAse*I (Promega, M6101) to eliminate possible genomic DNA contaminations, and stored at -80°C until use. Total RNA was then used for cDNA synthesis with random primers (Promega, C1181) and M-MLV Reverse Transcriptase RNase H- (Solis BioDyne, 06-21-010000) according to the manufacturer's protocol. PCRs were performed with the SYBR green (Bio-Rad Laboratories) method in a Rotor Gene-Q Real-Time PCR thermal cycler (Quiagen). *ribosomal protein, large, P0* (*rplp0*) was used as internal standard in each sample in order to standardize the results by eliminating variation in mRNA and cDNA quantity and quality. The annealing temperature for PCR ranges from 58 to 60°C, depending on the primer set used. The cycling parameters were 95°C for 14 min, followed by 45 cycles at 95°C for 30 s, 30 s of annealing at the temperature selected for the pair of primers and 20 s of extension at 72°C. No amplification products were observed in negative controls and no primer-dimer formations in the control templates. The data obtained were analysed using the Rotor Gene-Q software (Qiagen). All analyses were performed in triplicate. Primer sequences are reported in S-Table 1.

**Protein extraction and western blotting analysis**

Pool of 15 embryos of 8- and 11-dpf *epg5*$^{-/-}$ and WT zebrafish, in fed conditions or eventually following 72 hours of starvation, were frozen in liquid nitrogen and mechanically homogenized in Tissue Extraction Reagent I (Invitrogen, FNN0071) added with protease inhibitors (Roche, COEDTAF-RO). Following a brief centrifugation, the supernatant was collected and the protein content was determined by BCA assay (Thermo-Fisher Scientific, 23225). 30 µg of total proteins per sample were mixed with a reducing agent-containing loading buffer (Thermo-Fisher Scientific, NP0008), boiled, and loaded onto 12% polyacrilamide pre-cast gels (Thermo-Fisher Scientific, NP0341). Following SDS-PAGE, proteins were transferred onto a PVDF membrane (Thermo-Fisher Scientific, 88520) which was subsequently saturated with 5% non-fat milk in TBS-T, and hybridized with primary (anti-LC3 1:1000, Thermo fisher Scientific, PA1-16930; anti β-actin 1:2000, Sigma-Aldrich, A5316) and secondary (HRP-conjugated goat anti-rabbit or anti-mouse IgG-Fc fragment, Bethyl laboratories inc., A120-111P and A90-131P). The signal was revealed using SuperSignal West Pico Chemiluminescent Substrate (Thermo-Fisher Scientific, 340779).

**Morphological and histological analysis**

*epg5*$^{-/-}$ and WT zebrafish were fixed for 24 h in Bouin's solution at room temperature. The samples were dehydrated through a graded series of ethanol, infiltrated with xilene and embedded in Paraplast plus (Leica, 39602004). The samples were serially cut into 7/8-µm sections on a LKB microtome. After rehydration, the sections were stained with haematoxylin and eosin and mounted with Eukitt (BioOptica, 09-00100) for microscopic examination.

**Electron Microscopy**

WT and *epg5*$^{-/-}$ zebrafish larvae (8 and 11 days) and adult were fixed with Karnovsky fixative (2.5% glutaraldehyde and 2% paraformaldheyde in 0.1 M cacodylate buffer) for 3 h at 4°C, washed with 0.1 M cacodilate buffer, post-fixed with osmium tetroxide for 2 h and embedded in EPON 812. Ultrathin sections were stained with uranyl acetate and lead citrate and observed at Philips EM400 operating at 100 kV.

**Birefringence assay**

Muscle birefringence was analysed by placing anesthetized embryos mounted in methyl cellulose 2% in $H_20$ on a glass polarizing filter and covering with a second polarizing filter on a Leica M165 FC microscope. Embryos were photographed with a Nikon DS-Fi2 digital camera using the bright field. The top filter was twisted until it was possible to see the light refracting through the striated muscle. Pixel intensity in the trunk region was measured with ImageJ software. Values were normalized for samples area because of the slight differences in the size between mutants and WT in analysed stages. Three independent clutches of 10 larvae per genotype and treatment were analysed for their muscle birefringence. Data are represented as means ± SEM and statistical significance was determined by Student's t-test.

**Whole mount in situ hybridization (WMISH)**

Zebrafish embryos were fixed overnight at 4°C in 4% paraformaldehyde (PFA, Sigma) in phosphate-buffered saline (PBS) at the required stages of development. WMISH was performed as previously described (Thisse and Thisse, 2008). DIG-labelled epg5-riboprobe was synthesized by *in vitro* transcription with T7 or Sp6 RNA polymerases (Roche), following the manufacturer's instructions and after plasmid linearization as reported on S-Table 2.

**Alcian blue staining**

Larvae were fixed in 4% paraformaldehyde, rinsed in acidic ethanol and stained with Alcian blue as described. Unbound stain was removed by repeated rinsing with acidic ethanol and 3 washes in KOH 0.5%, $H_20_2$ 3% in $H_2O$ prior to whole-mount imaging. In addition, Alcian Blue staining was quantified as the total integrate density after removing background using a defined threshold in the middle-intestine area (area and threshold were constant in all the samples) using ImageJ. Dimensions of alcian spots were measured using imageJ and counted as mature cells if Area > 19.6 $\mu m^2$ (diameter 5 $\mu m$) and as immature if Area < 19.6 $\mu m^2$.

**Fluorescent staining with acridine orange**

For acridine orange fluorescent staining, live larvae were submerged in a solution containing a final concentration of 5 mg/ml of acridine orange in Fish Water, and incubated at 28.5°C for 30 min in the dark. Larvae were then washed several times with Fish Water and mounted in low-melting agarose for positioning and confocal microscope image acquisition. Quantification of apoptotic acridine orange positive spots were performed using the 3D-object counter plug-in of imageJ software, using a constant area and a constant threshold for all samples.

**Growth rate curve**

WT and *epg5*$^{-/-}$ larvae at 6 dpf were placed into 2,5 l fish tanks. 8 random fish were photographed twice a week from 6 dpf to 2 months, using the Leica 165 DM and the Nikon DS-FiS. This protocol was repeated in two independent experiments. Measures were obtained using imageJ.

**Amputation of the caudal fin**

Fish were anesthetized with tricaine to cut the final part of their caudal fin. 5 days after the amputation, the fins were photographed using the Leica 165 DM and the Nikon DS-FiS. The re-growth area was then measured using imageJ. The measure is composed by the mean length of the third superior fin ray, the third inferior fin ray and the central one, which is also the shorter.

**Imaging**

For imaging, transgenic embryos and larvae were anesthetized with 0.04% tricaine, embedded in 0.8% low-melting agarose and placed on a depression slide. The Nikon C2 confocal system using the software NIS ELEMENTS was used to record images. WMISH-

stained embryos were mounted in 87% glycerol in PBT (PBS plus 0.1% Tween 20) or cleared and mounted in 2:1 benzyl benzoate/benzyl alcohol, observed under a Leica M165 FC microscope, and photographed with a Nikon DS-Fi2 digital camera. Histology samples were photographed on a Leica DMR using a Nickon DS-Fi2 digital camera.
All images were analysed with Fiji (ImageJ) software.

**Statistical analysis**

Statistical analysis was performed using Graph Pad Prism V6.0. Data are presented as the means ± SEM except for the growth rate analysis. Statistical analysis of comparison between WT and mutant fish lines was performed by Student's *t*-test. The p values are summarized with the following symbols: *p<0.05, **p<0.01, ***p< 0.001, ****p<0.0001.

## RESULTS

### Zebrafish 5'-UTR *epg5* characterization and expression patterns during zebrafish development

*epg5* is present on the zebrafish genome as a single gene located on chromosome 5. Since no *epg5* experimentally determined sequences were available at the beginning of this work, we performed a 5'-RACE analysis with RNA extracted from 4-hpf (hour post fertilization) embryos to obtain a 363 nt sequence formed by a first non-coding and 3 coding exons of this gene. The transcript begins with a 5'-UTR of 117 nt (AC_MG775431). The experimentally determined partial transcript matches with the Genbank XM_009301680 and XM_005165361 sequences whereas it is slightly different with respect to the NM_001110525 that presents a different first exon and result in a 13-amino acid shorter protein and a different N-terminal region of 4 aa (see S-Fig. 1, panel A).

To investigate the temporal expression pattern of zebrafish *epg5* gene we performed an RT-qPCR analysis on cDNA obtained from different developmental stages ranging from 0 hpf to 6 dpf (days post-fertilization) (Fig. 1, panel A) and a gene-specific primer set designed to span two introns, to reveal any contaminating genomic DNA (EPG5-F/EPG5-R, S-Fig. 1, panel B for primer position). To compare differential gene expression over time, all values were adjusted to the stage with the lowest expression level, corresponding at 8 hpf which was set at an arbitrary unit of 1.

This analysis revealed that *epg5* transcripts were maternally deposited into the oocytes with the highest concentration at 0 and 2 hpf. Thereafter transcripts declined throughout the first 8 hpf, being replaced at a low level by the corresponding embryonic mRNAs until 6 dpf, the last stage examined (Fig. 1, panel A). To analyse the spatio-temporal expression of maternal and zygotic *epg5* mRNAs during zebrafish development, whole-mount *in situ* hybridization (WMISH) was performed on WT ovulated oocytes and embryos from 0.2 hpf to 6 dpf using a digoxigenin-labeled antisense *epg5* mRNA probe of 363 nt covering the 5'-UTR and the N-terminus. In oocytes, maternal *epg5* mRNA was spread throughout the central ooplasm, as shown in Fig. 1, panel B. At the 1-cell stage (0.2 hpf) transcripts were restricted in the blastodisc area, whereas no or very low signal was found at 8 and 12 hpf, in agreement with RT-qPCR results showing a minimum of *epg5* mRNA concentration at these stages. At 1 dpf, the zygotic *epg5* expression was ubiquitously observed, although at low level, and mainly concentrated in the head and in the trunk. At 3 dpf the transcript was localized in the oral cavity and heart region and at 6 dpf mainly in oral cavity and intestine,

vibratome transversal sections of 6-dpf stained larvae confirmed the epg5 expression in the above listed districts (data not shown). In adult *epg5* expression was analysed by RT-PCR and confirmed in the following tissues: gonads, brain, intestine, muscle, heart, liver and caudal fin (Fig. 1, panel C).

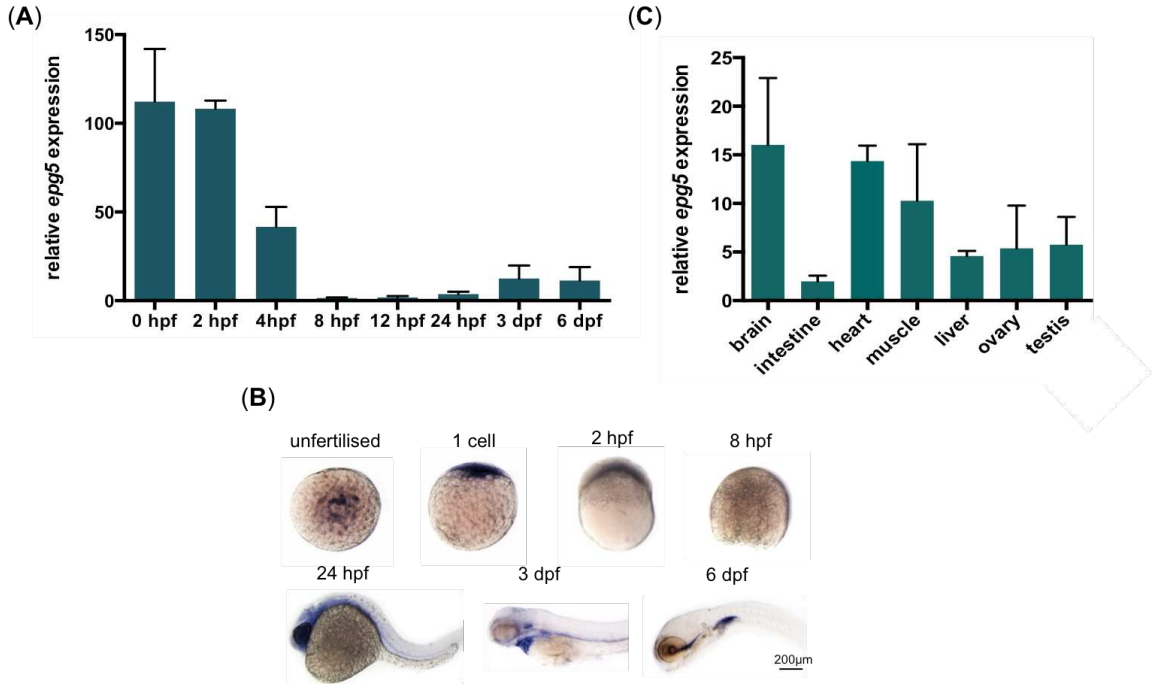


**Fig. 1. *epg5* expression patterns during zebrafish development**. (A) RT-qPCR analysis of zebrafish *epg5* expression. The graph shows the relative *epg5* transcript abundance in whole zebrafish embryos, from 0 to 6 dpf, as determined by RT-qPCR. Error bars indicate ±SEM. Data were generated from three biological replicates, pool of 15 embryos each. (B) Spatio-temporal expression of *epg5* transcripts during zebrafish development as evidenced by WMISH performed at the indicated stages. All embryos are lateral views with the animal pole up (1 cell and 12 hpf) and head pointing to the left (1, 3 and 6 dpf). Bar = 200 µm. (C) Graph showing the relative epg5 transcript abundance in zebrafish adult tissues, as determined by RT-qPCR. Error bars indicate ±SEM. Data were generated from four adult zebrafish (two male and two female).

## Generation and characterization of stable zebrafish *epg5* mutant lines by targeted mutagenesis

To generate a Epg5 loss of function zebrafish model, we mutated the zebrafish *epg5* gene using a CRISPR/Cas9 approach. In order to delete almost all the functional protein, the CRIPSR sequence was designed on the third exon (corresponding to the second coding exon). Two sgRNAs were injected together with the *cas9* mRNA (grey highlighted on S-Fig. 1). Only the second sgRNA resulted in mutagenesis at the expected target site in F0 injected embryos, as confirmed by sequencing of PCR fragments which revealed the presence of targeted mutation beginning in the proximity of the target CRISPR sequence. Two heterozygous F1 carriers with a 20- and a 13-nucleotide deletion were

selected from offspring of F0 outcrosses and used to obtain the F2 generation. Both deletions resulted in frameshift mutations that lead to premature stop codons located 62 and 61 aa after the first methionine, respectively. The putative encoded proteins contained 51 and 49 aa of the zebrafish Epg5 plus 11 and 12 new aa resulting respectively from the 20- and 13-nucleotide deletion. The two lines showed the same effects on autophagy process and thus, after the first analyses that were performed with both mutant lines, we chose to use the line resulting from the 20-nucleotides deletion. The line, named *epg5*$^{ia31/ia31}$ in ZFIN database, will be called *epg5*$^{-/-}$ hereafter (Fig. 2, Panel A).

Due to the unavailability of a zebrafish Epg5-specific antibody we could not experimentally verify the absence of the corresponding protein in our mutants. Thus, we investigated whether the introduced mutation resulted in variation of the transcribed product by means of quantitative RT-PCR (RT-qPCR) of *epg5* of 8-dpf (days post-fertilization) homozygous mutant and WT larvae. This analysis showed a statistically significant reduction of *epg5* transcript levels to less than 35% of those measured in WT fish (Fig. 2, Panel B), a result that is consistent with nonsense-mediated mRNA decay (NMD) due to premature stop codon (Baker and Parker, 2004), and suggests that the mutation might result in the loss of Epg5 functions. Moreover, WMISH analysis of 1- and 2-dpf embryos from homozygous parents showed, as expected from the previous results, a consistent reduction of *epg5* transcripts (Fig. 2, Panel C).

The remaining *epg5* mRNA can be translated due to the occurrence of 57 in frame alternative translation-initiation sites (AUG) downstream of the premature stop codon (XM_005165361.4). However, analysis with the program TIS Miner (http://dnafsminer.bic.nus.edu.sg/Tis.html; Liu and Wong, 2003) and the program ATGpr (http://atgpr.dbcls.jp; Salamov *et al.*, 1998) revealed that only a reduced number present a correct Kozak consensus sequence.

Finally, the mutated region was analysed by RT-PCR and sequencing, confirming the presence of the mutation in the remaining *epg5* transcripts of homozygous mutants (data not shown).

*epg5* mutant homozygous embryos, obtained by heterozygous mating, were phenotypically similar to control siblings and segregated according to a Mendelian ratio, as resulted by genotyping analysis of single embryos. Also, survival rate during development was normal, indicating that Epg5 deficiency did not affect early embryo viability.

Furthermore, offspring from incrossed homozygous *epg5* mutants raised to adulthood were viable and fertile, thus excluding that survival of homozygous fish derived from

heterozygous females was essentially due to the compensative effects of maternal *epg5* transcripts or proteins.

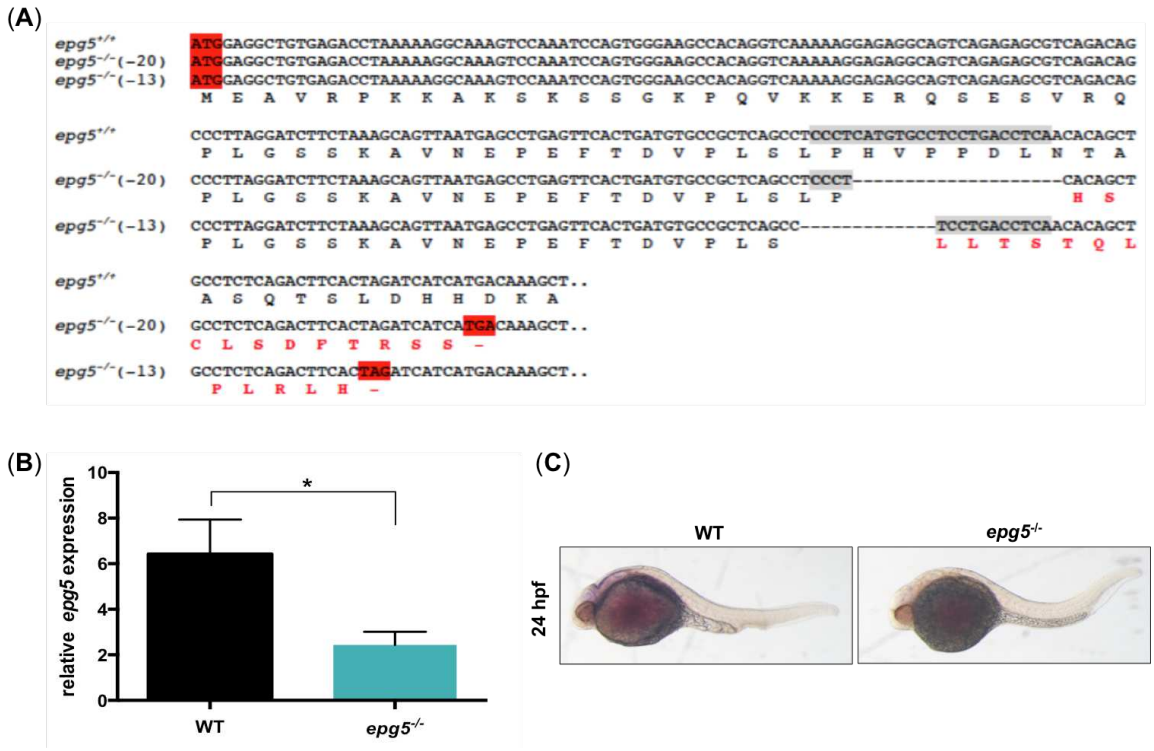


**Fig. 2. Knockout of the zebrafish *epg5* gene**. (A) Nucleotide and amino acid sequences to show the − 13 bp and − 20 bp deletion mutations, revealed by DNA sequencing analysis in the *epg5* CRISPR target site. Each deleted nucleotide is represented by a dash. CRISPR targeted site, highlighted in grey with the protospacer-adjacent motif (PAM) sequence in bold, was designed on second coding exon corresponding to the third of the gene. The *epg5* sequence is represented starting from the start codon to the newly formed stop codons resulting from the introduced frameshifts in the coding region, both highlighted in red. The new amino acids resulted by nucleotide loss are labelled in bold red. (B) qRT-PCR of *epg5* mRNA of 8 dpf mutant larvae compared to control shows a statistically significant reduction of *epg5* expression. Values represent the mean ± SEM. Data were generated from three biological replicates, pool of 15 embryos each. Statistical significance was determined using two tail Student's *t*-test, **P* < 0.05. (C) *epg5* expression analysis in WT and 1-dpf mutant embryos by whole-mount *in situ* hybridization. Embryos are lateral views with head pointing to the left.

### *epg5* knockdown results in impaired autophagosome-lysosome fusion and response to starvation

To test if the predicted loss of the Epg5 protein results in autophagy impairment, we performed a Western blot analysis with proteins extracted from 8- and 11-dpf *epg5*$^{-/-}$ and WT larvae. This analysis revealed, in fed conditions, a slightly and not significant higher level of lipidated Lc3 (Lc3-II) in 8-dpf mutant larvae with respect to WT, the membrane-bound form of this protein localized specifically on the autophagosome membrane. Interestingly, Lc3-II levels were much higher in mutants at 11 dpf and also statistically significant. As the latter is a substrate for autophagic degradation and LC3-II is continuously generated and degraded during the autophagic flux, their accumulation

on zebrafish mutants confirmed the expected block of autophagic degradation pathway leading to accumulation of undegraded autophagic vacuoles (Fig. 4, panel A).
In accordance with western blot results, electron microscopy analysis of *epg5*$^{-/-}$ 11-dpf larvae (Figure 3, panel B) displayed clear muscle alterations consistent with a block of the autophagic flux. An extensive accumulation of cytoplasmic debris, most of them membrane-bound, were detected among myofibrils. Several double membrane-bound structure, often including non-degraded organelles (i.e.. mitochondria, endoplasmic reticulum membrane, glycogen granules), consistent with autophagosomes, were found, while lysosomes were very rare. Some swollen mitochondria were detected, while the sarcoplasmic reticulum and the nuclear structure were apparently unaffected. The accumulation of autophagosomes was detected in non-degenerating myofibers, suggesting an early involvement of the autophagy defect in *epg5*$^{-/-}$ muscle phenotype. Fed 8 dpf *epg5*$^{-/-}$ larvae displayed subsarcolemmal accumulation of membranous structures and some mitochondria with dilation of the outer membrane, while autophagosomes were sporadically detected, confirming the absence of significant differences with aged-matched WT larvae, as detected by western blot. Although to a lesser extent, the accumulation of autophagosomes containing non degraded mitochondria or cytoplasmic material was found also in the muscle of *epg5*$^{-/-}$ adult fish. On the other hand, autophagosomes were never detected in WT 11- dpf larvae and adult fish.

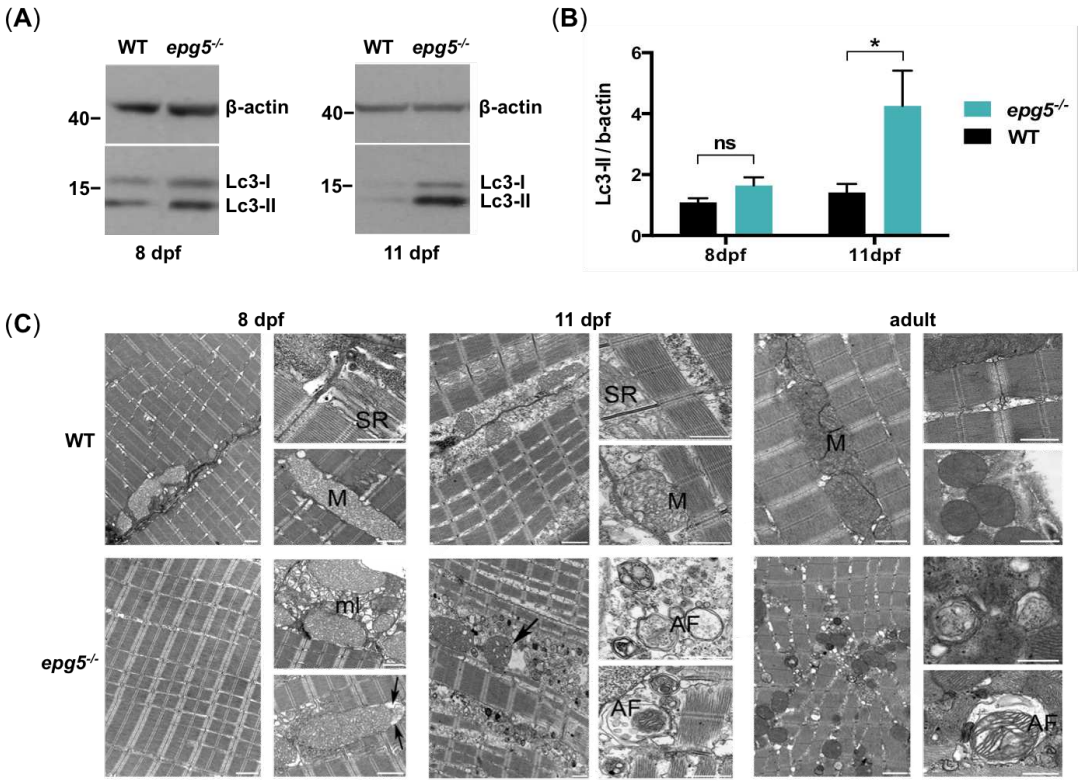


**Fig. 3. Autophagy impairment of zebrafish *epg5* mutants.** (A) Representative Western blot of LC3 of WT and *epg5*$^{-/-}$ larvae at 8- and 11-dpf, and (B) quantitative analysis of band intensities. LC3-II was standardized by ß-actin concentrations. Asterisks indicate that the LC3-II expression was significantly higher in 11-dpf homozygous mutants with respect to WT. Statistical significance was determined by one tail Student's *t*-test, **P* < 0.05; n = 4. (C) Ultrastructural analysis of skeletal muscle of WT and *epg5*$^{-/-}$ larvae and adult. 8- and 11-dpf WT larvae, as well as WT adult (upper panels) display well organized myofibrils with subsarcolemmal mitochondria (M) and a well-developed sarcoplasmic reticulum (SR). 8-dpf *epg5*$^{-/-}$ larvae do not show significant changes of the organization of muscle fibers with respect to WT larvae, except for some subsarcolemmal membrane-like structures (ml), some dilated mitochondria (m). Changes suggestive of altered autophagic flux, as autophagosomes (AF), are evident 11-dpf *epg5*$^{-/-}$ larvae. Although to a lesser extent, autophagosomes are also present in adult *epg5*$^{-/-}$ zebrafish. Ultrastructural analysis was performed with 5-6 larvae for each condition. Scale bar, 1 µm.

Due to the essential role of Epg5 during starvation-induced autophagy, we analysed mutant's response after 3 days of fasting condition. The experiment started at 5 dpf, around the onset of zebrafish exogenous feeding and thus before the yolk has been completely depleted, and ended at 8 dpf. Western blotting analysis of total proteins of 8-dpf larvae showed again, in fed condition, a lower increase in mutant larvae with respect to control. Lc3-II level had further increased after starvation both in control and mutant larvae but this increase was significantly much higher on *epg5*$^{-/-}$ samples (Fig. 4, Panel A).

As skeletal muscle is one of the tissues with the highest rates of autophagy vesicle formation during fasting to ensure cell survival through autophagic degradation of cytoplasm component (Bonaldo and Sandri, 2013), we analysed skeletal muscle

birefringence, an experimental approach that allow to measure *in vivo* reduction in the amount of myofibril or myofibril organization, either due to muscle atrophy or damage.
Although birefringence levels were similar in fed condition, starvation resulted in a marked and significant reduction of skeletal muscle birefringence, indicating muscular fibres decrease, both in control and *epg5*$^{-/-}$ larvae. However, the *epg5*$^{-/-}$ larvae birefringence reduction was much consistent and statistically different from control (Fig. 4, panel B). Moreover, birefringence analysis did not show a patch-like pattern, as expected with dystrophic models that usually display a random detachment of fibres from myosepta, but an overall reduction suggesting a general loss of fibres.
Consistent with a block of the autophagic flux, 3 days starvation induced a clear accumulation of autophagosomes both in *epg5-/-* 8dpf larvae and adult fish. By contrast, aged-matched fasted WT individuals showed mitochondrial alterations, while autophagosomes and cytoplasmic debris were only occasionally detected (Fig. 4 panel C).

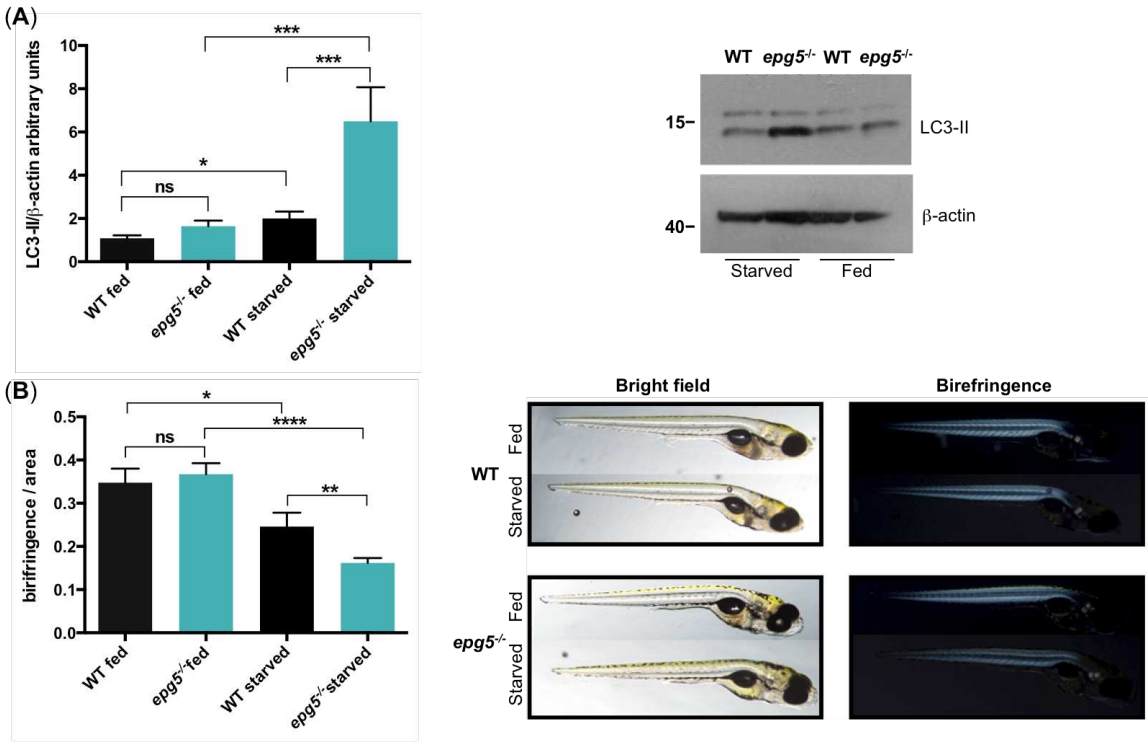

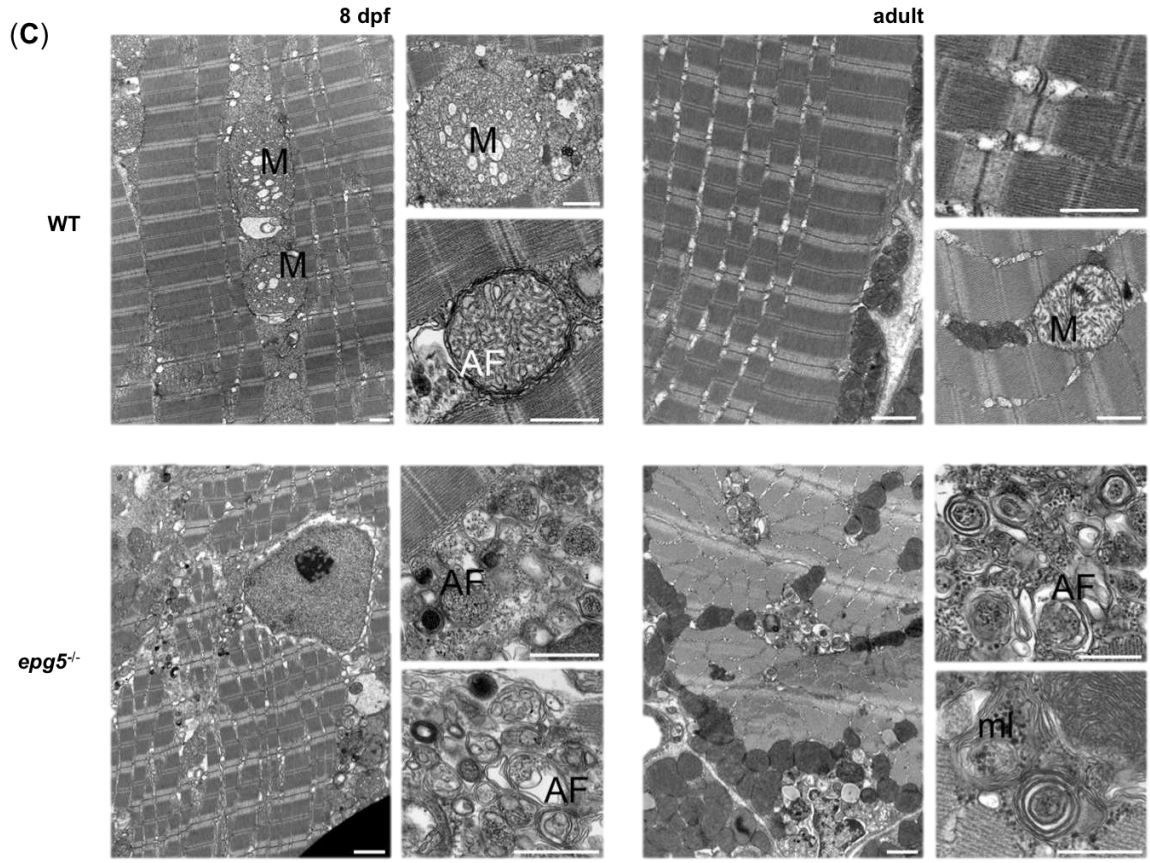


**Fig. 4. Starving response of zebrafish *epg5* mutants.** (A) Representative Western blot of LC3 of 8-dpf WT and *epg5*$^{-/-}$ larvae, in basal (fed) and fasting condition, and quantitative analysis of band intensities after standardization with bactin concentrations. Lc3-II expression was higher in homozygous mutants with respect to WT and, upon starvation, mutant larvae exhibited a higher and statistically significant increase of this autophagy marker. Statistical significance was determined by one tail t-test. Data are presented as mean ± SEM and were generated from three biological replicates with pools of 15 larvae. (B). An overall reduction of muscle birefringence was observed in WT and *epg5*$^{-/-}$ larvae after three days of starvation, consistent with a myopathic phenotype. Bright field images of WT and *epg5*$^{-/-}$ larvae are shown for reference. In *epg5*$^{-/-}$ larvae starvation resulted in a highly significant reduction in birefringence compared to WT controls. Quantification data were calculated by dividing the integrate density of refracted light by the total area of the fish (ImageJ), normalizing the birefringence for the fish dimensions. Data are presented as mean ± SEM. Statistical significance was determined by Student's t-test, *P < 0.05; **P < 0.01; ***P < 0.001. Total samples analysed deriving from three different experiments each with 15 larvae for genotypes and treatment. (C) Eight dpf larvae (left panels) and adult WT and *epg5*$^{-/-}$ mutant (right panels) starved for 3 days were studied by transmission electron microscopy analysis. In agreement with a block of the autophagic flux, *epg5*$^{-/-}$ larvae and adult mutants display an accumulation of autophagosomes (AF) and membrane-like structures (ml). In contrast, 8 dpf larvae and adult WT display enlarged mitochondria (M) and rare autophagosomes (AF). Ultrastructural analysis was performed with 5-6 larvae for each condition. Scale bar, 1µm.

### Knockout of *epg5* seems to affect the development of goblet cells in the intestine

Due to the high expression of *epg5* transcripts on intestine of zebrafish larvae, as established by WMISH, and to the increased Lc3-II level on 11-dpf mutant larvae that suggest an activation of the autophagy process likely due to starvation, we used Alcian

blue staining to analyse mucins secreted by goblet cells in the mid-intestinal region, where these cells are restricted during larval stages (Wallace et al., 2005). A substantial and statistically significant decrease in alcian blue-stained goblet cell area was detected in *epg5*$^{-/-}$ compared to WT 6-dpf larvae (Fig. 5, Panel A). Moreover, as dimension of these cells is linked to their maturation (Chen et al., 2012) we counted both mature cells (area equal or larger than 19.6 µm$^2$, diameter 5 µm) and immature cells (area lower than 19.6 µm$^2$) and found a significant lower total number of goblet cells in 6 dpf *epg5*$^{-/-}$. The difference is clearly due to a significant reduced mature Goblet cell number in mutant larvae intestine (Fig. 5, panel B). Moreover, an increased occurrence of cell death was detected on intestine of 6-dpf mutant larvae, as assayed by acridine orange staining (Fig. 5, panel C).

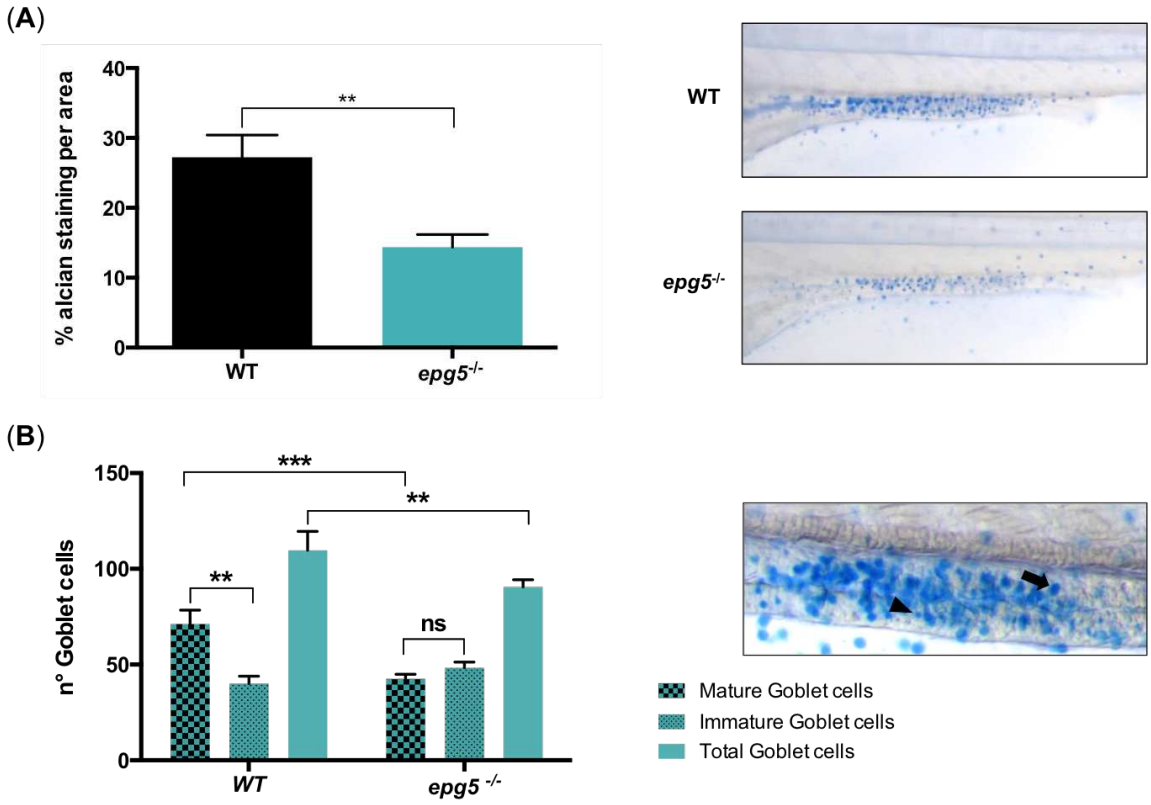

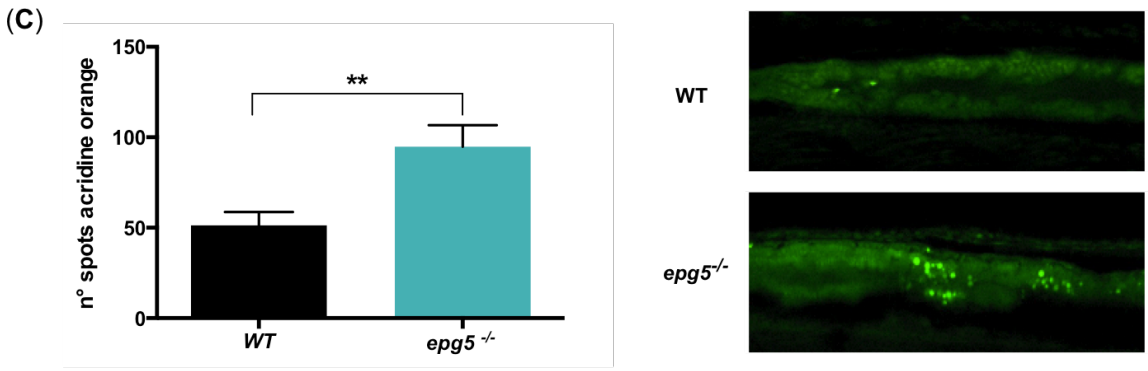


**Fig. 5.** (A). Whole mount alcian blue staining was performed with WT and mutant 6-dpf zebrafish larvae to detect mucin-containing goblet cells. The graph reports quantification of average mucin area/goblet cell in WT (n = 16) and *epg5*$^{-/-}$ (n = 11) larvae, ± SEM. Statistical significance was determined by Student's t-test. On the right two representative images of WT and mutant alcian blue stained larvae.
(B) Quantification of the number of total, mature (arrow) and immature (arrowhead) goblet cells in 6-dpf zebrafish larvae (WT, n = 7; *epg5*$^{-/-}$, n = 11), mean ± SEM. Statistical significance was determined by Student's t-test. On the right representative images of a WT stained larvae to identify mature and immature goblet cells.
(C) Analysis of cell death by means of acridine orang staining (WT, n = 10; *epg5*$^{-/-}$ n = 10), mean ± SEM. Statistical significance was determined by Student's t-test, *P < 0.05; **P < 0.01; ***P < 0.001. On the right two representative images of WT and mutant acridine orange stained larvae.

As the delay of maturation of goblet intestinal cells and the starvation phenotype of 11-dpf mutant larvae suggested a possible impairment of intestinal adsorptive capabilities, we analysed body length as a measure of larvae growth rate. Compared to WT, mutant larvae from incrossed homozygous displayed a slight but significant lower growth rate between 6 to 19 dpf (Fig. 6, Panel A). By 20 dpf, the delay in body lengthening was recovered and length variations were no longer statistically significant.
In order to exclude that length differences could be due to different genotypes or to the lack of *epg5* maternal transcripts, the same analysis was performed at 15 dpf with sibling clutches derived from heterozygous female per homozygous male parents. Also in this case the length difference was statistically significant (Fig. 6, Panel B).

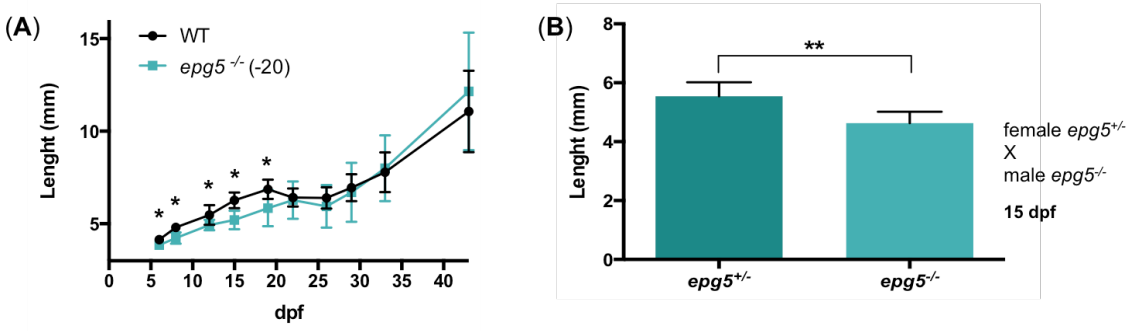

**Fig. 6.** (A) Growth curve of WT and *epg5*$^{-/-}$ larvae deriving from homozygous parents (6 to 44 dpf), mean ± SD. Asterisks indicate that the body length of *epg5*$^{-/-}$ larvae is slight but significantly lower than WT from 6 to 19 dpf. Statistical significance was determined by multiple t-test comparing each age group to the corresponding WT control using the Holm-Sidak method. Each age group was analysed individually without assuming a consistent SD; *P < 0.05, (n = 16 for each point), data presented as mean ± SD. (B) Body length of siblings at 15 dpf from outcross between a heterozygous female and a homozygous male. Statistical significance was determined by Student's t-test, **P < 0.01; *epg5*$^{-/-}$, n = 8; *epg5*$^{+/-}$, n = 7. Data presented as mean ± SEM.

**Loss of zebrafish *epg5* does not results in motor neuron developmental defects**

Motor neuron development has been analysed by comparing heterozygous and homozygous *epg5* mutants in Tg(mnx1:GFP) (formerly hb9:GFP) (Flanagan-Steet *et al.*, 2005) transgenic background, in which spinal motor neurons and their processes are labelled with GFP. At 25 and 52 hpf motor neuron development was the same in both genotypes in term of number and axon arborisation (S-Fig. 2), thus excluding a developmental problem linked to *epg5* silencing.

**epg5 knockdown impairs zebrafish caudal fin regeneration**

Analysis of 3-mpf (month post fertilization)-old zebrafish 5 days after amputation (dpa) showed a reduced caudal fin regeneration (S-Fig. 3) in *epg5*$^{-/-}$ compared to WT.

**Morphological analysis of *epg5*$^{-/-}$ mutants**

Comparative morphological analysis was performed with 7 WT and 8 *epg5*$^{-/-}$ adult zebrafish of both sexes and age ranging from 4 to 13 mpf and revealed defects on gonads and heart. Moreover, inflammation areas were detected on more than one sample as well as development of a chordoma tumor in a 10-mpf old female mutant. No clear alterations were visible on intestinal tissue except that, in some cases, the intestinal mucosa presented a sloughing epithelium at the folds tips (S-Fig. 4).

All WT adult female analysed presented asynchronous ovaries, which contain follicles of all stages of development ranging from primary to full growth stage. Similar results were also obtained with two *epg5*$^{-/-}$ female (4 and 8 mpf). However, histological analysis of two *epg5*$^{-/-}$ female (9 and 10 mpf) showed an impaired oocyte maturation with clear reduced ovarian size and presence of only primary and pre-vitellogenic follicles, suggesting a block of follicle maturation. Ovary morphology resembles that of a female immature zebrafish (Fig. 7, panel A and S-Fig. 5). All adult testes of WT were organized into tubules that contain sperm and all stages of spermatogenesis. Instead testes of *epg5* mutants presented morphological modification including tissues disorganization and empty tubules (asterisks) (Fig. 7, panel B and S-Fig. 6), drastically reduced dimension and increased fibrous connective tissue within the testicular stroma (S-Fig. 6, 11-mpf

mutant). These results are in agreement with the reduced egg production of *epg5*$^{-/-}$ female and the reproductive capabilities of both sexes showed by these mutants starting from around 8/10 months of age.

Moreover, according with Vici syndrome, *epg5*$^{-/-}$ adults present a dilated heart and reduction of the compact myocardium as well as of the trabecular network (Fig. 7, panel C and S-Fig. 7). Moreover, in one *epg5*$^{-/-}$ heart, clumps of red cell were seen between ventricular trabeculae (Fig. 7, panel C).

Additionally, a 10-mpf-old *epg5*$^{-/-}$ female developed a chordoma, an uncommon malignant tumor arising from notochord remnants usually occurring in the axial skeleton (Burger *et al.*, 2014; Cooper *et al.*, 2015). In our sample, as in those reported by Cooper and co-workers (2015) the neoplasia was found in the alimentary tract and not in the axial skeleton. Morphology of the tumor was in agreement with Cooper tumor description with masses/nodules containing cells similar to those of the notochord scattered throughout the intestine and separated each other by fibrous bands (Fig. 7, panel D and S-Fig. 8).

Finally, areas with infiltration of inflammatory cells were found in different samples of *epg5*$^{-/-}$ adults, such as fragments of exocrine pancreatic tissues of 11-mpf *epg5*$^{-/-}$ male (Fig. 7, panel E and S-Fig. 9), near the testis of 4-mpf *epg5*$^{-/-}$ male (Fig. 7, panel E) or above of the chordoma cist (Fig. 7, panel D and S-Fig. 8). In 11-mpf *epg5*$^{-/-}$ male, the pancreatic tissue was seemingly reduced and altered on its morphology (S-Fig. 9).

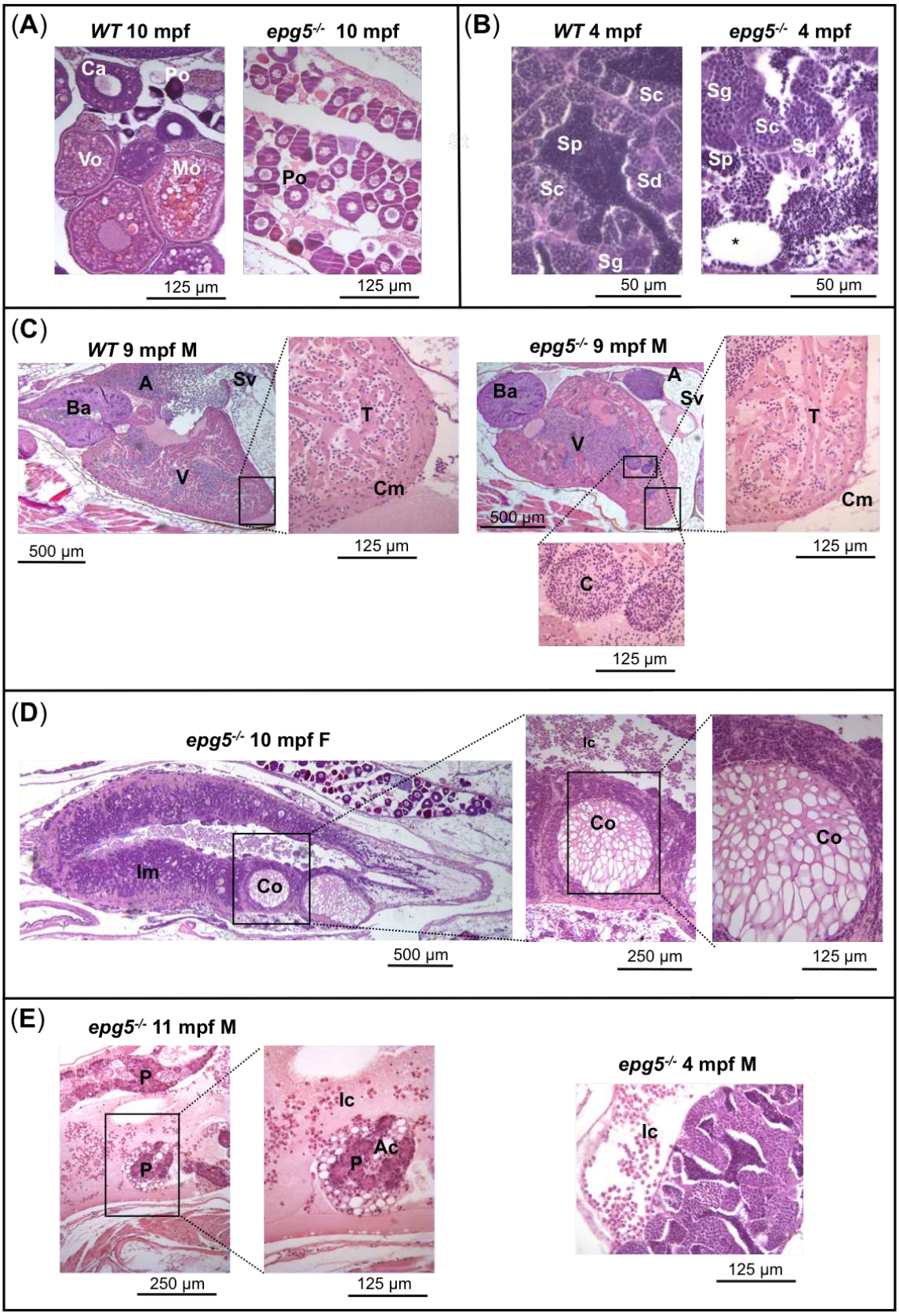


**Fig. 7.** (A) Effects of Epg5 deficiency on ovarian morphology in a female zebrafish mutant (10 mpf) in comparison with a control fish at the same age. Mutant ovary contains only immature stage I oocytes of

the perinucleolar stage (PO) whereas WT ovary contains oocytes at different developmental stages; PO, CA, cortical alveolus stage oocyte; VO, vitellogenic stage oocyte; MO, mature oocytes.
(B) Effects of Epg5 deficiency on testicular morphology in a male zebrafish mutant (4 mpf) in comparison with a control fish at the same age. Spermatozoa (Sp) and all stages of spermatogenesis, spermatogonia (Sg), spermatocytes (Sc), spermatids (Sd), were present on WT testis whereas the structure were disorganised on the mutant sample that also contained empty tubules (*).
(C) Effects of Epg5 deficiency on heart morphology in a male zebrafish mutant (9 mpf) in comparison with the heart of a control fish at the same age. The boxed regions are enlarged beneath to compare compact myocardium between the two genotypes. Sv, sinus venosus, A, atrium, Ba, bulbus arteriosus, V, ventricle, Cm, compact myocardium; C, clumps of red cells.
(D) Presence of intestinal chordoma in a female zebrafish mutant (10 mpf). Multiple tumor cists were present in the intestinal wall which mucosa appeared altered and also substituted by fibrotic tissue. Im = intestinal mucosa; Co = intestinal chordoma.
(E) Presence of inflammatory infiltrating cells (Ic) around small fragments of exocrine pancreatic tissue in a male mutant zebrafish (11 mpf) and in proximity of the testis of 4 mpf mutant. P, pancreas, Ac, adipous cells.

**Analysis of the reduced autophagosome-lysosome fusion by means of zebrafish transgenic lines**

To analyse the autophagy flux in *epg5*$^{-/-}$, mutant lines were generated in *lc3* (labelling autophagosome), *rab7* (labelling late endosome and lysosome), *rab5* (labelling early endosome) and *lamp1* (labelling mature lysosome) transgenic backgrounds.

Each transgenic mutant line has been analysed alone or after the preparation of double transgenic mutant lines in order to study co-localization of fluorescence signals. Fluorescence analysis was performed using sibling larvae and followed by genotyping.

In agreement with western blotting and electron microscopy results, analysis of Lc3 puncta at 6 dpf showed a weak increase and thus the experiment was repeated at later stages to obtain a statistically significant difference. However, Lamp1 and Rab7 (Fig. 8, panel A) fluorescence signals were severely accumulated in *epg5*$^{-/-}$ mutant muscle of 6-dpf larvae confirming that silencing of Epg5 resulted on block of the autophagosomes fusion with lysosomes. Instead, Rab5 fluorescence signal was not different between genotypes suggesting that maturation of early endosome to late endosome was not compromised by Epg5 loss (Fig. 8, panel A).

Mutant larvae showed a non-significant increased ratio of co-localization of Lc3 with Rab7 (data not shown). In contrast, we found that the fusion of Lc3-positive puncta with early endosome, as indicated by the co-localization of LC3 with early endosome-associated membrane proteins (Rab5), was increased in *epg5* mutants (Fig. 8, panel B) in agreement with the results obtained by Wang and co-workers with *C. elegans* epg5 mutant (2016).

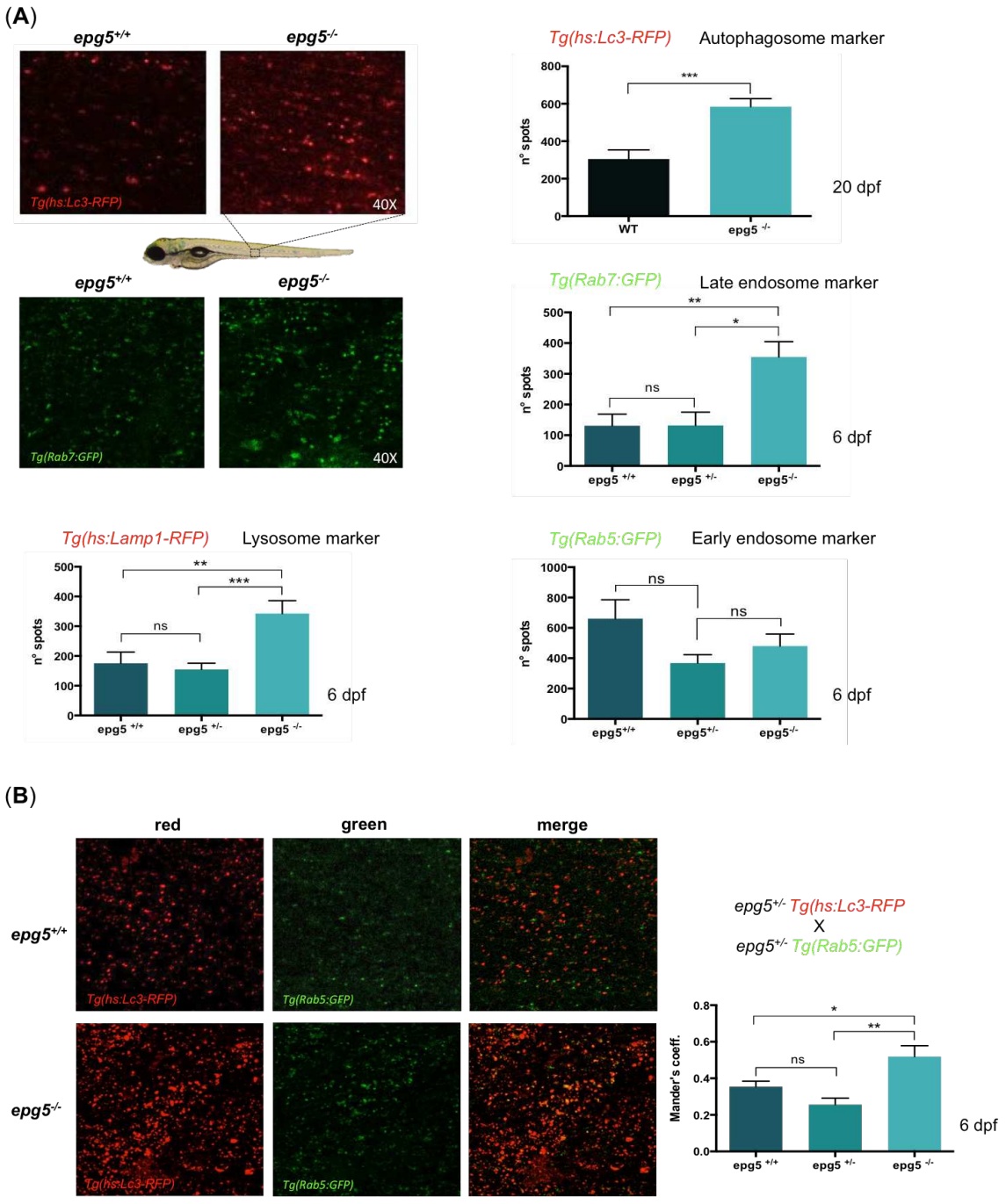


**Fig. 8.** (A) Representative images and fluorescence spot quantification Rab7, Rab5 and Lamp1 of 6-dpf siblings deriving from epg5 heterozygous mutants in the respective transgenic background. Analysis of Lc3-II spots was performed comparing WT and epg5 homozygous mutants in transgenic background at 20 dpf. Data are represented as mean ± SEM (n = 30 for each transgenic line analysed). (B) Quantification of the colocalization between Rab5 spots (green) and Lc3 spots (red) Lamp1 of 6-dpf siblings (n=22) deriving from epg5 heterozygous mutants in Rab5/Lc3 double transgenic background using Mander's coefficient. Statistical significance was determined by Student's t-test, *P < 0.05; **P < 0.01; ***P < 0.001.

**DISCUSSION**

In this work, we generated two viable and fertile zebrafish lines bearing a homozygous mutation in the *epg5* gene to knockout the cellular activity of the encoded protein. This was achieved by CRISPR/Cas9 deletion of a 13 and 20-nucleotide segment in exon 3 (second coding exon) of the *epg5* gene. Both deletions resulted in a frame-shift leading to premature stop codons that blocked translation after about 60 aa. The mutant line characterization was performed using the -20 nt line, signed *epg5*$^{ia31/ia31}$ and called *epg5*$^{-/-}$ hereafter.

As measured by qRT-PCR analysis with primers designed after the CRISPR target region, the overall *epg5* transcript level was reduced by 65% in *epg5*$^{-/-}$ mutants compared to WT, due to the nonsense-mediated mRNA decay (NMD) machinery, a surveillance pathway that prevents truncated protein formation (Baker and Parker, 2004). Due to the non-complete efficiency of the NMD machinery and the presence of several in frame alternative downstream start codons, we cannot exclude potential alternative translation initiation events using the un-degraded *epg5* mRNAs, leading to truncated protein products with at least partially retained functions. The lack of a zebrafish specific C-terminal Epg5 antibody prevented us to analyse the consistency of the protein eventually translated. However, the full penetrance of dysfunctional autophagy in zebrafish *epg5*$^{-/-}$ larvae, as confirmed by western blotting analysis of the autophagy marker Lc3-II, suggests that alternative starting codons downstream of the mutation could be not highly efficient. Thus, we may assume that in our mutant line Epg5 silencing was functionally obtained.

Impairment of the fusion of autophagosomes with lysosomes, the cellular function in which Epg5 is involved as an effector of Rab7 (Wang *et al.*, 2016), was confirmed in zebrafish *epg5*$^{-/-}$ mutant lines by several different approaches including, beside Western blotting analysis, electron microscopy of muscle tissues at different ages and condition, analysis of starvation-induced effects on autophagy flux and muscle birefringence, tail fin regeneration and evaluation of fluorescence of mutant larvae in autophagy and vesicle trafficking reporter transgenic backgrounds.

The *epg5*$^{-/-}$ mutant line was viable and fertile but analysis of reproductive behaviour revealed a premature reduction of reproductive capabilities or a complete infertility starting from 8-10 months, when zebrafish reproductive capabilities are normally at the highest level. This result was confirmed by histological analysis of the gonads, which presented, in both sexes, alteration of the architecture, reduction of the organ dimension or, in female, an apparent block of the oocytes maturation process. The Epg5

involvement on spermatogenesis was before suggested by the work of Herpin and co-workers (2015) who found this protein as essential for clearance of germplasm and mitochondria during germ cell specification and to preserve adult testis morphology in the medaka model organism. KO of Epg5 caused the loss of medaka reproductive capacity although no pathological features were reported regarding female gonads. A significant contribution of autophagy on reproduction was reported also in mouse. Germ cell-specific mouse Atg7 KO resulted in male and female fertility problems as this autophagy gene was found to be required for acrosome biogenesis during spermatogenesis and to protect from oocytes over-loss (Song *et al.*, 2015; Wang *et al.*, 2014). Although the molecular mechanism underlying the reproductive impairment in zebrafish *epg5*$^{-/-}$ needs to be further characterized, these results emphasize the critical role of autophagy on gametogenesis and reproduction.

The histological analysis displayed also pathological features link to cardiomyopathy, detection of areas with invasion of inflammatory cells and, in one case, development of a tumour. These multisystem effects can be explained by the Epg5 wide expression in zebrafish during development and adult life, as shown by WMISH and RT-PCR analysis of adult tissues. Moreover, the results are in agreement with the features of Vici syndrome (Cullup *et al.*, 2013) and confirm the involvement of the autophagy pathway in the development and functioning of multiple organ systems.

Whereas dysfunctional autophagy was confirmed in all experiments performed, structural and degenerative changes due to the Epg5 silencing in adult zebrafish mutants presented both common (cardiomyopathy, that is also an important characteristic of Vici syndrome) as well as uncommon features and thus penetrance of the mutant phenotype differs between the individuals analysed. In humans, the *EPG5* gene contains 44 exons encoding a protein of 2579 amino acids. Mutations linked to the Vici syndrome so far identified, are widely distributed along the entire gene and the great majority of mutations lead to formation of a premature stop codon and eventually to the production of a truncated proteins of different size (Ebrahimi-Fakhari *et al.*, 2015, Byrne *et al.*, 2016). Severity of the pathological features differ between patients and was suggested to be determined by the residual amount of functional EPG5 protein (Kane *et al.*, 2016, Byrne *et al.*, 2016). In zebrafish mutants, a variability in the residual Epg5 function due to the potential use of downstream start codons could explain the difference in phenotype severity as well as onset of some pathological features during adult life.

Growth impairment, a common feature to both Vici patients (Byrne *et al.*, 2016) and Epg5 knockout mice (Zhao *et al.*, 2013a), was observed also in zebrafish mutants. In this

model, the reduction in body length was limited to the larval stage, just after the beginning of the autonomous feeding, a process that partially overlaps with completion of yolk depletion. Due to initial difficulty with prey capture, zebrafish larvae undergo a critical period, that last 7-10 days starting from first feeding (Chinaa and Holzmana, 2014). During this period, *epg5* mutant larvae showed a significant reduction in total goblet cell number and in their maturity, thus reflecting a possible delay in intestine development and functionality. This could result in a lower nutrient assimilation, leading to reduced growth. Moreover, the lower mucus quantity could determine susceptibility to intestinal inflammation which explain the higher apoptotic cell number in mutant's intestine. In fact, these high-molecular-weight glycoproteins exert a protective and homeostatic role on intestinal mucosa, as underlined by the phenotypes of mice deficient in Agr2, a protein essential for synthesis and maturation of the intestinal mucin2, and muc2 KO mice (Park *et al.*, 2009; Van der Sluis *et al.*, 2006). Moreover, it is known that autophagy is deeply involved on intestinal epithelium homeostasis, as demonstrated by chronic intestinal inflammation as a consequence of dysfunctional autophagy mechanism (Randall-Demllo *et al.*, 2013).

The delay in the assimilation competence can also explain the difference in autophagosomes detected in fed condition in muscle tissue of 8- and 11-dpf and confirmed by the Western blotting analyses: at 8-dpf the mutant larvae can still derive energy from the remaining yolk whereas at 11 dpf the likely reduced energy from the intestinal absorption need to be integrated by activation of the autophagy process thus resulting in the increased number of autophagosomes.

Other features of the Vici syndrome such as pulmonary abnormalities associated to recurrent infections, were found also in mice bearing Epg5 as well as Atg14, Fip200, Atg5 and Atg7 deletion. The elevated inflammatory response seems to protect from lethal influenza A virus (IAV) challenge (Lu *et al.*, 2016).

Interestingly, the histological examination of our adult mutant zebrafish revealed areas with infiltration of inflammatory cells, suggesting that, also in zebrafish, *epg5* KO could interfere with the immune system.

In humans, *EPG5* was initially named KIAA1632 and was identified among a group of genes found to be mutated in breast cancer tissues (Sjöblom *et al.*, 2006; Halama *et al.*, 2007), a finding shared with other genes implicated in the autophagy machinery (Levine and Kroemer, 2008). Although the identification in one out of eight adult mutants analysed, of a chordoma tumor is too limited to draw clear correlation with cancer, this result is interesting. This tumour, normally associated to aged adult zebrafish, showed instead an early onset in this mutant. Noteworthy is also the finding that rapamycin, an

inducer of autophagy, can delay chordoma formation in a zebrafish model for chordoma and improves survival of tumour-bearing fish (Burger *et al.,* 2014).
In conclusion, this zebrafish model could represent a new tool for studying Epg5 functions and its involvement on Vici syndrome. Moreover, this mutant line can allow selection of drugs acting as autophagy stimulators without the need to block the autophagy flux as this it is naturally interrupted.

**ACKNOWLEDGMENTS**

The authors wish to acknowledge Prof. Michel Bagnat (Department of Cell Biology, Duke University Medical Center, Durham, NC) for providing hsp:Lc3-RFP and hsp:Lamp1-RFP plasmid, Prof. Marino Zerial (Max Planck Institute of Molecular Cell Biology and Genetics, Dresden, Germany) for providing Tg(h2afx:EGFP-Rab5c)$^{mw5}$ and Tg(h2afx:EGFP-Rab7)$^{mw7}$. Moreover, authours wish to aknowledge L. Pivotti and Dr. M. Milanetto for their valuable assistance in the fish facility.

**REFERENCES**

**Baker K. E. and Parker R. 2004.** Nonsense-mediated mRNA decay: terminating erroneous gene expression. *Curr Opin Cell Biol* 16, 293-299.

**Bonaldo P. and Sandri M. 2013.** Cellular and molecular mechanisms of muscle atrophy. Dis Model Mech Jan;6(1):25-39.

**Burger A., Vasilyev A., Tomar R., Selig M.K., Nielsen G.P. 2014.** A zebrafish model of chordoma initiated by notochord-driven expression of HRASV12. Dis Model Mech Jul;7(7):907-13.

**Byrne S., Dionisi-Vici C., Smith L., Gautel M., Jungbluth H. 2016.** Vici syndrome: a review. Orphanet J Rare Dis. Feb 29; 11:21.

**Chen Y. C., Lu Y.F., Li I.C., Hwang S.P. 2012.** Zebrafish Agr2 is required for terminal differentiation of intestinal goblet cells. PLoS One.;7(4): e34408.

**China V., Holzman R. 2014.** Hydrodynamic starvation in first-feeding larval fishes. Proc Natl Acad Sci U S A. Jun 3;111(22):8083-8.

**Clark S. B., Winter M., Cohen A.R., Link B.A. 2011.** Generation of Rab-based transgenic lines for in vivo studies of endosome biology in zebrafish. Dev Dyn. Nov; 240(11): 2452–2465.

**Cooper T.K., Murray K.N., Spagnoli S., Spitsbergen J.M. 2015.** Primary intestinal and vertebral chordomas in laboratory zebrafish (Danio rerio). Vet Pathol. 2015 Mar;52(2):388-92.

**Cullup T., Kho A. L., Dionisi-Vici C., Brandmeier B., Smith F., *et al.,* 2013.** Recessive mutations in EPG5 cause Vici syndrome, a multisystem disorder with defective autophagy. Nat. Genet. 45, 83-87.

**Ebrahimi-Fakhari D., Saffari A., Wahlster L., Lu J., Byrne S., *et al.*, 2016.** Congenital disorders of autophagy: an emerging novel class of inborn errors of neuro-metabolism. Brain. Feb;139(Pt 2):317-37.

**Ehmke N., Parvaneh N., Krawitz P., Ashrafi M.R., Karimi P., *et al.*, 2014.** First description of a patient with Vici syndrome due to a mutation affecting the penultimate exon of EPG5 and review of the literature. Am J Med Genet A. Dec;164A (12):3170-5.

**Ellis K., Bagwell J., Bagnat M. 2013.** Notochord vacuoles are lysosome-related organelles that function in axis and spine morphogenesis. J Cell Biol. 2013 Mar 4; 200(5): 667–679.

**Flanagan-Steet H., Fox M. A., Meyer D., Sanes J. R. 2005.** Neuromuscular synapses can form in vivo by incorporation of initially aneural postsynaptic specializations.

Development 132, 4471–4481.

**Flicek P., Amode M.R., Barrell D., Beal K., Billis K., *et al.,* 2014.** Nucleic Acids Res. Ensembl :D749-55.

**Gagnon J.A., Valen E., Thyme S.B., Huang P., Akhmetova L. *et al*., 2014.** Efficient mutagenesis by Cas9 protein-mediated oligonucleotide insertion and large-scale assessment of single-guide RNAs. PLoS One, 9, e98186.

**Halama N., Grauling-Halama S.A., Beder A., Jäger D. 2007.** Comparative integromics on the breast cancer-associated gene KIAA1632: clues to a cancer antigen domain. Int J Oncol. 2007 Jul;31(1):205-10.

**Herpin A., Englberger E., Zehner, M., Wacker R., Gessler M., *et al.*, 2015.** Defective autophagy through epg5 mutation results in failure to reduce germ plasm and mitochondria. FASEB J. 29, 4145–4161.

**Hori I., Otomo T., Nakashima M., Miya F., Negishi Y., *et al.,* 2017.** Defects in autophagosome-lysosome fusion underlie Vici syndrome, a neurodevelopmental disorder with multisystem involvement. Sci Rep. Jun 14;7(1):3552.

**Kane M.S., Vilboux T., Wolfe L.A., Lee P.R., Wang Y. 2016.** Aberrant splicing induced by the most common EPG5 mutation in an individual with Vici syndrome. Brain. Sep;139(Pt 9):e52.

**Kimmel C.B., Ballard W.W., Kimmel S.R., Ullmann B., Schilling T.F. 1995.** Stages of embryonic development of the zebrafish. Dev Dyn 203: 253-310.

**Levine B. and Kroemer G. 2008.** Autophagy in the pathogenesis of disease. Cell 132, 27–42.

**Liu H., Wong L. 2008.** Data mining tools for biological sequences. J Bioinform Comput Biol. Apr;1(1):139-67.

**Lu Q., Yokoyama C.C., Williams J.W., Baldridge M.T., Jin X. *et al*. 2016**. Homeostatic Control of Innate Lung Inflammation by Vici Syndrome Gene Epg5 and Additional Autophagy Genes Promotes Influenza Pathogenesis. Cell Host Microbe. 2016 Jan 13;19(1):102-13.

**Meeker N. D., Hutchinson S. A., Ho, L. and Trede N. S. 2007.** Method for isolation of PCR-ready genomic DNA from zebrafish tissues. *Biotechniques* 43, 610, 612, 614.

**Miao G., Zhao Y.G., Zhao H., Ji C., Sun H., *et al.*, 2016.** Mice deficient in the Vici syndrome gene Epg5 exhibit features of retinitis pigmentosa. Autophagy. 2016 Dec;12(12):2263-2270. Epub Oct 7.

**Park S.W., Zhen G., Verhaeghe C., Nakagami Y., Nguyenvu L.T., 2009.** The protein disulfide isomerase AGR2 is essential for production of intestinal mucus. Proc Natl Acad Sci U S A. Apr 28;106(17):6950-5.

**Randall-Demllo S., Chieppa M., Eri R. 2013.** Intestinal epithelium and autophagy: partners in gut homeostasis. Front Immunol. Sep 30;4:301.

**Salamov A.A., Nishikawa T., Swindells M.B. 1998.** Assessing protein coding region integrity in cDNA sequencing projects. Bioinformatics. Jun;14(5):384-90.

**Sjoblom, T., Jones, S., Wood, L.D., Parsons, D.W., Lin, J. *et al.,* 2006.** The consensus coding sequences of human breast and colorectal cancers. Science 314, 268–274.

**Song Z.H., Yu H.Y., Wang P., Mao G.K., Liu W.X., *et al.*, 2015.** Germ cell-specific Atg7 knockout results in primary ovarian insufficiency in female mice. Cell Death Dis. 2015 Jan 15;6:e1589.

**Thisse C., Thisse B. 2008.** High-resolution in situ hybridization to whole-mount zebrafish embryos. Nat Protoc 3: 59-69.

**Tian Y., Li Z., Hu W., Ren H., Tian E. *et al.* 2010.** E. elegans screen identifies autophagy genes specific to multicellular organisms. Cell Jun 11;141(6):1042-55.

**Van der Sluis M., De Koning B.A., De Bruijn A.C., Velcich A., Meijerink J.P. 2006.** Muc2-deficient mice spontaneously develop colitis, indicating that MUC2 is critical for colonic protection. Gastroenterology. Jul;131(1):117-29.

**Wallace K.N., Akhter S., Smith E.M., Lorent K., Pack M. 2005.** Intestinal growth and differentiation in zebrafish. Mech Dev. Feb;122(2):157-73.

**Wang H., Wan H., Li X., Liu W., Chen Q., *et al.,* 2014.** Atg7 is required for acrosome biogenesis during spermatogenesis in mice. Cell Res. Jul; 24(7):852-69.

**Wang Z., Miao G., Xue X., Guo X., Yuan C. *et al*. 2016.** The Vici Syndrome Protein EPG5 Is a Rab7 Effector that Determines the Fusion Specificity of Autophagosomes with Late Endosomes/Lysosomes. Mol Cell. 2016 Sep 1;63(5):781-95

**Westerfield M. 1995.** The Zebrafish Book. A Guide for the Laboratory Use of Zebrafish (Danio rerio), 3rd Edition. Eugene, OR, University of Oregon Press.

**Zhao H., Zhao Y.G., Wang X., Xu L., Miao L., *et al.*, 2013.** Mice deficient in Epg5 exhibit selective neuronal vulnerability to degeneration. J Cell Biol. Mar 18;200(6):731-41.a

**Zhao Y.G., Zhao H., Sun H., Zhang H. 2013b.** Role of Epg5 in selective neurodegeneration and Vici syndrome. Autophagy. Aug;9(8):1258-62.

## SUPPLEMENTARY MATERIAL

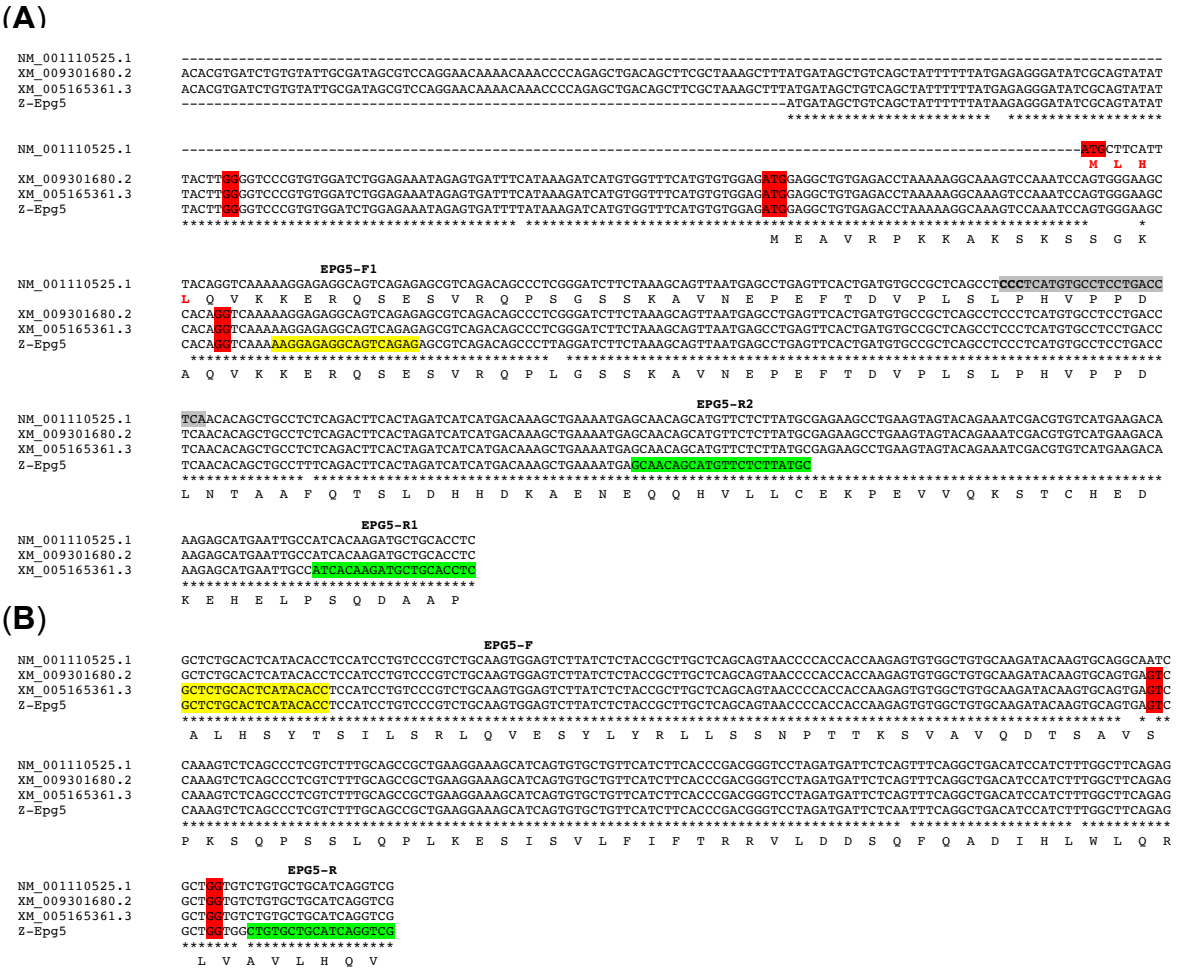


**S-Fig. 1.** (A) Alignment between three Epg5 NCBI reference sequences and the experimentally determined one by means of 5'-RACE analysis and sequencing. Sense primers are labelled in yellow whereas antisense in green. The CRISPR/Cas9 target sequence is in grey with the protospacer-adjacent motif (PAM) sequence in bold. The ATG start codon as well as the intron/exon junctions are in red. (B) Alignment of the cDNA fragment used for qPCR analysis. The gene-specific primer set was designed to span two introns.

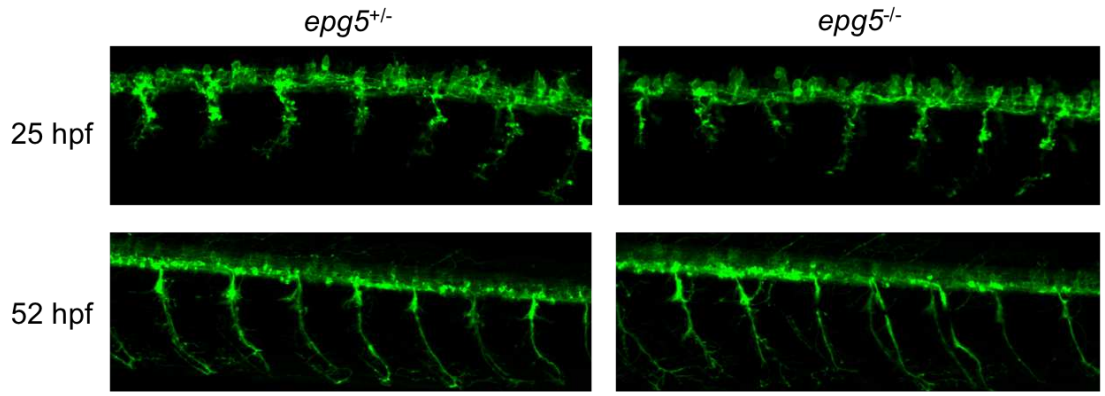


**S-Fig. 2.** Representative confocal micrographs of motor neuron axons exiting the spinal cord in control *epg5*$^{+/-}$ (left) and *epg5*$^{-/-}$ mutant (right) Tg(hb9:GFP) zebrafish embryos at 25 and 52 hpf.

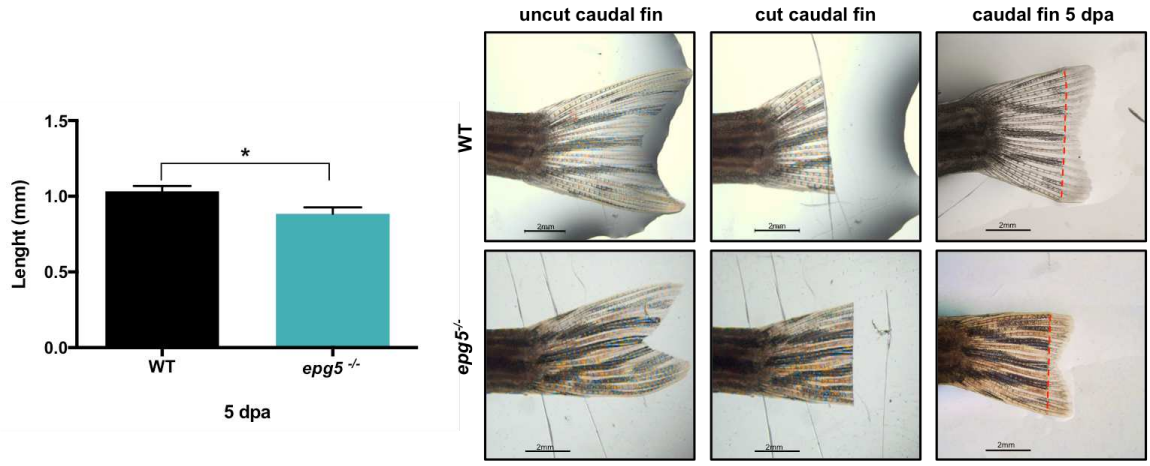


**S-Fig. 3.** Caudal fin regeneration is impaired *epg5*$^{-/-}$ mutants. (A) Caudal fin regeneration was reduced 5 dpa (days post amputation) in *epg5*$^{-/-}$ mutants, compared with WT 3-mpf zebrafish. Statistical significance was determined by Student's t-test, with WT, n = 20; *epg5*$^{-/-}$, n = 20, data presented as mean ± SEM.

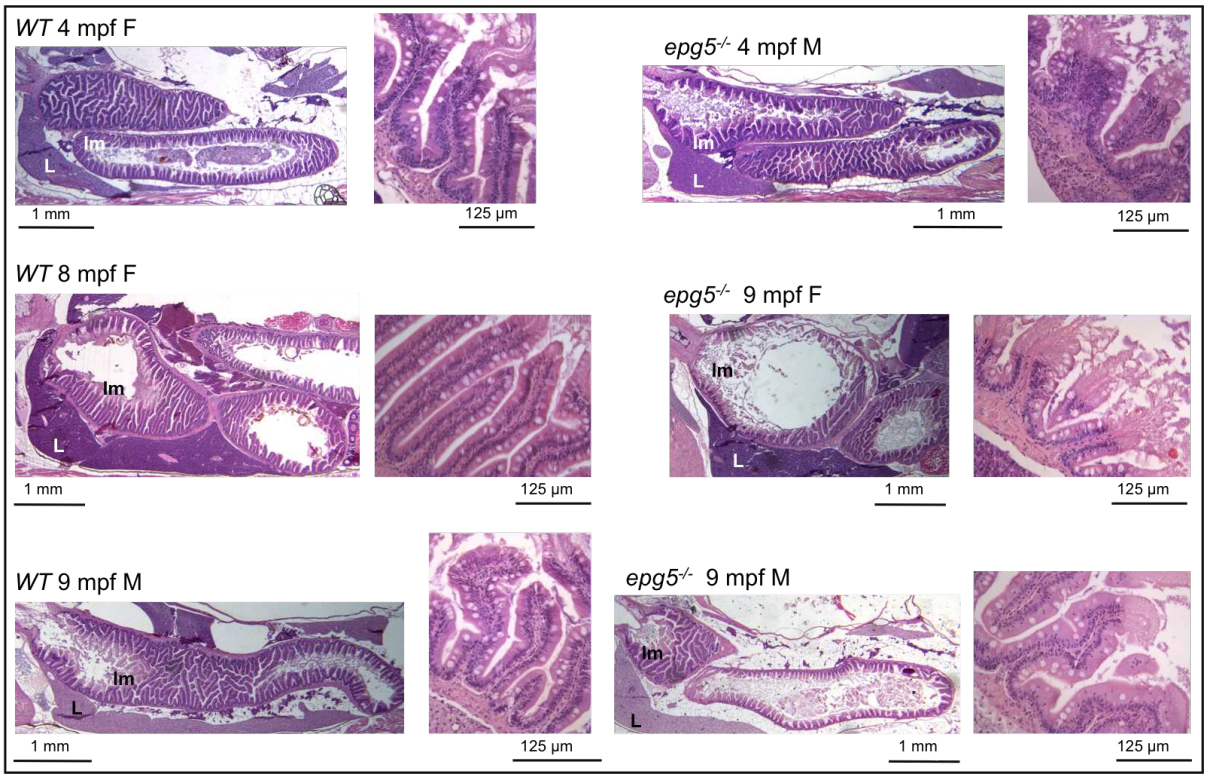


**S-Fig. 4.** Effects of Epg5 deficiency on intestinal morphology in adult zebrafish mutants in comparison with control fish at the same age. No clear alterations were present in mutant samples except for a sloughing epithelium at the folds tips of intestinal mucosa. lm = intestinal mucosa; L, liver.

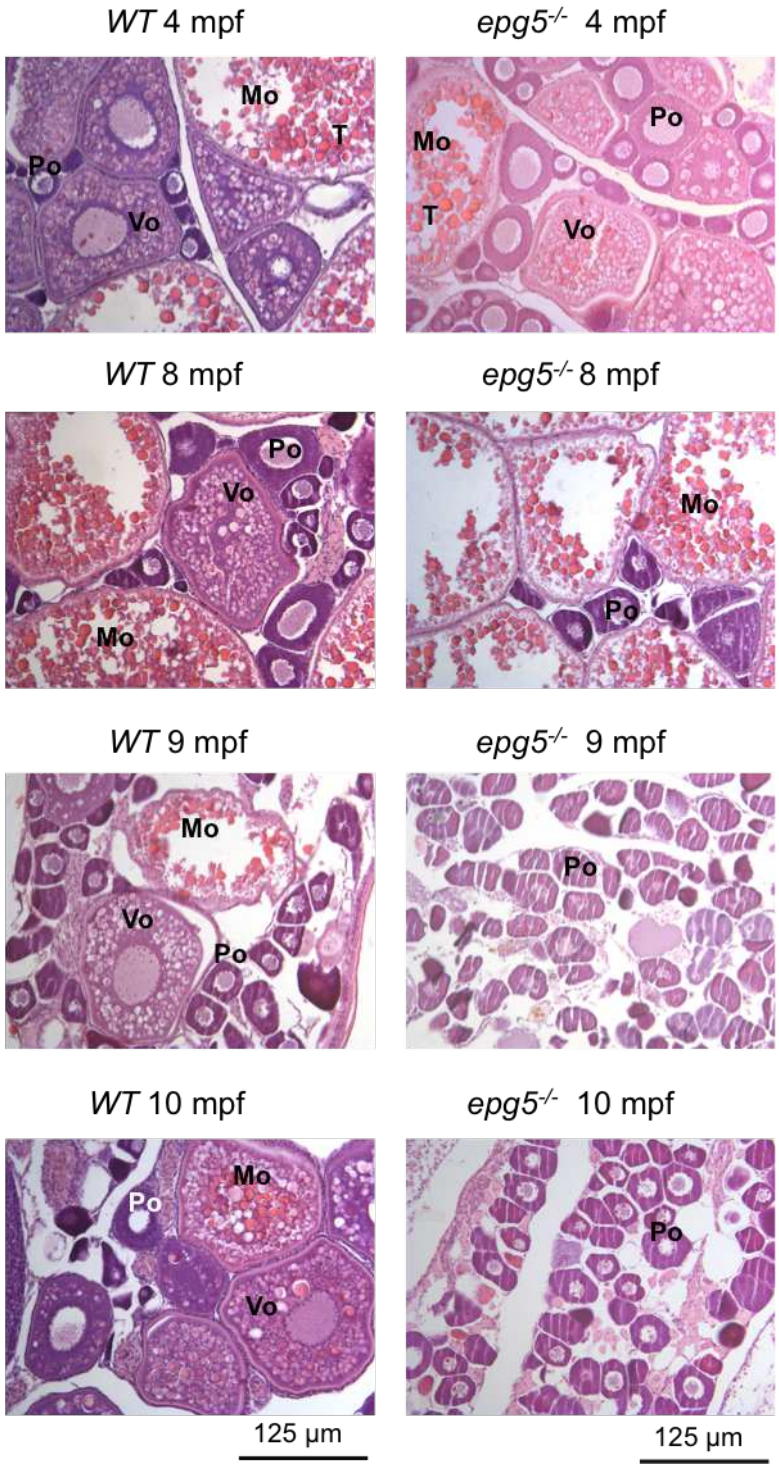


**S-Fig. 5.** Effects of Epg5 deficiency on ovarian morphology in adult zebrafish mutants in comparison with control fish at the same age. Two of the four ovaries analysed contains only primary and pre-vitellogenic follicles, suggesting a block of follicle maturation. PO, primary oocytes, CA, cortical alveolus stage oocyte; VO, vitellogenic stage oocyte; MO, mature oocytes.

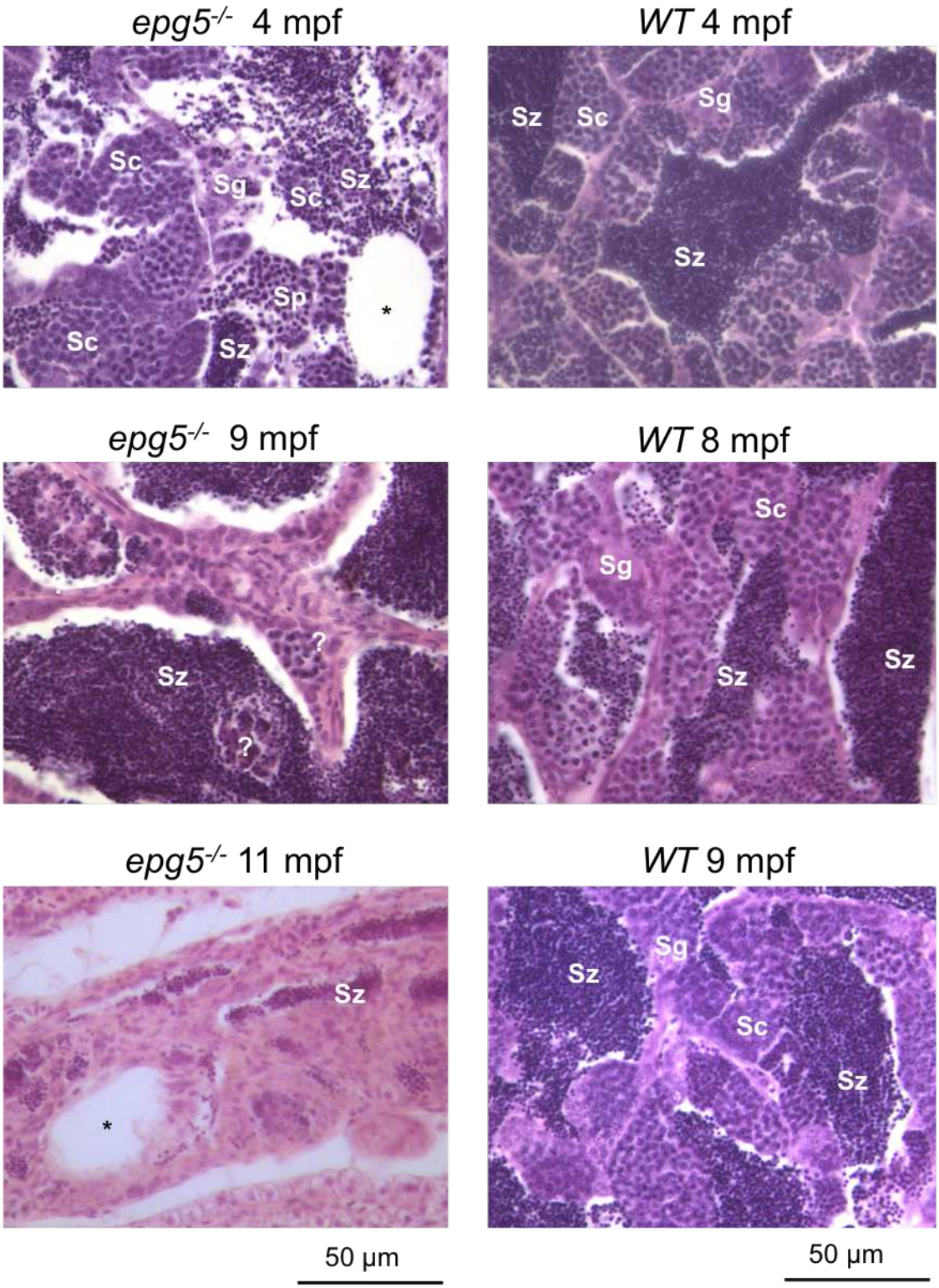


**S-Fig. 6.** Effects of Epg5 deficiency on testicular morphology in adult zebrafish mutants in comparison with control fish at the same age. Testicular tissues disorganization, empty tubules (asterisks), reduced dimension or increased fibrous connective tissue within the testicular stroma were present in almost all mutant samples analysed. Spermatozoa (Sp) and all stages of spermatogenesis, spermatogonia (Sg), spermatocytes (Sc), spermatids (Sd), were present on WT testis whereas the structure were disorganised on the mutant sample that also contained empty tubules (*).

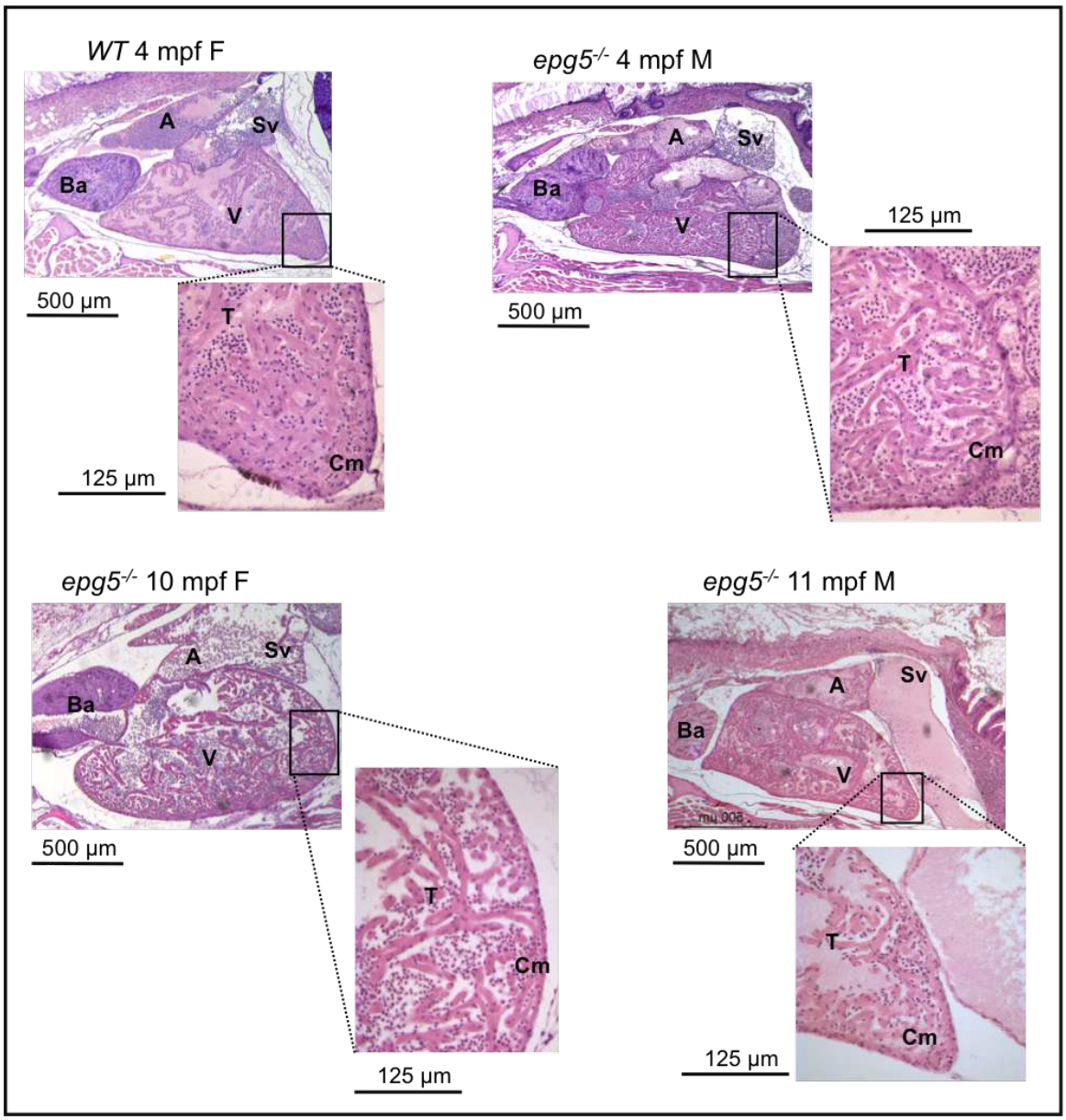


**S-Fig. 7.** Effects of Epg5 deficiency on heart morphology in adult male (M) and female (F) zebrafish mutants (10-11 mpf) in comparison with heart of control fish at the same age. The boxed regions are enlarged beneath to compare compact myocardium and underline its reduction between the two genotypes. Sv, sinus venosus, A, atrium, Ba, bulbus arteriosus, V, ventricle, Cm, compact myocardium; C, clumps of red cells.

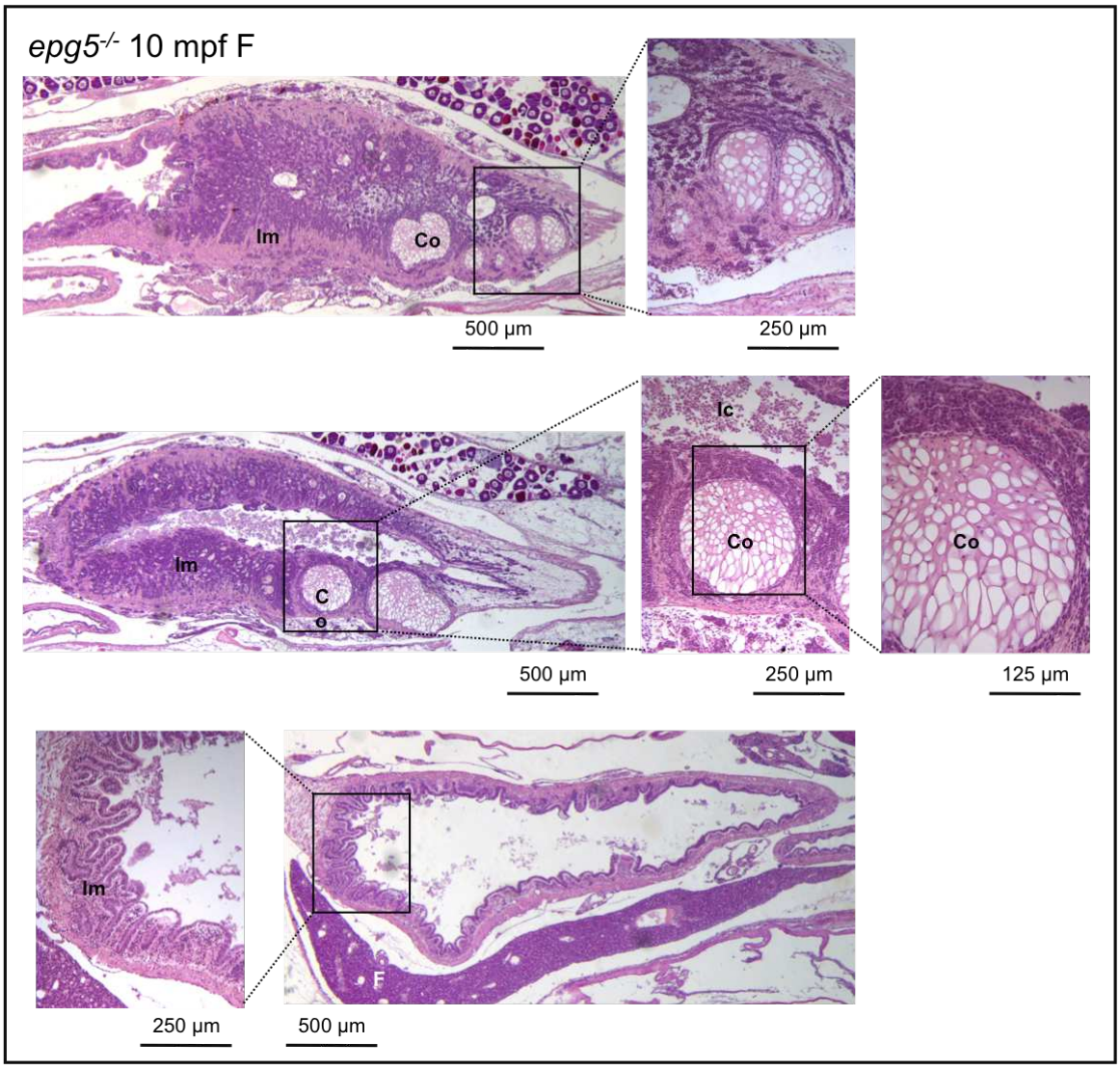


**S-Fig. 8.** Longitudinal sections at different levels of the intestine of a female zebrafish mutant (10 mpf) showing the presence of an intestinal chordoma. Multiple tumor cists were present in the intestinal wall which mucosa appeared altered and also substituted by fibrotic tissue. Botton section shows a clear alteration in the intestinal mucosa folds. Im = intestinal mucosa; Co = intestinal chordoma.

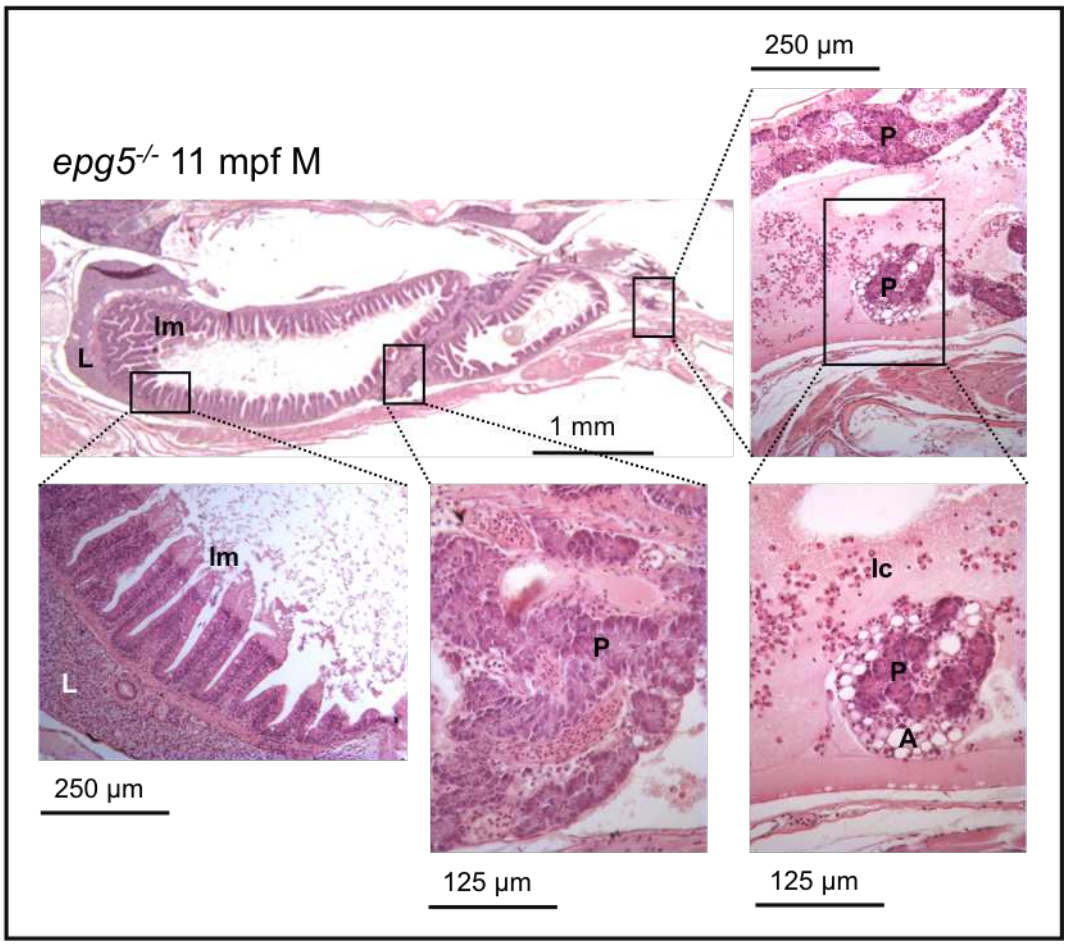


**S-Fig. 9**. Longitudinal sections of a male zebrafish mutant (11 mpf) showing reduction and alteration of the pancreatic tissue. Fragments of pancreas were also found surrounded by inflammatory infiltrating cells. Im, intestinal mucosa, L, liver, P, pancreas, A, adipose cell, Ic, infiltranting cells.

**S-Tab. 1.** Table of PCR, RT-qPCR, 5'-RACE oligos and CRISPR target site (Gagnon et al., 2014) used in this work.

| **Oligo name** | **Sequence** |
|---|---|
| Constant oligo | AAAAGCACCGACTCGGTGCCACTTTTTCAAGTTGATAACGGACTAGCCTTATTTTAACTTGCTATTTCTAGCTCTAAAAC |
| *Epg5* site specific oligo | ATTTAGGTGACACTATA***TGAGGTCAGGAGGCACATGA***TTTTAGAGCTAGAAATAGCAAG |

*Bold and italic sequence correspond to gRNA

| **Gene** | **Accession** | **Use** | | **Primer (5'–3')** |
|---|---|---|---|---|
| *epg5* | MG775431 | 5'-RACE | R1 | GAGGTGCAGCATCTTGTGAT |
| | | | R2 | GCATAAGAGAACATGCTGTTGC |
| *epg5* | XM_009301680 | screening sequencing | F1 | AAGGAGAGGCAGTCAGAG |
| | | | R1 | GAGGTGCAGCATCTTGTGAT |
| *epg5* | XM_009301680 | qPCR | F | GCTCTGCACTCATACACC |
| | | | R | CGACCTGATGCAGCACAG |
| *rplp0 (arp)* | NM_131580 | qPCR | F | CTGAACATCTCGCCCTTCTC |
| | | | R | TAGCCGATCTGCAGACACAC |

**S-Tab. 2.** List of markers used in the whole-mount in situ hybridization analyses.

| **Gene** | **GenBank cDNA reference** | **Vector** | **Endonuclease and RNA polymerase** |
|---|---|---|---|
| z-epg5-3'-UTR | Submitted to EMBL | pGEM | ApaI, Sp6 |

Chapter 1

# Zebrafish *ambra1a*$^{-/-}$ and *ambra1b*$^{-/-}$ mutant analysis suggests activation of paralogs compensation and confirms sub-functionalization following gene duplication

**In preparation**

## INTRODUCTION

Ambra1 is a positive regulator of the Beclin-1 dependent program of autophagy (Fimia *et al*., 2007), but thanks to its intrinsically disordered structure is involved in other important cellular processes such as development, apoptosis and cell proliferation (Cianfanelli *et al.,* 2015). In mouse indeed, Ambra1 has shown to be essential for the proper nervous system development during embryogenesis (Fimia *et al.,* 2007). Moreover, mice *ambra1* KO present early embryonic lethality, severe abnormalities in the neural tube development, uncontrolled cell proliferation and excessive cell death (Fimia *et al.,* 2007). Similarly, silencing of the zebrafish paralogous genes by morpholinos knockdown resulted in lethality within 12 dpf and the impairment of neural tube, muscle and heart development (Benato *et al.,* 2013; Skobo et al., 2014; this work). Moreover, also in zebrafish the *ambra1* silencing resulted in reduction of the autophagy, and in an increase of cell proliferation and apoptosis (Benato *et al.,* 2013).

In the last few years the genetic reverse approach in zebrafish research have been radically changed by the development of new genome editing tools, such as zinc finger nucleases (ZFNs), transcription activator-like effector nucleases (TALENs) and in particular the CRISPR/Cas9 system (Hwang *et al.,* 2013) that have facilitated the zebrafish generation of specific mutant lines.

Moreover, the gene editing approach to assess gene function revealed, in many cases, great differences between mutant and morphant phenotypes (Kok *et al*., 2015). The more severe morphant phenotype must be due to off-target effects of morpholinos targeting other transcripts in a non-specific way (Kok *et al*., 2015). The authors suggested the use of morpholinos approach only in comparison with results form a mutant zebrafish line. However, Rossi and coo-workers (2015) demonstrated the activation of a compensatory transcriptional activity that can explain the mild or apparently absent mutant phenotype (Rossi *et al*., 2015).

In this study, we generated and characterized the zebrafish *ambra1a*$^{-/-}$ and *ambra1b*$^{-/-}$ mutant lines, using CRISPR/Cas9 mutagenesis. Analysis of the *ambra1a*$^{-/-}$ line suggests activation of paralogs compensation process. These lines will allow us to separately analyse the function of Ambra1a and Ambra1b proteins as well as their interaction in the

double mutant line, as larvae can complete development and survive at least during larval stages. Moreover, the lack of female adult *ambra1b*$^{-/-}$ mutants identified a specific function for this gene in reproduction.

## MATERIAL AND METHODS

### Zebrafish maintenance and care

Wild type and mutant zebrafish were staged and maintained according to standard procedures (Kimmel *et al*., 1995; Westerfield, 1995). Embryos were obtained by natural mating and raised at 28.5°C in Petri dishes containing fish water and kept in a 13:11 light-dark (LD) cycle. For screening and *in vivo* imaging, embryos and larvae were anesthetized with 0.04% tricaine (Sigma-Aldrich, E10521). All husbandry and experimental procedures complied with European Legislation for the Protection of Animals used for Scientific Purposes (Directive 2010/63/EU) and were previously authorized by the University of Padua, Body for the Protection of Animals (OPBA-Project Number 568/2016).

### Generation and genotyping of *ambra1a* and *ambra1b* mutant lines

*ambra1a*$^{-/-}$ and *ambra1b*$^{-/-}$ zebrafish mutants were generated by CRISPR/Cas9-mediated genome editing. Single guide RNAs (sgRNA) were designed, using the CHOPCHOP software (https://chopchop.rc.fas.harvard.edu), to specifically target a CRISPR sequence on exon 4 (third codifying exon) of the *ambra1a* gene (HE602022) and on exon 2 (first coding exon) of *ambra1b* (FR846230). BLAST analysis of the target sequences revealed no specific binding with other genes. The two sgRNAs, (sequence GGATGGAGAGGTCAGAATCTGG for *ambra1a*) and (AGCGAGGAGCTCGTATGCTGGGG for *ambra1b*), were generated according to Gagnon *et al*. (2014) and *in vitro* transcribed using the MEGAshortscript T7 kit (Life Technologies, AM1354). *Cas9* mRNA was transcribed from linearized pCS2-NLS-zCas9-NLS plasmid (Addgene, Plasmid #47929) using mMessage Machine SP6 kit (Life Technologies, AM1340).

Fertilized eggs were injected with 1 nl of a solution containing 400 ng/uL Cas9 mRNA and 150 ng/uL sgRNA, using Phenol Red as injection marker. Genomic DNA was extracted from 5-dpf larvae derived from individually injected eggs to verify the presence of mutations and confirm the activity of the guide RNAs. F0 injected embryos were raised to adulthood and selected by genotyping. Individuals of F1 generation from the outcross of F0 founders with WT were raised and genotyped to confirm germline transmission of the mutation. Heterozygous mutants harbouring the identified mutations were then

outcrossed with WT for two generation and then incrossed to obtain the homozygous mutants (F4 generation).

**DNA extraction and genotyping**

Genomic DNA was extracted from single 5-dpf larvae euthanized with a lethal dose of tricaine (MS222) using the HotSHOT protocol (Meeker *et al*., 2007). Biopsies from the caudal fin of larvae and adult fish, anesthetized with tricaine, were used for fin clips DNA extraction. Genomic DNA was then extracted from these specimens with the HotSHOT protocol (Meeker *et al*., 2007).

Mutations in F0 were detected using heteroduplex mobility assay (HMA). In this case, genomic fragments at the target sites were amplified by PCR with 5x HOT FIREPol® Blend Master Mix (Solis BioDyne, 04-25-00125) and the locus-specific primers Am1a-hrmF/Am1a-R2 for *ambra1a* and Am1b-F5/Am1b-R2 for *ambra1b*. All primers are listed in S-Table 1. PCR conditions were as follows: 15 min at 95°C followed by 35 cycles at 95°C for 20 s, 60°C for 30 s and 72°C for 30 s. The resultant PCR amplicons were analysed by electrophoresis on a 15% polyacrylamide gel (Life Technologies, NP0323PK2). For confirmation, PCR products from fish harbouring indel mutations were subjected to direct sequencing. Poly Peak Parser software (http://yosttools.genetics.utah.edu/PolyPeakParser/) was used for identification and sequence characterization of heterozygous mutant carriers generated by genome editing.

For the screening of F2 and F3 generations, PCR products were resolved with Gel Red-stained 3% agarose low EEO gel (Fisher BioReagents, BP160-500) to identify *ambra1a*$^{+/+}$, *ambra1a*$^{+/-}$, *ambra1a*$^{-/-}$ as well as *ambra1b*$^{+/+}$, *ambra1b*$^{+/-}$, *ambra1b*$^{-/-}$ genotypes. Fragments at the target sites were amplified by PCR with 5X HOT FIREPol® Blend Master Mix (Solis BioDyne, 04-25-00125) and the locus-specific primers (Am1a-hrmF3/Am1a-R1 and Am1b-hrmF/Am1b-hrmR2, listed in S-Table 1).

**MO microinjection**

MO (Gene Tools) injection was performed with ATG-MOs against the translate initiation sites of either *ambra1a* or *ambra1b* transcripts (MO-*ambra1a*-ATG and MO-*ambra1b*-ATG). All MOs were previously described and validated (Benato *et al*., 2013; Skobo et al., 2014). A lower MOs dosage with respect to first MO analyses (Benato et al., 2013; Skobo et al., 2014) was used in order to reduce embryo mortality and to obtain a better differentiation of the resulting phenotypes. Specifically, for each MO 4 ng were injected in the yolk of 1-cell stage embryos. Injections were performed under a dissecting

microscope using a microinjector attached to a micromanipulator (Leica Microsystems). MOs-injected embryos were then incubated in 1x fish water solution at 28.5 °C.

**Whole-mount in situ hybridization (WMISH)**

Zebrafish embryos were fixed overnight at 4°C in 4% paraformaldehyde (PFA, Sigma) in phosphate-buffered saline (PBS) at the required stages of development. WMISH was performed as previously described (Thisse and Thisse, 2008). DIG-labeled riboprobes (S-Table 2) were synthesized, after plasmid linearization, by *in vitro* transcription with T7 or Sp6 RNA polymerases (Roche), following linearization as described in the manufacturer's instructions.

**Imaging**

For imaging, transgenic embryos and larvae were anesthetized with 0.04% tricaine, embedded in 0.8% low-melting agarose and placed on a depression slide. WMISH-stained embryos were mounted in 87% glycerol in PBT (PBS plus 0.1% Tween 20) or cleared and mounted in 2:1 benzyl benzoate/benzyl alcohol, observed under a Leica M165 FC microscope, and photographed with a Nikon DS-Fi2 digital camera.

**Statistical analysis**

Statistical analysis was performed using Graph Pad Prism V6.0. Record of morphants phenotypes is presented as % of the total and represents the means of 3 biological replicates. Statistical analysis was performed with the chi-square test between groups of phenotypes. The p values are summarized with the following symbols: *$p<0.05$, **$p<0.01$, ***$p< 0.001$, ****$p<0.0001$.

## RESULTS

### Generation of stable zebrafish *ambra1a*$^{-/-}$ and *ambra1b*$^{-/-}$ mutant lines by CRISPR-Cas9 mutagenesis

We targeted both *ambra1* paralogue genes using a CRISPR/Cas9 approach. The CRISPR sequences were selected on the fourth exon (coding exon 3) and on the second exon (coding exon 1) of *ambra1a* and *ambra1b* respectively. Both sgRNA injections resulted in mutagenesis in F0 injected embryos, as confirmed by sequencing. Heterozygous F1 carriers harbouring 11 nucleotides insertion and 8 nucleotides deletion were selected respectively for *ambra1a* and *ambra1b* (Fig. 1). F1 heterozygous were than outcrossed and screened to obtain the F2 generation. Both mutations resulted in shift in the reading frame that leads to premature stop codons. The putative encoded Ambra1a mutated protein contained 188 amino acids (aa) of which the first 120 correspond to the original protein and the last 68 resulted from the reading frame alteration (Fig. 1, panel A). The putative encoded Ambra1b mutated protein contained 47 aa of which the first 19 correspond to the original protein and the last 28 resulted from the reading frame alteration (Fig. 1, panel B).

Both mutant lines did not display clear phenotypes during the first stages of development.

(**A**)

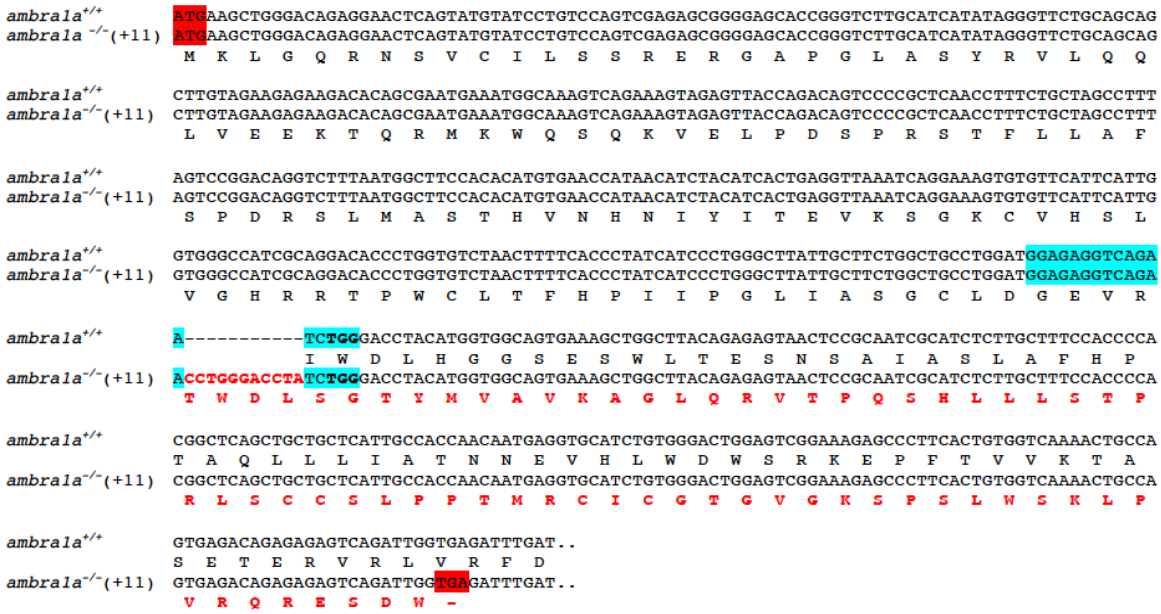

(**B**)


**Fig. 1.** Nucleotide and amino acid sequences showing the + 11 (panel A) and − 8 bp (panel B) mutations, as revealed by DNA sequencing analyses of zebrafish ambra1a and ambra1b mutant lines. Both *ambra1* sequences are represented starting from the start codon to the newly formed stop codons caused by frameshifts in the coding region. Both start and stop codons are highlighted in red. CRISPR targeted sites are highlighted in light blue with the protospacer-adjacent motif (PAM) sequence in bold. (A) In *ambra1a* sequence, the 8-nucleotide insertion and the consequent 68 new aa are shown in red and bold. (B) In *ambra1b* sequence, each deleted nucleotide is represented by a dash and the consequent 28 new aa are shown in red and bold.

### Zebrafish *ambra1a*$^{-/-}$ mutant line

Zebrafish *ambra1a*$^{-/-}$ mutants obtained from heterozygous carriers were viable and showed normal development, without any evident phenotype. Siblings segregated according to a Mendelian ratio, as resulted by genotyping analyses of 5-dpf larvae.

Moreover, both homozygous mutants deriving from a heterozygous or a homozygous parental cross reached sexual maturity and reproduced, thus demonstrating that survival of homozygous fish derived from heterozygous females was not due to the presence of maternal *ambra1a* transcripts or proteins.

Since the antibody against zebrafish Ambra1a was not available, we could not use western blotting analysis to verify the absence of the corresponding protein in the mutants. Thus, we analysed the possible reduction of *ambra1a* transcription in the mutant line using whole mount *in situ* hybridization (WMISH) analysis of 24-hpf WT and *ambra1a*$^{-/-}$ embryos. This analysis showed, in *ambra1a*$^{-/-}$ embryos, a clear reduction of *ambra1a* transcripts together with an increase of *ambra1b* gene expression levels with respect to the WT control (Fig. 2). Moreover, expression pattern of *ambra1b* in *ambra1a*$^{-/-}$ mutants seemed more widespread than in WT and similar to the WT expression pattern of *ambra1a* gene (Fig. 2).

This result is in agreement with the activation of nonsense-mediated mRNA decay (NMD) process due to an uncorrected mRNA termination (Baker and Parker, 2004). Moreover, the altered expression pattern of *ambra1b* gene in the *ambra1a*$^{-/-}$ line could be explained by a functional compensation between the two *ambra1* paralogous genes in zebrafish.

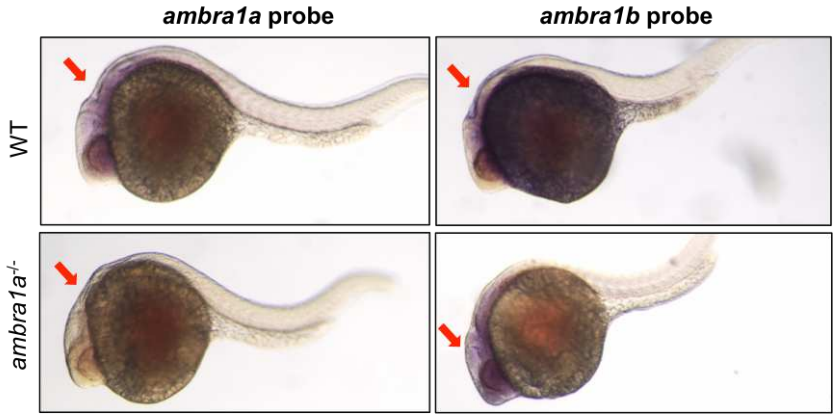


**Fig. 2.** *ambra1a* and *ambra1b* expression analysis in WT and 1-dpf mutant embryos by whole mount *in situ* hybridization. Embryos are lateral views with head pointing to the left.

### Compensatory effects of the paralogous *ambra1b* gene in the *ambra1a*$^{-/-}$ mutant line

Due to the lack of an evident mutant phenotype and to WMISH expression results above described, we investigated the compensatory effect exercised by the *ambra1b* gene in *ambra1a*$^{-/-}$ mutants by analysis of effects due to injection of the previously validated *ambra1a* and *ambra1b*-ATG-MOs (Benato *et al.,* 2013; Skobo *et al*., 2014).

As theoretically expected, *ambra1a*$^{-/-}$ mutants were weakly sensitive to *ambra1a*-ATG-MO, as the gene was already silenced, and this resulted in a significant different percentage of dead, abnormal and normal phenotypes when compared with WT embryos injected with *ambra1a*-ATG-MO. This result confirmed both the presence of a null mutant for Ambra1a protein and the specificity of the MO we used, given the lack of significant off-target effects in the mutant line.

On the contrary, *ambra1a*$^{-/-}$ mutants were strongly sensitive to ambra1b-MO knockdown as demonstrated by the higher percentages of dead and abnormal phenotypes compared with the results obtained after WT embryos injection with *ambra1b*-ATG-MO (Fig. 3). The stronger phenotype obtained was in agreement with the increase of morphant phenotype severity obtained by co-injection of both MOs (Benato *et al*., 2013; Skobo *et al* ., 2014).

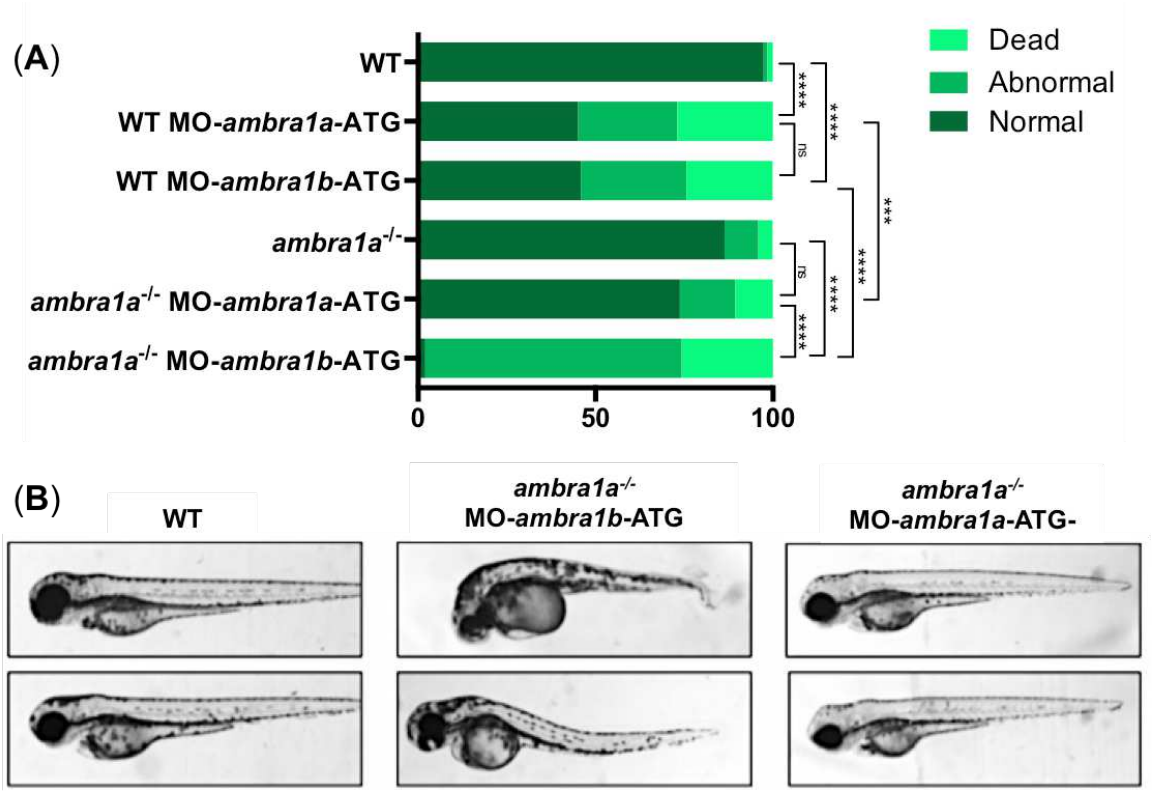


**Fig. 3.** (A) Percentage of normal, abnormal and dead in 3-dpf WT and *ambra1a*$^{-/-}$ mutant larvae with or without co-injection with *ambra1a*-ATG-MO and *ambra1b*-ATG-MO. For each treatment about 150 larvae were analysed. Statistical analysis was performed using chi-squared test, * P<0,05 ** P<0,01 *** P<0,001. (B) Representative images of the phenotype obtained after injection of *ambra1*-MOs on *ambra1a*$^{-/-}$ embryos.

### Zebrafish *ambra1b*$^{-/-}$ mutant line

Zebrafish *ambra1b*$^{-/-}$ mutants obtained from heterozygous carriers were viable and presented a normal survival rate during development, indicating that Ambra1b deficiency did not affect early embryo viability. Also for this mutant line, siblings segregated according to a Mendelian ratio.

However, until now, *ambra1b*$^{-/-}$ mutants were obtained only by heterozygous parental cross. Indeed, among more than 70 mutants homozygous fish identified by fin clips genotyping of heterozygous derived offspring, no female was morphologically identified. Moreover, anatomical examination of 4 adult *ambra1b*$^{-/-}$ mutants confirmed that the individuals examined were males.

The lack of female adults prevented us to generate homozygous offspring, useful for mutant phenotypical analysis during first developmental stages and for the study of possible compensatory effects of *ambra1a* paralogous gene. Moreover, in homozygous embryos, the maternal *ambra1b*$^{-/-}$ mRNA was always present in the zygote.

**Zebrafish *ambra1a*$^{-/-}$ *ambra1b*$^{-/-}$ double mutant line**

To analyse more in detail *ambra1a* and *ambra1b* function during development, and the compensation between the two paralogs, we attempted to obtain ambra1a/b double mutant line. Genotyping of progeny (100 adult individuals) from *ambra1a*$^{-/-}$*ambra1b*$^{+/-}$ female and *ambra1a*$^{+/-}$*ambra1b*$^{-/-}$ male fish did not reveal double homozygous mutants, despite the fact that the expected double mutant ratio is 25% (Fig 4).

However, as no clear phenotypes between embryos and larvae were identified and all of these seemed to develop normally, we genotyped the offspring derived from this breading at different developmental stages. The results suggested that a normal development occurred during the first larval stages (as revealed by the correct Mendelian proportion calculated at 5 and 13 dpf). However, genotyping of 43 individuals (29 dpf of age) revealed the presence of only one double mutant, presenting a phenotype characterized by strongly reduced body dimension with respect to double heterozygous siblings, likely consequent to a severe developmental delay (Fig 4). Although the double mutant did not present a suffering phenotype he was anesthetised with tricaine and sacrificed.

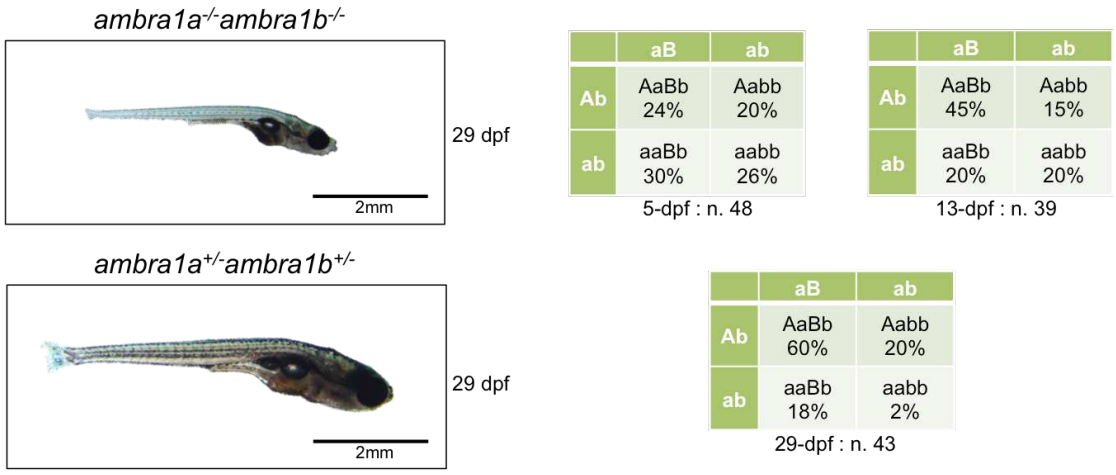


**Fig. 4.** On the left picture of the oldest double homozygous mutant found in the screening of double heterozygous progenies, compared to a double heterozygous sibling. On the right, Punnett Square showing the percentage of each phenotype obtained from genotyping analysis of *ambra1a*$^{-/-}$*ambra1b*$^{+/-}$ females and *ambra1a*$^{+/-}$*ambra1b*$^{-/-}$ male progenies.

## DISCUSSION

We have generated, by CRISPR/Cas9 targeted mutagenesis, two viable zebrafish lines harbouring a specific mutation in each *ambra1* genes, to study the functions of these proteins during development.

*ambra1a*$^{-/-}$ mutants were viable and fertile and did not present a clear phenotype. Validation of the *ambra1a* gene KO was not possible by protein analysis due to the lack of a specific antibody. However, *ambra1a* transcript level in the mutant line, as analysed by WMISH, was clearly reduced when compared to WT, due to the nonsense-mediated mRNA decay (NMD), an efficient machinery that prevents the production of truncated proteins (Chang *et al*., 2007).

Consistent with results reported by other authors (Kok *et al*., 2015; Novodvorsky *et al*., 2015; Eve *et al*., 2017) we also experienced differences of mutant versus morphant phenotypes. However, analysing the expression pattern of the paralogous gene *ambra1b* in the *ambra1a*$^{-/-}$ mutant, we noted, not only an increased signal, but also a different expression pattern with respect to WT and similar to the normal *ambra1a* pattern. This result suggested a possible functional compensation between the two paralogous genes, supported also by the reduction in *ambra1a* transcripts. Compensatory effects between the two paralogous *ambra1* genes were confirmed, in this work, by MOs injection experiments that also verified the specificity of *ambra1a*-ATG-MO used in this and in previous works and the consistency of *ambra1a* null mutants.

These results are in agreement with the genetic compensation described by Rossi and coo-workers (2015) that reported not only the expected up-regulation of paralogous genes but also the activation of different but related genetic pathways when the KO gene was present in single copy.

Actually, the NMD process was recently linked not only to a general cellular quality control system but also to a dynamic regulation of the transcriptomes in response to different physiological conditions (Lykke–Andersen *et al.,* 2015). Moreover, an efficient NMD pathway and the consequent increase of mutated mRNA degradation was found to result in a milder phenotype. To explain this, it was suggested that NMD could work as a machinery that shapes transcriptomes and thus regulates the compensatory response in order to mitigate the severity of the mutant phenotypes (Schuermann *et al*., 2015; EL-Brolosy and Stainier, 2017). In these situations, analysis of transcriptomes and proteomes will allow to identify the transcriptionally altered genes that could also represent target for functional studies and drug discovery.

Although double *ambra1* mutants were present in the progenies of double heterozygous parents, they were not able to survival after larval stages. Differently from mice in which *ambra1* KO is embryonic lethal (Fimia *et al*., 2007), double *ambra1* mutants survive at least during larval stages, likely thanks to maternal *ambra1b* transcripts that consent to overcome first development. Concerning this, the double mutant line will allow the study of *ambra1* functions at least until 20-30 dpf, without the rescued phenotype due to the functional compensation played by the two genes.

An unexpected but very interesting result was obtained with the *ambra1b*$^{-/-}$ line in which all adult homozygous mutant fish were males, suggesting a critical role of *ambra1b* in sexual determination and/or ovary development in zebrafish. According to this, a higher expression level of *ambra1b* was measured by qPCR in the ovary respect to other adult organs and also to the relative expression of the paralogous *ambra1a gene* (unpublished results).

In the last years a crucial connection between autophagy and reproductive functions has been suggested by the increasing number of publications on this topic related to both male and female (see the review of Lim and Song, 2014). KO of autophagy related genes determines fertility reduction (as reported in the Chapter I of this thesis with the zebrafish *epg5* mutant line), impairment of spermatogenesis in mice (Atg7 mice KO, Wang *et al*., 2014) and medaka (Epg5 medaka KO, Herpin *et al.*, 2015), premature loss of female germ cells (Atg7 and Beclin 1 mice KO, Gawriluk *et al.,* 2011; Song *et al.,* 2015).

The last report is particularly interesting in relation of our results because, in zebrafish, primordial germ cells (PGCs) number may directly regulate gonadal transformation and early depletion of PGC cells can promote testis formation (Tzung *et al.,* 2014).

Given the different phenotypes of the Ambra1 mutants**,** at least with respect of the gonads development, this result underlined also the sub-functionalization of the two paralogous genes, favouring their maintaining in zebrafish genome.

Analysis of sexual differentiation and gonad development in the *ambra1b*$^{-/-}$ line will help in the future to deepen the link between autophagy and reproduction.

**REFERENCES**

**Baker K. E. and Parker R. 2004.** Nonsense-mediated mRNA decay: terminating erroneous gene expression. Curr Opin Cell Biol 16, 293-299.

**Benato F., Skobo T., Gioacchini G., Moro I., Ciccosanti F., *et al*. 2013.** Ambra1 knockdown in zebrafish leads to incomplete development due to severe defects in organogenesis. Autophagy 9: 476-495.

**Chang, Y.F., Imam J.S. and Wilkinson M.F. 2007.** The nonsense-mediated decay RNA surveillance pathway. Annu Rev Biochem 76, 51-74.

**Cianfanelli, V., Fuoco, C., Lorente, M., Salazar, M., Quondamatteo, F., *et al*. 2015.** AMBRA1 links autophagy to cell proliferation and tumorigenesis by promoting c-Myc dephosphorylation and degradation. Nat. Cell Biol. 2015. 17, 20-30.

**El-Brolosy M.A. and Stainier D.Y. 2017.** Genetic compensation: A phenomenon in search of mechanisms. PLoS Genet. Jul 13;13(7):e1006780.

**Eve A.M., Place E.S., Smith J.C. 2017.** Comparison of Zebrafish *tmem88a* mutant and morpholino knockdown phenotypes. PLoS One. Feb 13;12(2):e0172227.

**Fimia G.M., Stoykova A., Romagnoli A., Giunta L., Di Bartolomeo S., *et al*. 2007.** Ambra1 regulates autophagy and development of the nervous system. *Nature*. 447:1121-5.

**Gagnon J.A., Valen E., Thyme S.B., Huang P., Akhmetova L. *et al*., 2014.** Efficient mutagenesis by Cas9 protein-mediated oligonucleotide insertion and large-scale assessment of single-guide RNAs. PLoS One, 9, e98186.

**Gawriluk T.R., Hale A.N., Flaws J.A., Dillon C.P., Green D.R., *et al.,* 2011.** Autophagy is a cell survival program for female germ cells in the murine ovary. Reproduction. Jun;141(6):759-65.

**Herpin A., Englberger E., Zehner, M., Wacker R., Gessler M., *et al.*, 2015.** Defective autophagy through epg5 mutation results in failure to reduce germ plasm and mitochondria. FASEB J. 29, 4145–4161.

**Hwang W.Y., Fu Y., Reyon D., Maeder M.L., Tsai S.Q., *et al*., 2013.** Efficient In Vivo Genome Editing Using RNA-Guided Nucleases. Nat Biotechnol. Mar; 31(3): 227–229.

**Kimmel C.B., Ballard W.W., Kimmel S.R., Ullmann B., Schilling T.F. 1995.** Stages of embryonic development of the zebrafish. Dev Dyn 203: 253-310.

**Kok F.O., Shin M., Ni C.W., Gupta A., Grosse A.S., *et al.* 2015.** Reverse genetic screening reveals poor correlation between morpholino-induced and mutant phenotypes in zebrafish. Dev Cell.;32(1):97–108.

**Lim HJ, Song H. 2014.** Evolving tales of autophagy in early reproductive events. Int J Dev Biol. 2014;58(2-4):183-7. doi: 10.1387/ijdb.130337hl.

**Lykke-Andersen S. and Jensen T.H. 2015.** Nonsense-mediated mRNA decay: an intricate machinery that shapes transcriptomes. Nat Rev Mol Cell Biol. Nov;16(11):665-77.

**Meeker N. D., Hutchinson S. A., Ho, L. and Trede N. S. 2007.** Method for isolation of PCR-ready genomic DNA from zebrafish tissues. *Biotechniques* 43, 610, 612, 614.

**Novodvorsky P., Watson O., Gray C., Wilkinson R.N., Reeve S., *et al.,* 2015.** Mutant Zebrafish Do Not Recapitulate Morpholino-Induced Vascular and Haematopoietic Phenotypes. PLoS One. Oct 27;10(10):e0141611.

**Rossi A., Kontarakis Z., Gerri C., Nolte H., Hölper S., *et al*., 2015.** Genetic compensation induced by deleterious mutations but not gene knockdowns. Nature. Aug 13;524(7564):230-3.

**Schuermann A., Helker C.S., Herzog W. 2015.** Metallothionein 2 regulates endothelial cell migration through transcriptional regulation of vegfc expression. Angiogenesis. Oct;18(4):463-75.

**Skobo T., Benato F., Grumati P., Meneghetti G., Cianfanelli V., *et al.* 2014.** Zebrafish *ambra1a* and *ambra1b* knockdown impairs skeletal muscle development. PLOS One, 9(6):e99210.

**Song Z.H., Yu H.Y., Wang P., Mao G.K., Liu W.X., *et al*., 2015.** Germ cell-specific Atg7 knockout results in primary ovarian insufficiency in female mice. Cell Death Dis. Jan 15;6:e1589.

**Thisse C., Thisse B. 2008.** High-resolution in situ hybridization to whole-mount zebrafish embryos. Nat Protoc 3: 59-69.

**Tzung K.W., Goto R., Saju J.M., Sreenivasan R., Saito T. *et al*. 2014.** Early Depletion of Primordial Germ Cells in Zebrafish Promotes Testis Formation. Stem Cell Rep 4: 61-73.

**Wang H., Wan H., Li X., Liu W., Chen Q., *et al*., 2014.** Atg7 is required for acrosome biogenesis during spermatogenesis in mice. Cell Res. Jul;24(7):852-69.

**Westerfield M. 1995.** The Zebrafish Book. A Guide for the Laboratory Use of Zebrafish (Danio rerio), 3rd Edition. Eugene, OR, University of Oregon Press.

## SUPPLEMENTARY MATERIAL

**S-Table 1.** Primers used for screening of the mutants by electrophoresis and sequencing.

| Usage | Name | Sequence |
|---|---|---|
| PCR electrophoresis | Am1a- hrmF3 | TGGCTGCCTGGATGGAGAG |
| PCR electrophoresis | Am1a-R1 | ATTACGGCAACTTTTGCACC |
| Sequencing | Am1a-hrmF | TGAGGTTAAATCAGGAAAGTGT |
| Sequencing | Am1a-R2 | GACCACAGTGAAGGGCTC |
| PCR electrophoresis | Am1b-hrmF | GAAACTCTGTGCTGATCCTGT |
| PCR electrophoresis | Am1b- hrmR2 | CGTGTTCGGTCTTCCACCAG |
| Sequencing | Am1b-F5 | GCGTGCTGCTGAGTTAGTG |
| Sequencing | Am1b-R2 | GGCTTTAACAATTATATGCTGC |

**S-Table 2.** List of markers used in the whole-mount in situ hybridization analyses.

| Gene | Reference | GenBank cDNA reference | Vector | Endonuclease and RNA polymerase |
|---|---|---|---|---|
| z-am1a1-3'-UTR | Benato *et al*., 2013 | XM_002667669 | pGEM | ApaI, Sp6 |
| z-am1b-3'-UTR | Benato *et al*., 2013 | XR_084457 | pGEM | SalI, T7 |

# Zebrafish *ambra1a* and *ambra1b* silencing affects heart development

**Advanced draft**

**ABSTRACT**

In zebrafish two paralogous genes, *ambra1a* and *ambra1b*, both required for the autophagic process and during development, encode the protein Ambra1, a positive regulator of early steps of autophagosome formation. As evidenced by whole mount in situ hybridization (WMISH) both transcripts are expressed in the heart region. In this work, we analyse the ambra1a and ambra1b knockdown effects on heart development by means of morpholino oligonucleotides (MOs). Silencing of the two proteins by ATG-MOs affects heart morphogenesis resulting in a small, string-like heart with pericardial oedema, whereas treatment with SPLIC-MOs does not results on clear cardiac phenotypes, indicating the importance of maternally supplied ambra1 transcripts. Co-injection of both ATG-MOs determines a more severe cardiac phenotype with a prominent pericardial oedema. The morphants cardiac phenotypes were effectively rescued by co-injection of MOs with human AMBRA1 mRNA pointing up the conservation of Ambra1 functions during evolution. WMISH of myosin light chain 7 (*myl7*) as well as ATG-MOs microinjection on a green heart zebrafish transgenic line revealed defects with the heart jogging process followed by imperfect cardiac looping. Moreover, WMISH of *pitx2c* transcripts, which at the 21-somite stage are expressed on the left plate mesoderm, showed both bilateral or reversed pitx2c expression in Finally, co-injections of *ambra1* ATG-MOs with *hAMBRA1* mRNA mutated in the PP2A binding sites (*AMBRA1*$^{PXP}$) was not able to rescue the cardiac phenotypes in the same way as human *AMBRA1* mRNA and treatment of zebrafish embryos with the specific inhibitor of PP2A, cantharidin, showed similar developmental cardiac defects. These results suggested a possible role of Ambra1 proteins in heart development, involving the binding site for the PP2A phosphatase.

Chapter 3

## INTRODUCTION

AMBRA1 (activating molecule in BECN1-regulated autophagy) is a 140 kDa, intrinsically disordered, adaptor protein involved in a plethora of cellular processes (Cianfanelli *et al.*, 2015a). AMBRA1 primarily belongs to the regulatory network of autophagy, an evolutionarily-conserved catabolic process essential to remove intracellular protein aggregates and unnecessary or damaged organelles (Cianfanelli *et al.*, 2015b). In resting conditions, AMBRA1 docks to the cytoskeleton the autophagy initiation complex containing ULK1, VPS34 and BECN1. Upon autophagy induction, AMBRA1 is able to relocalize this complex to the endoplasmic reticulum, where it allows the nucleation of the autophagic vesicles named "autophagosomes" (Di Bartolomeo *et al.*, 2010). AMBRA1 contributes to autophagy induction also by interacting with the E3-ligase TRAF6, that is responsible of binding an activating Lys63-ubiquitin chain to ULK1 (Nazio *et al.*, 2013).

More recently, a role for AMBRA1 in the regulation of cell proliferation was demonstrated (Cianfanelli *et al.*, 2015c). Through a conserved Proline-rich domain, the dephosphorylated form of AMBRA1 interacts with the catalytic subunit of the protein phosphatase PP2A (PP2Ac). The AMBRA1-PP2Ac complex destabilizes the proto-oncogene c-Myc, leading to an overall reduction of its pro-proliferative activity. Conversely, under anabolic conditions, the nutrient-availability sensor mTOR (mammalian Target Of Rapamycin) phosphorylates AMBRA1, thus determining not only autophagy inhibition, but also increased cell proliferation (Cianfanelli *et al.*, 2015c).

The biological importance of AMBRA1 is further confirmed by the extent to which AMBRA1 deficiency can interfere with embryonic development *in vivo*. The first evidences for a role of AMBRA1 in vertebrate development came from a study of large-scale mutagenesis based on gene-trapping in mice (Stoykova *et al.*, 1998; Fimia *et al.*, 2007). Mice homozygous for a gene-trap mutation in the *Ambra1* locus (*Ambra1*$^{gt/gt}$) die at late stages of development and show severe defects in the central nervous system (Fimia *et al.*, 2007).

We approached the study of AMBRA1 in vertebrate development by mean of another model organism, particularly appropriate for developmental studies due to the external fertilization and the almost complete transparency until adulthood: zebrafish (*Danio rerio*; Kimmel *et al.*, 1995). Bioinformatic analyses revealed that AMBRA1 is highly conserved in evolution and there are two paralogues of the mammalian *Ambra1* gene in the zebrafish genome, *ambra1a* and *ambra1b* (Benato *et al.*, 2013; Skobo *et al.*, 2014). A strong downregulation of these two zebrafish genes was successfully achieved by mean

of a morpholino-based strategy, and Ambra1 deficiency resulted in dramatic defects in organogenesis and subsequent embryonic lethality (Benato *et al.*, 2013). A generalized disorganization of skeletal myofibers was also evident both in ambra1 morphants and in *Ambra1*$^{gt/gt}$ mouse embryos (Skobo *et al.*, 2014).

Preliminary observations suggested us a possible involvement of heart defects in the observed phenotype of *ambra1* zebrafish morphants, since pericardial oedema was particularly evident (Benato *et al.*, 2013). In zebrafish, heart precursors are recruited to form the heart tube in a two-step process that requires the orchestration of different signalling pathways, including Fgf and TGFβ (Liu and Stainier, 2012; Bakkers, 2011). Subsequently the heart tube forms a right-sided loop and the specification of cardiac chambers takes place (Bakkers, 2011). Moreover, heart morphogenesis in zebrafish can be easily monitored by taking advantage of a myocardium-reporter fish (Huang *et al.*, 2003), making this animal model a precious resource for the study of human heart congenital defects (Bakkers, 2011).

Here we give the first full description of a clear developmental defect in the heart of zebrafish *ambra1* morphants. Our data suggest that this phenotype relies on a defective activity of the cellular signalling dependent on PP2A.

## MATERIALS AND METHODS

### Animal maintenance and handling

Zebrafish (AB strain) were raised, staged and maintained according to standard protocols (Kimmel *et al.*, 1995; Westerfield, 1995). Embryos were obtained by natural spawning and cultured in zebrafish fish water solution (50x: 25 g Instant Ocean, 39.25 g CaSO4, 5 g NaHCO3 for 1 L) at 28.5°C with a photoperiod of 13 h light/11 h dark. The developing embryos were kept in an incubator at 28°C. For *in vivo* imaging, embryos were anesthetized with 0.04% tricaine (Westerfield, 1995). Embryos of the transgenic line Tg(*7xTCF*$^{mut}$*-1.2ins:EGFP*) presenting a green heart were used for assessing looping development (Facchinello *et al*., 2016). Tg(*fli1::EGFP*) instead was used to analyse vascular system development in morphants (Lawson *et Weinstein*, 2002). All husbandry and experimental procedures complied with European Legislation for the Protection of Animals used for Scientific Purposes (Directive 2010/63/EU) and were previously authorized by the University of Padova, Body for the Protection of Animals (OPBA-Project Number 568/2016).

### MO microinjection

MO (Gene Tools) treatment was performed with MOs against the ATG translation initiation sites of either *ambra1a* or *ambra1b* transcripts (MO-*ambra1a*-ATG and MO-*ambra1b*-ATG) and with splice-blocking MOs designed at the exon 3 / intron 3 junction sequence of both genes (MO-*ambra1a*-splice and MO-*ambra1b*-splice). As controls, we used five-nucleotide-mismatched control MOs (MO-*ambra1a*-5m and MO-*ambra1b*-5m) (Benato *et al.*, 2013; Skobo *et al.*, 2014). All MOs were previously described and validated (Benato *et al.*, 2013). As in the analysis of Ambra1 involvement of skeletal tissue development (Skobo *et al.*, 2014), lower MOs dosages were used in order to reduce embryo mortality. Specifically, for each MO, 8,2 ng were injected in the yolk of 1-cell stage embryos, whereas the dosage was halved in the co-injection experiments. Injections were performed under a dissecting microscope using a microinjector attached to a micromanipulator (Leica Microsystems). MOs-injected embryos were then incubated in 1x fish water solution at 28.5 °C up to the desired stages of development.

### RNA synthesis and injections

For rescue experiments, human *AMBRA1* cDNA (*hAMBRA1*) (Fimia *et al.*, 2007) as well as human *AMBRA1* cDNA mutated in the PP2A binding sites (*AMBRA1*$^{PXP}$) (Cianfanelli *et al.*, 2015) were removed from the corresponding pLPCX plasmids (*pLPCX-hAMBRA1* and

*pLPCX- AMBRA1*$^{PXP}$) with the restriction enzymes *Eco*RI and *Cla*I, and subcloned in the pCS2+ vector to obtain the pCS2+*hAMBRA1* and pCS2+*hAMBRA*$^{PXP}$ constructs. The corresponding full-length RNAs were transcribed using the T3 promoter and the mMessage Machine kit (Ambion) according to the manufacturer's instructions, after plasmid linearization with *Hind*III restriction enzyme. The RNAs were polyadenylated at the 3'-termini using a Poly(A) Tailing Kit (Invitrogen, AM1350). After preliminary experiments with different dosages ranging from 400 to 100 pg/embryo, the 200 pg/embryo dosage was selected for the injection in one-cell stage embryos of *hAMBRA1* and *hAMBRA1*$^{PXP}$ mRNA respectively.

**Heart dissection**

Whole hearts were extracted manually from 3-dpf WT and morphant embryos using a green heart transgenic line to help tracking the cardiac tissues, as described by Burns and MacRae (2006). Before heart extraction, embryos were anesthetized with Tricaine-S, placed in a microcentrifuge tube with Lebovitz's L-15 medium plus 10% fetal bovine serum (Invitrogen). Hearts were separated from total embryos by drawing and expelling the embryos through a 6-mL syringe with a 19-gauge syringe needle. Disrupted embryos were then size fractioned using two different mesh filters. Zebrafish fluorescent hearts were collected with a p20 pipet under fluorescent microscopy, frozen and stored at −80°C until RNA extraction.

**RNA extraction, reverse transcription and quantitative polymerase chain reaction (qPCR)**

Total RNA was extracted from pools (100-200) of 3 dpf WT and morphants hearts using NucleoSpin RNA XS (Macherey-Nagel, 740902) according to the manufacturer's instructions. The RNA samples were kept at -80°C until use.

For qPCR, 1 µg of total RNA obtained was used for cDNA synthesis, employing FIREScript Reverse Transcriptase Kit (Solis BioDyne, 06-13-00050) and following the manufacturer's protocol. PCRs were performed with SYBR green method in on a Rotor-Gene Q real-time analyser (Qiagen). The reaction conditions were as follows: enzyme activation at 95°C for 15 min followed by 45 cycles of denaturation (30 s at 95°C), annealing (30 s at 60°C) and extension (20 s at 72°C). Fluorescence monitoring occurred at the end of each cycle. The extension phase of the last cycle was prolonged by 10 min. Primer specificity and the absence of primer-dimer formation during real-time PCR analysis was indicated in each sample by the presence of a single peak in the dissociation (melting) curve at the end of the amplification program. The specificity of each primer set was also analysed by

sequencing the obtained fragment. *b-actin-2* mRNAs were used as normalizers in each sample in order to standardize the results by eliminating variations in mRNA and cDNA quantity and quality. Modification of gene expression is represented with respect to the control, sampled at the same time of the treatment. The primer sequences were reported in supplementary S-Table 1.

**Whole mount in situ hybridization (WMISH) and morphological analysis**

Zebrafish embryos were fixed overnight in 4% paraformaldehyde (PFA, Sigma) in phosphate-buffered saline (PBS) at the required stages of development. WMISH was performed as previously described (Benato *et al.*, 2013).

Antisense DIG-labeled riboprobes were synthesized by *in vitro* transcription with T7 or Sp6 RNA polymerases supplemented with digoxigenin-UTP (Roche), following the manufacturer's instructions. Supplemental S-Table 2 reports restriction enzymes and RNA polymerases used for linearization and transcription.

For histological analysis, zebrafish WMISH-stained larvae at 5 dpf were fixed in 4% paraformaldehyde at RT for 2 h and processed into an alcohol–xylene series followed by paraffin embedding (Paraplast plus, Leica, 39602004). Samples were serially cut into 7 μm sections on a LKB microtome. After rehydration, sections were stained with haematoxylin and eosin and mounted with Eukitt (BioOptica, 09-00100) for microscopic examination.

**Proliferation analysis using whole mount immunohistochemistry**

Proliferation was analysed in WT and ambra1 morphant embryos at 90% epiboly (9 hpf) by whole mount immunohistochemistry with anti-phosphohistone H3 antibody (polyclonal rabbit Millipore, 1:1000) according to the manufacturer instructions and revealed with NBT/BCIP solution (Roche). Phospho-H3 immunostaining was quantified by counting the number of positive cells present in ten embryos of each category.

Zebrafish embryos were fixed overnight in 4% paraformaldehyde in PBS at 4°C. For rescue experiments both *hAMBRA1* and *hAMBRA1*$^{PXP}$ mRNA were used.

**Zebrafish embryos treatment**

WT embryos were incubated with different concentrations of the PP2A specific inhibitor, cantharidin (2.5 to 5 μM) starting from 4 hpf. Embryos were then analysed at 2 and 3 dpf using bright-field microscopy.

**Imaging**

For confocal microscopy, fixed embryos were embedded in 0.8% low-melting agarose and placed on a depression slide, and a Nikon C2 confocal system was used to record images.

WMISH-stained embryos were mounted in 87% glycerol in PBT (PBS plus 0.1% Tween 20) or cleared and mounted in 2:1 benzyl benzoate/benzyl alcohol, observed under a Leica DMR microscope, and photographed with a Leica DC500 digital camera.

**Statistical analysis**

Statistical analysis was performed using chi-square test comparing the groups of phenotypes in the rescue experiment (GraphPad Prism Software V6.0). Student T-test was used to analyse PH3 spots in the whole mount immunohistochemistry at 9 hpf and to test the RT-qPCR data.* P<0,05; ** P<0,01; *** P<0,001;****P<0,0001.

## RESULTS

### *ambra1a* and *ambra1b* transcripts are expressed in the cardiac region during heart development

Whole mount *in situ* hybridization (WMISH) showed that both zebrafish *ambra1* transcripts are present in the heart region of 2-dpf embryos and thus during heart development. Indeed, *ambra1* transcripts localized in the same position of myosin light chain 7 (*myl7*) transcripts, a marker specific to cardiac tissue (S-Fig. 1). Moreover, the longer exposition time required by the *ambra1b* digoxigenin-labelled probe to label the cardiac region suggested a lower cardiac expression of these transcripts. Expression of both *ambra1* transcripts as well as the lower expression of *ambra1b* mRNA was finally confirmed by RT-qPCR analysis using cDNA from extracted hearts of 3-dpf WT embryos (S-Fig. 1). Moreover, this result was in agreement with previously RT-qPCR analysis of these paralogous genes which showed a higher ambra1a expression during development and at least until 6 dpf.

### Knockdown of *ambra1a* and *ambra1b* impairs cardiac development

To investigate the role of *ambra1a* and *ambra1b* during cardiac development, we injected validated antisense *ambra1*-MOs for both paralogous genes into 1-cell embryos to suppress translation of both maternal and zygotic mRNA (ATG MOs) or to silence zygotic transcription of the two genes (splice-blocking MOs) (Benato *et al.*, 2013; Skobo *et al.*, 2014). In agreement with previous results, the loss of both *ambra1* transcripts induces severe morphological defects, such as body growth delay, curved shape, neural tube defects and haemorrhagic pericardial oedema. Due to the reduced MOs doses used in these experiments, the phenotypes were less severe than those we previously described (Benato *et al.*, 2013).

Cardiac morphology was analysed at 3 dpf using bright-field microscopy. In WT and five-nucleotide-mismatched-morphant embryos (5M-morphants), the hearts appeared phenotypically indistinct with ventricle and atrium overlapping with each other. In contrast, both Ambra1-morphants, and in particular ambra1a, resulted in an elongated, string-like heart tube, displaying little overlapping between ventricle and atrium, and a marked pericardial oedema (Fig. 1). These results were also confirmed by histological analysis of 3-dpf WT and morphant embryos (S-Fig. 2).

Phenotype severity was variable but enhanced in embryos co-injected with MO-ambra1a-ATG and MO-ambra1b-ATG (Fig. 1). Treatment with SPLIC-MOs revealed no obvious difference between these morphants and WT or 5M-morphants embryos,

suggesting a fundamental role of maternally supplied *ambra1* transcripts during development. Co-injection of ATG-MOs with human *AMBRA1* mRNA rescued the cardiac phenotype of morphant embryos, thus underlining the specificity of morpholino-induced defects and the conservation of Ambra1 functions during evolution. On the other hand, co-injection of ATG-MOs with human *AMBRA1* mRNA mutated in the PP2A binding sites (*AMBRA1*$^{PXP}$) was not able to rescue the cardiac phenotypes (Fig. 1)

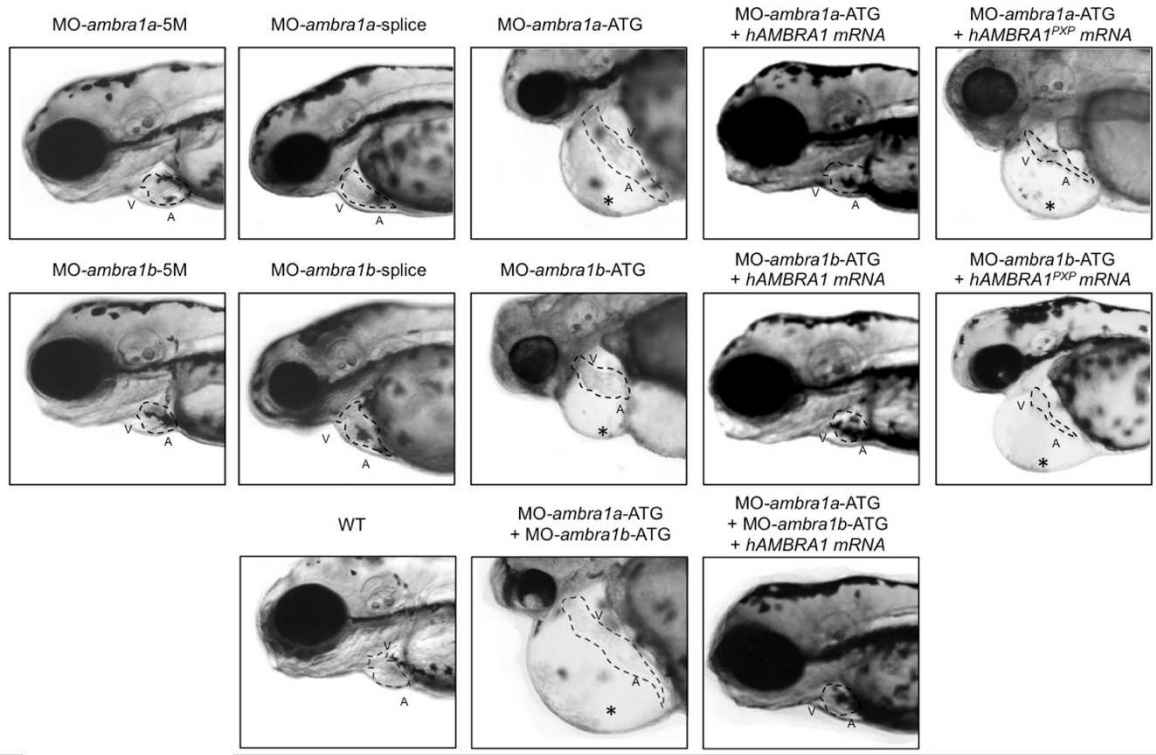


**Fig. 1.** Representative images under normal light of cardiac region of 3-dpf live embryos injected with the indicated MOs. ATG-morphant embryos show pericardial oedema and string-like heart tube when compared to WT and 5 m-control embryos. No visible abnormalities are evident in splice-morphants, whereas cardiac defects are enhanced in the double morphants. The phenotypic defects of ATG-morphant embryos are rescued by co-injection with human *AMBRA1* mRNA but not with the *AMBRA1*$^{PXP}$ mRNA. V, ventricle; A, atrium. Asterisks indicate blood pooling.

As impairment of heart development can be secondary to blood circulation and vascular defects, we used the transgenic line Tg(*fli1:EGFP*), which expresses GFP in endothelial cells including vasculature, blood cells, and endocardial cells (Lawson *et Weinstein*, 2002), to analyse vascular patterning in 2-dpf ambra1 morphants. As previously demonstrated by endogenous alkaline phosphatase analysis (Benato *et al*., 2013), the network of sub-intestinal vessels at the yolk stalk was reduced, in both ambra1-morphants with respect to WT, a result which could explain the delay in yolk depletion of morphant embryos. Moreover, intersegmental vessels in the trunk and tail were also

thinner and sometimes presented interruptions (S-Fig. 4). However, defects were not severe enough to suggest a direct correlation with impairment of heart development.

**Knock-down of zebrafish *ambra1a* and *ambra1b* genes causes aberrant cardiac looping and laterality defects**

In order to follow heart development, expression of the cardiomyocyte marker *myl7* was analysed at 20, 24 and 36 hpf in WT and *ambra1a*- and *ambra1b*-ATG morphants. At 24-hpf stage, the proper tubular heart shape, present in WT embryos, was completely absent in both morphants. Moreover, at 36 hpf, when the heart begins to loop in control embryos, heart tube appeared relatively straight and smaller in *ambra1*-morphants (Fig. 2 panel A). These results suggested a possible developmental delay, but also a possible heart looping failure.

As heart looping orientation defects are indicative of altered cardiac left-right patterning during development, we analysed the expression of *pitx2c,* a gene that controls heart laterality and that is normally expressed, induced by asymmetric Nodal signalling, on the left lateral plate mesoderm (LPM) at 21-somite stage.

This analysis revealed both bilateral or reversed *pitx2c* expression in both *ambra1* morphants, indicating that ambra1 knockdown interferes with heart laterality (Fig. 2, panel B). Moreover, the embryonic and transient sensory Rohon-Beard neurons, forming two columns on either side of the midline (Burdine *et al.*, 2016), when visualised by the *pitx*2c probe, were found correctly aligned in WT embryos whereas ambra1-morphants showed loss of the their regular organization (Fig. 2, panel B). Finally, a disorganised *pitx2c* expression pattern was also evident when the superficial cells of the yolk forming the hatching gland (Ji *et al.,* 2016) were taken into consideration. The specificity of *ambra1* knockdown effects was confirmed by co-injection with hAMBRA1 mRNA (Fig. 2, panel C) which allowed a clear rescue of a normal *pitx*2c expression pattern.

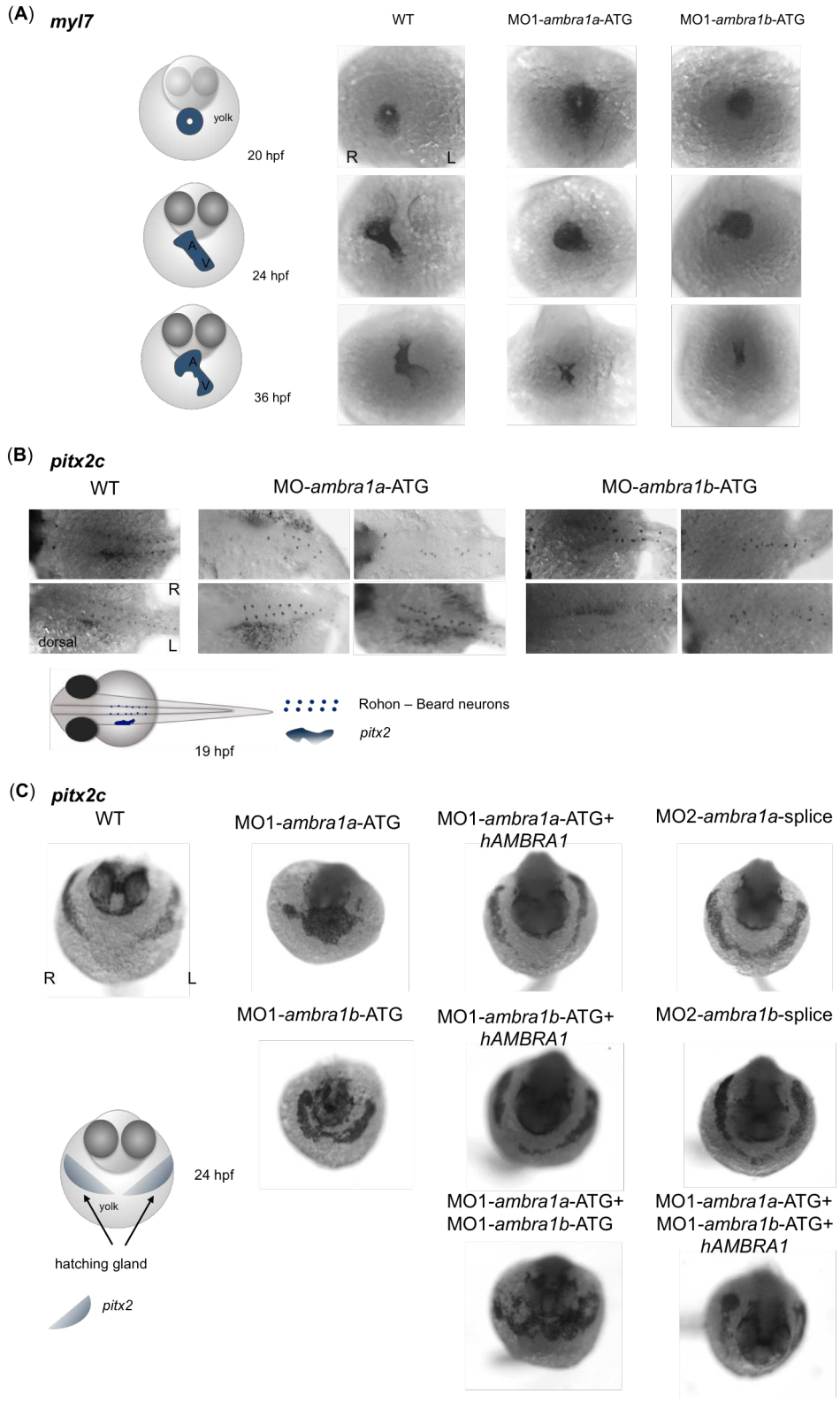


**Fig. 2.** (A) Representative *myl7* WMISH images of WT and *ambra1a* and *ambra1b* ATG-morphant embryos at 20, 24 and 36 hpf developmental stages. (B) Dorsal views of the lateral plate mesoderm of WT and *ambra1*-morphant embryos showing different expression patterns of *pitx2c* expression as indicated by Left (L) and right (R) symbols. Disorganization of presumptive Rohon-Beard neurons localization was observed in morphant embryos. (C) Ventral view of WT and *ambra1*-morphant embryos showing altered *pitx2c* expression in the hatching gland position and recovery after co-injection of *AMBRA1* mRNA.

Analysis of looping phenotypes by visualization of the developing atrium and ventricle was performed at 48 hpf using the zebrafish Tg(*7xTCF*$^{mut}$*-1.2ins:EGFP*) transgenic line (Facchinello *et al.,* 2016), which have the coding region for the EGFP protein located downstream the promoter of cardiac myosin *myl7*, a marker for both atrium and ventricle. Compared to WT control embryos, ATG-morphants exhibited looping defects we classified in four heart looping orientation groups, namely D-loop (right, normal), incomplete D-loop, complete and incomplete L-loop (left, reversed), no-loop (Fig. 3, panel A). The incorrect looping phenotypes of both morphant embryos were rescued by co-injection of h*AMBRA1* mRNA. The rescue was not total, as normally happens in these experiments. Recovery of the phenotype was instead very slight when *hAMBRA1*$^{PXP}$ mRNA was co-injected with the two MOs. Moreover, distribution of heart looping orientation groups was not statistically different between embryos treated with ambra1b-MO alone or co-injected with *hAMBRA1*$^{PXP}$ mRNA (Fig. 3, panel B).

Greater rescue efficiency was obtained when the general morphant phenotype was taken into consideration. In this case the differences between the rescue capabilities of *hAMBRA1* and the mutated *hAMBRA1*$^{PXP}$ messengers were lower and, at least in the case of ambra1a-MO, not statistically different (Fig. 3, panel C).

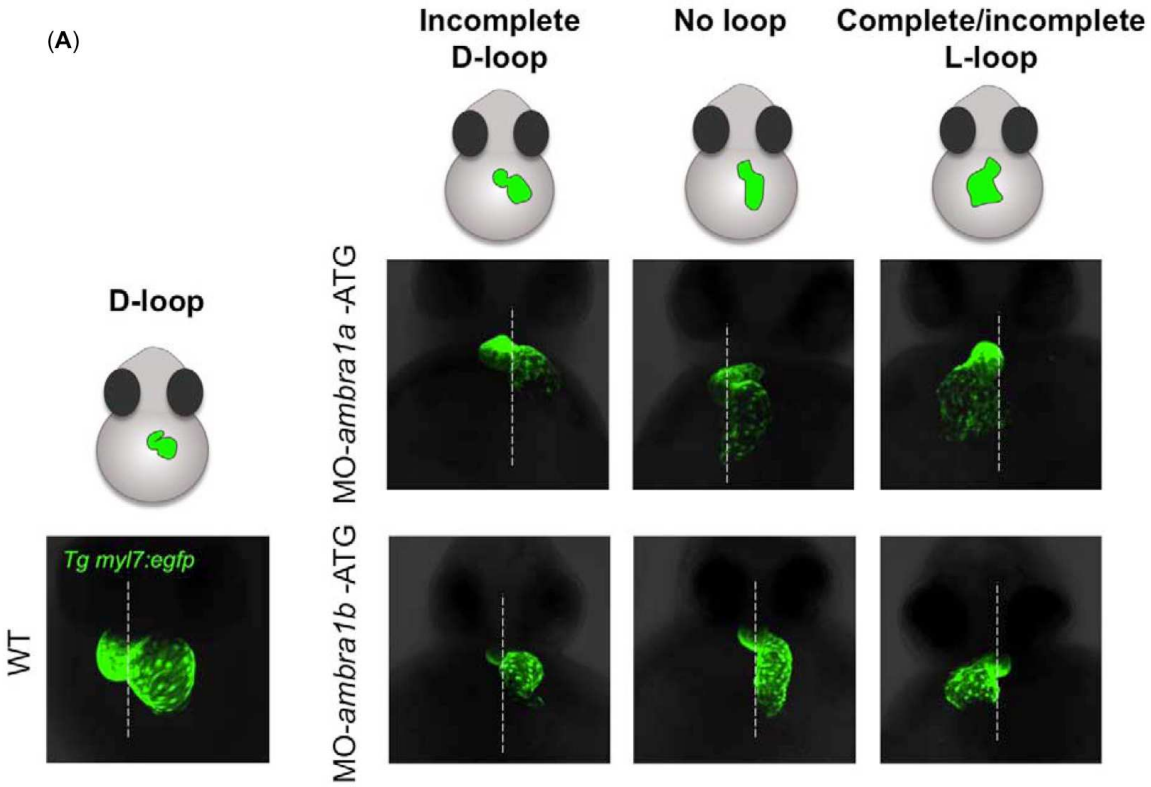

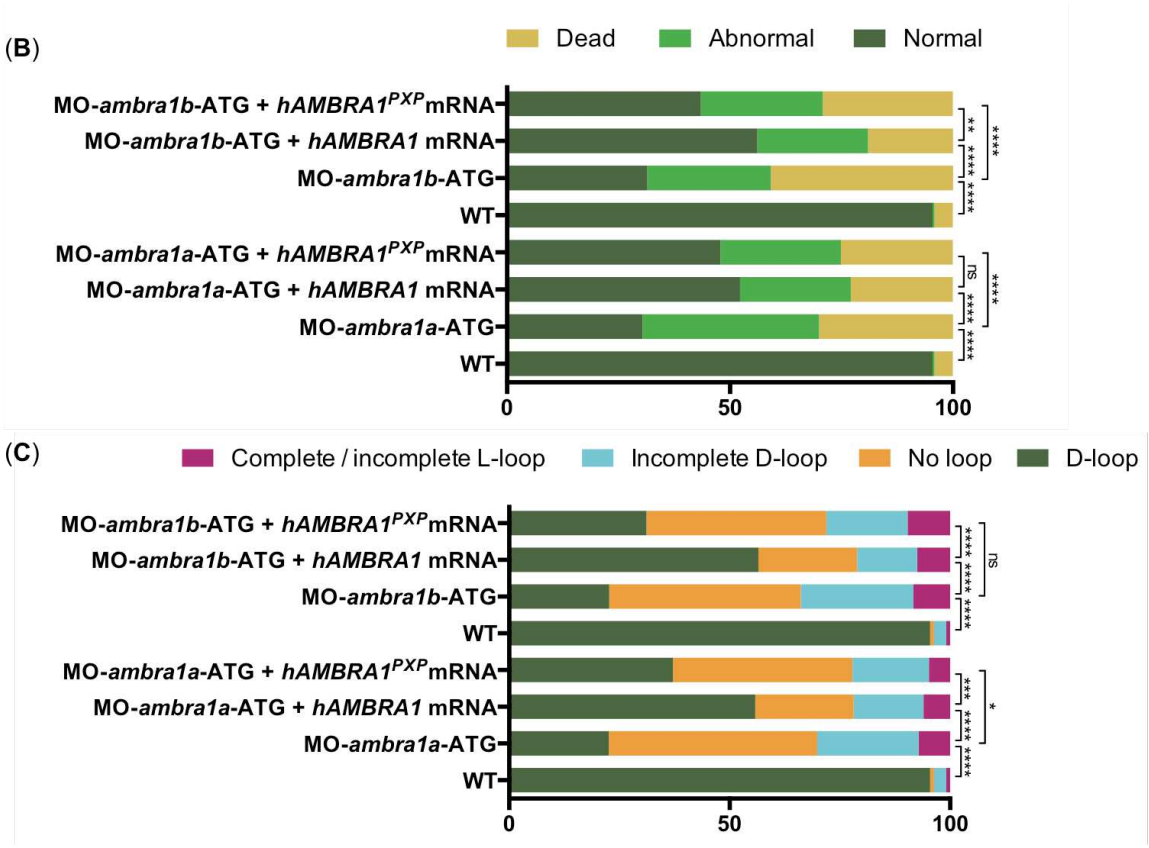


**Fig. 3.** (A) Three-dimensional reconstructions showing WT and *ambra1*-morphant hearts expressing the myocardial reporter transgene myl7:EGFP at 48 hpf and describing the incorrect phenotypes found in morphants in addition to the normal D-looping orientation. (B) Percentage of normal, abnormal and dead in WT and morphant embryos at 48 hpf and after rescue experiments with *hAMBRA1* and the mutated *hAMBRA1*$^{PXP}$ messengers. For each treatment 200 embryos were analysed. Statistical analysis was performed using chi-squared test,* P<0,05; ** P<0,01; *** P<0,001; **** P<0,0001. (C) Percentage of D-loop, incomplete D-loop, complete and incomplete L-loop, no-loop in WT and morphant embryos at 48 hpf and after rescue experiments with *hAMBRA1* and the mutated *hAMBRA1*$^{PXP}$ messengers. For each treatment 200 embryos were analysed. Statistical analysis was performed using chi-squared test; *P<0,05; ** P<0,01; *** P<0,001; **** P<0,0001.

## Proliferation analysis suggests conserved interaction of Ambra1 with PP2Ac in zebrafish and its involvement on heart development

Analysis of zebrafish sequences revealed the presence of one and two PP2A binding regions in Ambra1a and Ambra1b proteins, respectively (Supplemental Fig. 4).

In order to assess the involvement of zebrafish Ambra1 proteins in the regulation of cell proliferation and the role of the PP2A binding regions, we analysed this process in 9-hpf WT and morphant embryos by means of whole-mount immunohistochemistry with anti-phospho-histone H3. Moreover, co-injection with *hAMBRA1* and *hAMBRA1*$^{PXP}$ mRNAs was used to analyse the rescue effectiveness of the *AMBRA1* transcript mutated in the

PP2A binding regions. Silencing of both Ambra1a and Ambra1b proteins resulted in a statistically significant increase of cell proliferation (Fig. 4). Co-injection of *hAMBRA1* mRNA with both ATG-MOs restored the dividing cells number to the WT level. Conversely, co-injection with *hAMBRA1*$^{PXP}$ mRNA was not able to control cell proliferation (Fig. 4). This was particularly evident with ambra1b morphants, likely due to the presence of two PP2A binding regions (S-Table 2).

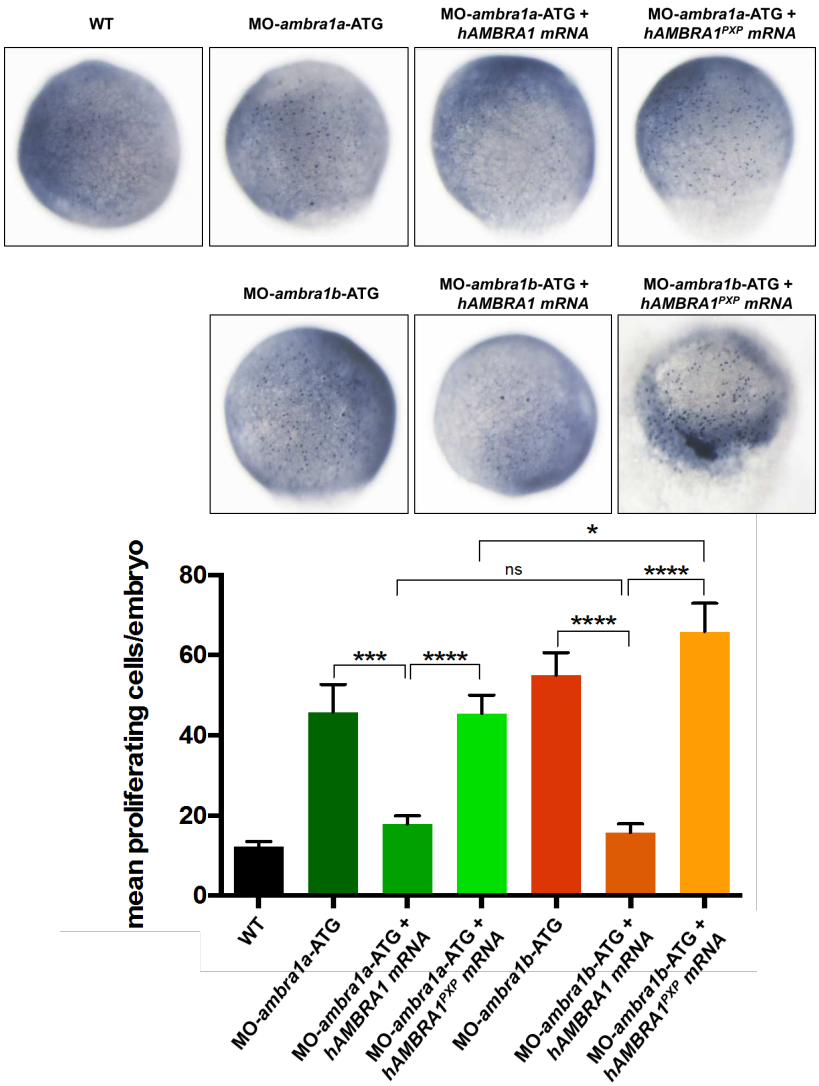


**Fig. 4.** Representative images of PH3 immunohistochemistry performed to analyse the embryo cell proliferation at the embryonic stage of 9 hpf. The proliferating cell numbers were counted and compared between WT, *ambra1a*- and *ambra1b*-morphant embryos and after rescue experiments with *hAMBRA1* and the mutated *hAMBRA1*$^{PXP}$ messengers. For each treatment were analysed 10 embryos and the experiment was performed two times. Statistical analysis was performed using Student's T-test. * $P < 0.05$, ** $P < 0.01$, *** $P < 0.001$, **** $P<0.0001$.

**Treatment with a PP2A specific inhibitor suggests a role of this protein in zebrafish heart development**

Cantharidin is a strong and specific inhibitor of protein phosphatase 2A (PP2A) (Li *et al*., 2010). To analyse the involvement of this protein in heart development, WT embryos were soaked in different concentrations of cantharidin (2.5 to 5 μM). The treatment was initiated at 4 hpf, before heart morphogenesis. Cantharidin treatment resulted, at the highest dose used, in a reduced survival rate. At intermediate concentrations, the inhibitor induced heart defects similar to those displayed by ATG-morphant embryos (Fig. 5).

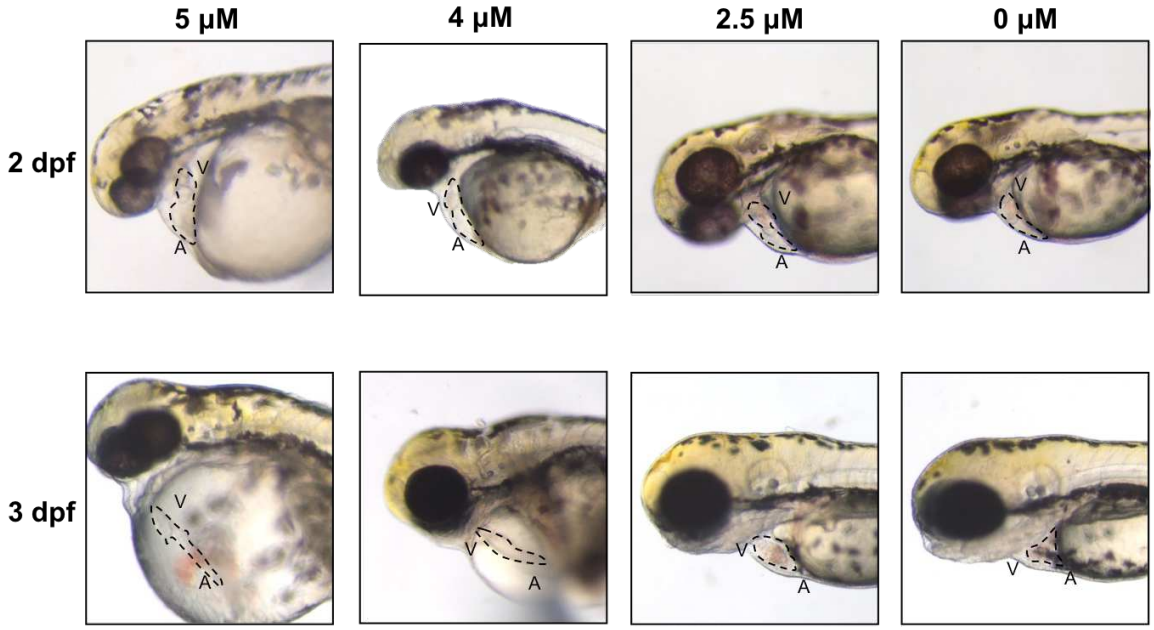


**Fig. 5.** Representative bight field micrographs of cardiac region of 2 and 3-dpf live embryos treated with the indicated concentrations of the PP2A inhibitor cantharidin.

Chapter 3

## DISCUSSION

The involvement of Ambra1 in vertebrate development was previously demonstrated both in mice (Fimia *et al*., 2017) and in zebrafish, where this protein is encoded by two paralogous genes named *ambra1a* and *ambra1b* (Benato *et al.*, 2014; Skobo *et al.*, 2014). In this work, we adopted a targeted protein depletion approach to analyse the effects of Ambra1 deficiency on cardiac morphogenesis and development, as a clear and severe heart phenotype was displayed by zebrafish *ambra1a/ambra1b* morphants in our previously works (Benato *et al.*, 2014; Skobo *et al.*, 2014).

The present work highlights for the first time a direct correlation between zebrafish *ambra1a* and *ambra1b* genes and cardiac development. Both genes are expressed in the cardiac region at 2-dpf stage, and their ablation resulted on morphants presenting a small, string-like heart with severe pericardial oedema. However, treatment with SPLIC-MOs, which target only zygotic *ambra1* transcripts, revealed no obvious difference between these morphants and WT or 5M-morphants embryos, indicating the fundamental importance of maternally supplied *ambra1* transcripts in early embryonic development. Importantly, *ambra1* genes knockdown resulted in ectopic expression of *pitx2c* gene, a well-known regulator of heart laterality, thus suggesting an early determination of the observed cardiac defects and the incorrect looping process. This was clearly visualized by analysing heart phenotypes on the green heart transgenic line, which allowed us to measure the rescue efficiency of *hAMBRA1* mRNA as well as of the human form mutated on both the PP2A binding region (*hAMBRA1*$^{PXP}$) (Cianfanelli *et al.*, 2015).

PP2A is a highly conserved and ubiquitously expressed phosphatase acting by dephosphorylating serine and threonine residues of critical cellular proteins such as Akt, p53, c-Myc and β-catenin (Seshacharyulu *et al.*, 2013). The holoenzyme plays key roles in development and several cell functions including cell proliferation and death, cytoskeleton dynamics, and signalling pathways regulation (Janssens and Goris, 2001). Moreover, a function as tumor suppressor has been suggested (Janssens *et al.*, 2005; Mumby, 2007; Seshacharyulu *et al.*, 2013).

The holoenzyme PP2A comprises a core dimer formed by catalytic (C) and scaffold (A) subunits, associated to a regulatory (B) subunit. The last is present in multiple isoforms conferring temporal and spatial specificity to its activity (Seshacharyulu *et al.*, 2013). In adult heart, PP2A dysfunction is clearly linked with cardiovascular diseases as the enzyme is one of the major phosphatases expressed in the heart, where its activity on ion channels and cardiac proteins can regulate membrane excitability and cardiac

excitation-contraction (DeGrande *et al.*, 2013). During development, the catalytic subunit of PP2A was found to be expressed in rat heart (Heller *et al.*, 1998). Moreover, knockout of zebrafish PR130, encoded by the largest transcript of protein phosphatase 2 regulatory subunit B, alpha (PPP2R3A), and acting as a regulatory subunit of PP2A, resulted in heart development impairment and cardiac looping defects (Yang *et al.*, 2016). Likewise, mouse B56γ, a PP2A regulatory subunit, was found to be required, by KO approach, for heart development. Additionally, PP2A containing B56δ regulatory subunit regulates phosphorylation state of HAND1 and HAND2 proteins, both involved on heart development (Firulli *et al.*, 2003). All these results suggest a role for the holoenzyme PP2A in cardiac development.

The human AMBRA1 possesses two conserved Proline-rich domains, allowing interaction with the catalytic subunit of the protein phosphatase PP2A (Cianfanelli *et al.*, 2015c). In zebrafish, Ambra1a and Ambra1b differ from each other for the presence of one or two PP2A binding sites, respectively. In this work, we confirmed the role of zebrafish Ambra1 proteins in cell proliferation regulation, as already proposed (Cianfanelli *et al.*, 2015), and in addition, we verified that proliferation regulation require interaction with PP2A. Indeed, whereas the rescue analysis with *hAMBRA1* mRNA rescued the number of proliferating cells in 9-hpf embryos to the WT level, these remained significantly high after co-injection with the mRNA for the human AMBRA1 mutated in its PP2A-interacting residues. Moreover, a possible interaction between Ambra1 and PP2A in the molecular process causing the heart phenotype is suggested by the rescue experiments performed with the two human *AMBRA1* messengers during cardiac development and by proliferation analysis during heart development.

Results obtained by silencing the two *ambra1* paralogous genes were slightly different and suggested a major role of the *ambra1a* isoform on cardiac development, as underlined by the more severe cardiac phenotype showed by ambra1a-morphants (Fig. 1). This result could also be explained by the higher *ambra1a* expression with respect to *ambra1b* during development (Benato *et al.*, 2013), and in particular in developing heart (S-Fig. 1).

Co-injection with mutated *hAMBRA1*$^{PXP}$ mRNA showed also a different rescue efficiency: the non-statistically different distribution of heart looping orientation groups between embryos treated with *ambra1b*-MO alone or co-injected with *hAMBRA1*$^{PXP}$ mRNA (Fig. 3, panel B) suggested a higher interaction of Ambra1b and PP2A with respect to Ambra1a, likely due to the presence of two PP2A binding sites in the former protein. Although partial, a significant rescue was instead obtained when *hAMBRA1*$^{PXP}$ mRNA was used together with *ambra1a*-MO. In agreement with Ambra1 capability of binding a great

number of regulatory partners, it is possible that Ambra1a isoform interacts with different proteins to influence heart morphogenesis. Concerning this point, it is noteworthy that also knockdown of zebrafish *cul4a*, another AMBRA1 interactor, interferes with cardiac development (Antonioli *et al.*, 2014).

Moreover, when the general phenotype of Ambra1a-morphants was taken into consideration, we didn't observe any difference in the rescue efficiency between *hAMBRA1* and *hAMBRA1*$^{PXP}$ mRNAs, thus suggesting that Ambra1a silencing effects could be minimally linked to PP2A interaction. Acquisition of distinct roles after ancestral gene duplication is required for the maintenance through evolution of different paralogous genes (Postlethwait *et al.*, 2004).

In conclusion, this study shows for the first time that both zebrafish Ambra1a and Ambra1b play an essential role in cardiogenesis, beside impacting on nervous system and skeletal muscle development as previously described (Benato *et al.*, 2013; Skobo *et al.*, 2014. Our results also suggest that involvement of Ambra1 proteins on heart development requires interaction with the holoenzyme PP2A.

**ACKNOWLEDGMENTS**

The authors wish to acknowledge Dr. N. Facchinello and Prof. F. Argenton for providing the transgenic lines Tg(7xTCFmut-1.2ins:EGFP) and Tg(fli1::EGFP). Moreover, authours wish to aknowledge L. Pivotti and Dr. M. Milanetto for their valuable assistance in the fish facility.

**REFERENCES**

**Antonioli M., Albiero F., Nazio F., Vescovo T., Perdomo A.B., *et al.*, 2014.** AMBRA1 interplay with cullin E3 ubiquitin ligases regulates autophagy dynamics. Dev Cell. Dec 22;31(6):734-46.

**Bakkers J. 2011.** Zebrafish as a model to study cardiac development and human cardiac disease. *Cardiovasc Res*. 91: 279–288.

**Benato F., Skobo T., Gioacchini G., Moro I., Ciccosanti F., *et al.*, 2013.** Ambra1 knockdown in zebrafish leads to incomplete development due to severe defects in organogenesis. Autophagy 9: 476-495.

**Burdine R.D., Grimes D.T. 2016.** Antagonistic interactions in the zebrafish midline prior to the emergence of asymmetric gene expression are important for left-right patterning. Philos Trans R Soc Lond B Biol Sci. 2016 Dec 19;371(1710). pii: 20150402.

**Burns C.G. and MacRae C.A. 2006.** Purification of hearts from zebrafish embryos. Biotechniques. 2006 Mar;40(3):274, 276, 278 passim.

**Cianfanelli V., De Zio D., Di Bartolomeo S., Nazio F., Strappazzon F., Cecconi F. 2015a.** Ambra1 at a glance. *J Cell Sci*. 128:2003-8.

**Cianfanelli V., Fuoco C., Lorente M., Salazar M., Quondamatteo F., 2015c.** AMBRA1 links autophagy to cell proliferation and tumorigenesis by promoting c-Myc dephosphorylation and degradation. *Nat Cell Biol*. 17:20-30.

**Cianfanelli V., Fuoco C., Lorente M., Salazar M., Quondamatteo F. 2015.** AMBRA1 links autophagy to cell proliferation and tumorigenesis by promoting c-Myc dephosphorylation and degradation. Nature Cell Biology, 17(1), 20-30.

**Cianfanelli V., Nazio F., Cecconi F. 2015b.** Connecting autophagy: AMBRA1 and its network of regulation. *Mol Cell Oncol*. 2:e970059.

**DeGrande S.T., Little S.C., Nixon D.J., Wright P., Snyder J. 2013.** Molecular mechanisms underlying cardiac protein phosphatase 2A regulation in heart. J Biol Chem. Jan 11;288(2):1032-46.

**Di Bartolomeo S., Corazzari M., Nazio F., Oliverio S., Lisi G. 2010.** The dynamic interaction of AMBRA1 with the dynein motor complex regulates mammalian autophagy. *J Cell Biol*. 191:155-68.

**Essner J.J., Branford W.W., Zhang J., Yost H.J. 2000.** Mesendoderm and left-right brain, heart and gut development are differentially regulated by pitx2 isoforms. Development. Mar;127(5):1081-93.

**Facchinello N., Schiavone M., Vettori A., Argenton F., Tiso N. 2016.** Monitoring Wnt Signaling in Zebrafish Using Fluorescent Biosensors. Methods Mol Biol. 2016;1481:81-94.

**Fimia G.M., Stoykova A., Romagnoli A., Giunta L., Di Bartolomeo S. 2007.** Ambra1 regulates autophagy and development of the nervous system. *Nature*. 447:1121-5.

**Firulli B.A., Howard M.J., McDaid J.R., McIlreavey L., Dionne K.M. 2003.** PKA, PKC, and the protein phosphatase 2A influence HAND factor function: a mechanism for tissue-specific transcriptional regulation. Mol Cell. Nov;12(5):1225-37.

**Heller F.A., Xue C., Fisher A., Everett A.D. 1998.** Expression and Mapping of Protein Phosphatase 2Aα in the Developing Rat Heart. Pediatric Research 43, 68–76

**Huang C.J., Tu C.T., Hsiao C.D., Hsieh F.J., Tsai H.J. 2003.** Germ-line transmission of a myocardium-specific GFP transgene reveals critical regulatory elements in the cardiac myosin light chain 2 promoter of zebrafish. *Dev Dyn*. 228:30-40.

**Janssens V. and Goris J. 2001.** Protein phosphatase 2A: a highly regulated family of serine/threonine phosphatases implicated in cell growth and signalling. Biochem. J.; 353: 417–439.

**Janssens V., Goris J. and Van Hoof C. 2005.** PP2A: the expected tumor suppressor. Curr. Opin. Genet. Dev. 2005; 15: 34–41.

**Ji Y., Buel S.M., Amack J.D. 2016.** Mutations in zebrafish *pitx2* model congenital malformations in Axenfeld-Rieger syndrome but do not disrupt left-right placement of visceral organs. Dev Biol. 2016 416(1):69-81.

**Kimmel C.B., Ballard W.W., Kimmel S.R., Ullmann B., Schilling T.F. 1995.** Stages of embryonic development of the zebrafish. Dev Dyn 203: 253-310.

**Lawson N.D. and Weinstein B.M. 2002.** In Vivo Imaging of Embryonic Vascular Development Using Transgenic Zebrafish. Developmental Biology 248, 307–318.

**Liu J., Stainier D.Y.. 2012.** Zebrafish in the study of early cardiac development. *Circ Res*. 110:870-4.

**Mumby M. 2007.** PP2A: Unveiling a Reluctant Tumor Suppressor. Cell 130:21-24.

**Nazio F., Strappazzon F., Antonioli M., Bielli P., Cianfanelli V. 2013.** mTOR inhibits autophagy by controlling ULK1 ubiquitylation, self-association and function through AMBRA1 and TRAF6. *Nat Cell Biol*. 15:406-16.

**Postlethwait J., Amores A., Cresko W., Singer A., Yan Y.L. 2004.** Subfunction partitioning, the teleost radiation and the annotation of the human genome. Trends Genet 20: 481–490.

**Seshacharyulu P., Pandey P., Datta K., Batra S.K. 2013.** Phosphatase: PP2A structural importance, regulation and its aberrant expression in cancer. Cancer Lett. 2013 Jul 10;335(1):9-18.

**Skobo T., Benato F., Grumati P., Meneghetti G., Cianfanelli V. *et al*. 2014.** Zebrafish ambra1a and ambra1b knockdown impairs skeletal muscle development. PLOS One, 9(6):e99210.

**Stoykova A., Chowdhury K., Bonaldo P., Torres M., Gruss P. 1998.** Gene trap expression and mutational analysis for genes involved in the development of the mammalian nervous system. *Dev Dyn*. 212:198-213.

**Westerfield M. 1995.** The Zebrafish Book. A Guide for the Laboratory Use of Zebrafish (Danio rerio), 3rd Edition. Eugene, OR, University of Oregon Press.

**Yang J., Li Z., Gan X., Zhai G., Gao J., *et al.,* 2016.** Deletion of Pr130 Interrupts Cardiac Development in Zebrafish. Int J Mol Sci. Nov 11;17(11). pii: E1746.

**Yelon D., Horne S.A., Stainier D.Y. 1999.** Restricted expression of cardiac myosin genes reveals regulated aspects of heart tube assembly in zebrafish. Dev Biol. Oct 1;214(1):23-37.

## SUPPLEMENTARY MATERIAL

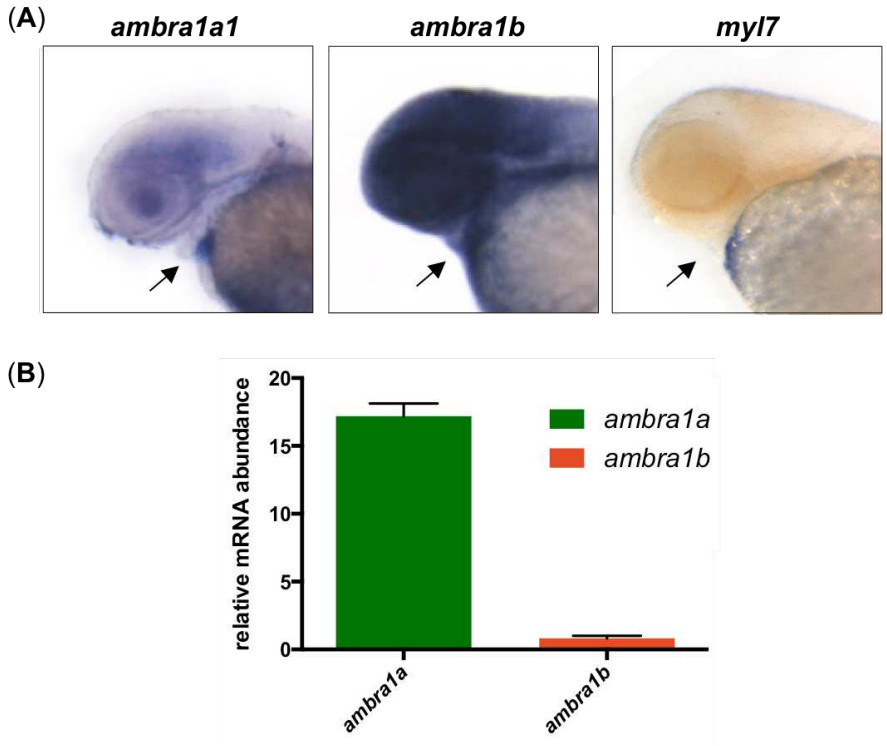


**S-Fig. 1.** (A) Whole-mount in situ hybridization analysis of *ambra1a*, *ambra1b* and *myl7* mRNA in the heart region of 3-dpf WT embryos. All embryos are lateral views with head pointing to the left. Both *ambra1* transcripts show a similar expression pattern with *myl7*, a cardiac marker, in the heart region. (B) The graph shows the relative mRNA transcript abundance of *ambra1a* and *ambra1b*, in 3-dpf zebrafish heart, as determined by RT-qPCR. Error bars indicate SEM.

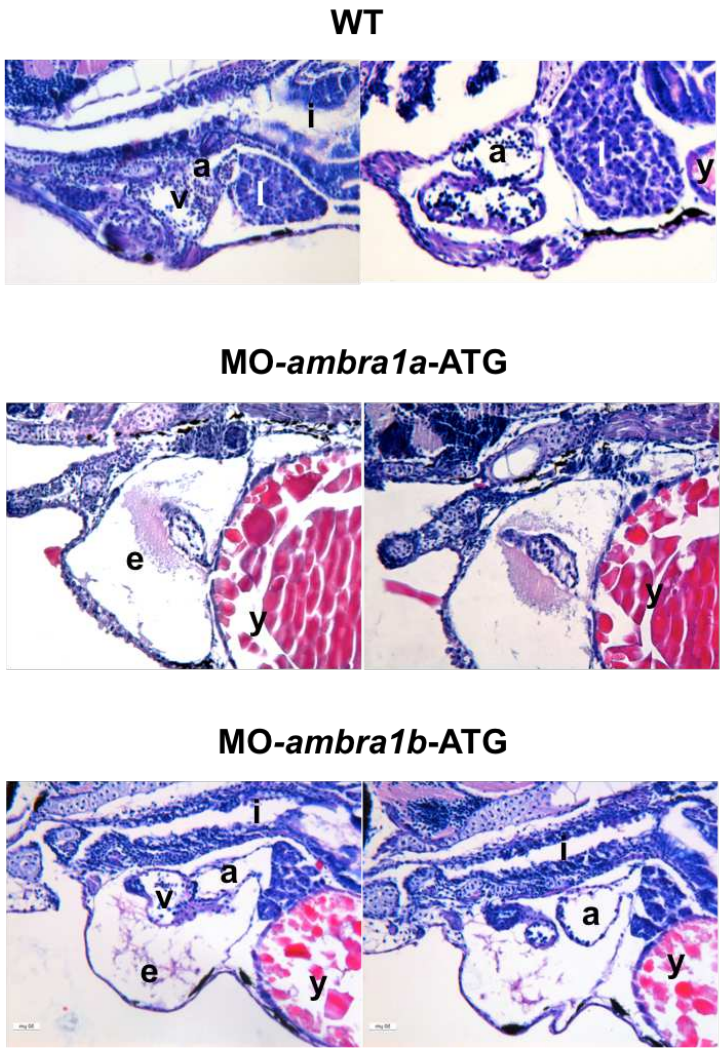


**S-Fig. 2.** Representative longitudinal sections of cardiac region of 5 dpf control and *ambra1* morphant embryos. The head is positioned to the left. In the WT and morphant heart, atrium and ventricle are visualized. All *ambra1*-morphant hearts, in particular *ambra1a*-morphants, display severe pericardial oedema. Morphants show a delay in yolk depletion. a, atria; v, ventricle; y, yolk; i, intestine; e, edema.

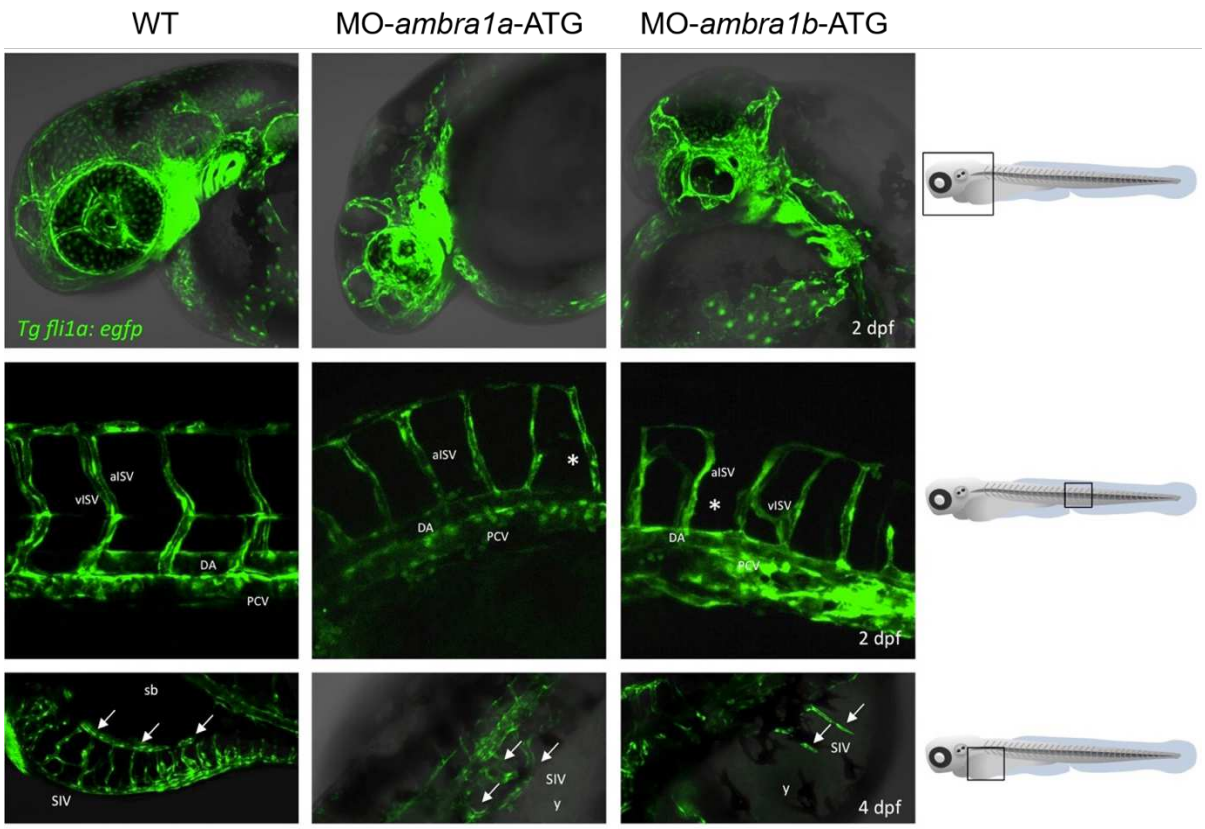


**S-Fig. 3.** Representative images of the vasculature in control or *ambra1a* and *ambra1b*-morphants using Tg(*fli1::EGFP*) embryos at 2 dpf. Whereas well-organized sub-intestinal vessels (SIVs) are present in WT larvae, *ambra1*-MOs-injected embryos present a slight reduction of SIVs and less defined intersegmental vessels in the trunk and tail. Bar= 200 µm. SIv, sub-intestinal vessels; ISV, Intersegmental vessel.

| | | | |
|---|---|---|---|
| hAMBRA1 PXP-1 | PQPSTER | hAMBRA1 PXP-2 | PQPSTER |
| zAmbra1a PXP-1 | - | zAmbra1a PXP-2 | PIPGPSS |
| zAmbra1b PXP-1 | PREPPSI | zAmbra1b PXP-2 | PTPETPA |

**S-Fig. 4.** PP2a binding regions found in Ambra1a and Ambra1b zebrafish proteins.

**S-Tab. 1.** Primer used for RT-PCR.

| Gene | Reference | Sequence |
|---|---|---|
| β-actin2_FW | This work | TGGGTATGGAATCTTGCGGT |
| β-actin2_RW | This work | GTGGGGCAATGATCTTGATCT |
| am1a-F1 | Benato *et al.*, 2013 | CTGCTGCTCATTGCCACC |
| am1a-R6 | Benato *et al.*, 2013 | CGCATCTCCACATCGTCC |
| am1b-F2 | Benato *et al.*, 2013 | AGGTGACGGACAGTCAGC |
| am1b-R6 | Benato *et al.*, 2013 | CCTACCATCACATAGCAGC |

**S-Tab. 2.** List of markers used in the whole-mount in situ hybridization analyses.

| **Gene** | **Reference** | **Vector** | **Endonuclease and RNA polymerase** |
|---|---|---|---|
| z-am1a1-3'-UTR | Benato *et al*., 2013 | pGEM | ApaI, Sp6 |
| z-am1b-3'-UTR | Benato *et al*., 2013 | pGEM | SalI, T7 |
| z-pitx2c | Essner *et al*., 2000 | pGEM | SpeI, T7 |
| z-myl7 | Yelon *et al.,* 1999 | pGEM | SacI, T7 |

## CONCLUDING REMARKS

This thesis describes the generation and characterization of zebrafish mutant lines for Ambra1 and Epg5, two fundamental proteins of the autophagic process.
Autophagy plays an essential role in many cell functions and processes. Its importance is underlined not only by a growing number of publications related to this field but also by the Noble Prize in Physiology and Medicine that was awarded to Yoshinori Ohsumi in 2016, for his “discoveries of the mechanisms for autophagy”.
Zebrafish are becoming an increasingly popular choice of model for the study of vertebrate biology, being well suited to not only for developmental studies but also as a disease model. Recently, to its advantages have been increased in the last years by the introduction of the gene editing approach, based on CRISPR/Ca9, that makes possible the generation of new mutant lines and also integration of previously reported knockdown phenotype.
In the Epg5 zebrafish mutant line developed in this thesis the autophagy role of this protein was confirmed using different experimental approaches.
Given its fundamental role in autophagosome maturation, together with the multi-systemic phenotype displayed by the mutants and compatible with the Vici syndrome clinical signs, we propose the use of this mutant line to study this disease. Moreover, as the autophagy flux is naturally blocked and the zebrafish is particularly suitable for high-throughput screening, this mutant line could represent a valuable model for autophagy inducer molecules, an experimental approach that we intend to follow in the next future.
Regarding the zebrafish mutant line for the paralogous genes *ambra1a* and *ambra1b*, they allowed the validation of the results obtained by morpholino knock-down in previous works and, in particular, on zebrafish heart development.
The functional compensation suggested by Rossi and co-workers (2015) to explain the differences in phenotype severity between morphants and morphants was also demonstrated in this work. Despite genetic compensation between the paralogous genes, our findings also indicate a possible sub-functionalization following gene duplication. In fact, all *ambra1b*$^{-/-}$ adults are males, suggesting that Ambra1 (in zebrafish Ambra1b), may play a role in ovary development and/or sexual determination that remains still unknown. This new finding, together with the possible role of Epg5 in reproduction, open a complete new field of research for our laboratory concerning the interplay between autophagy and reproduction.

**PUBBLICATION LIST**

Skobo T., Benato F., Grumati P., **Meneghetti G.**, Cianfanelli V., Castagnaro S., Chrisam M., Di Bartolomeo S., Bonaldo P., Cecconi F., Dalla Valle L. Zebrafish *ambra1a* and *ambra1b* knockdown impairs skeletal muscle development. Skobo PLoS One. 2014 12;9(6):e99210.

Facchinello N*, Skobo T*, **Meneghetti G**, Colletti E, Dinarello A, Tiso N, Costa R, Gioacchini G, Carnevali O, Argenton F, Colombo L, Dalla Valle L. nr3c1 null mutant zebrafish are viable and reveal DNA-binding- independent activities of the glucocorticoid receptor. Sci Rep. 2017 Jun 29;7(1):4371. * These two authors contributed equally to this article.

**PARTICIPATION TO COURSES**

Summer School; Scuole di Dottorato di Ricerca dell'Area Medica ciclo 30, September 21-25 2015, Padova, Italy.

International Workshop in Genome Engineering in Zebrafish, June 27-28 2017, MPI Frankfurt.

Workshop "Advanced Cellular Assay Technologies: High content Imaging and Label-Free DMR" in collaboration with Perkin Elmer on April 19 2017, Padova, Italy.

**MEETINGS AND ABSTRACTS**

DMM Scientific Meeting 2015, Università degli Studi di Padova, May 28-29, 2015, Padua, Italy.

DMM Scientific Meeting 2016, Università degli Studi di Padova, May 26-27, 2016, Padua, Italy.

12$^{th}$ International Conference on Zebrafish Development and Genetics, July 13-17, 2016, Orlando, Florida USA. Abstract/Poster: "Zebrafish *ambra1a* and *ambra1b* silencing affects heart development".

PhD student research program day, medical and biomedical sciences (XXX cicle), October 3, 2016, Padua, Italy. Talk: "Generation of *epg5* mutant zebrafish lines to study Epg5 functions during development and adult life".

1st ZebraFish Italian Meeting (ZFIM), 2-3 February 2017, Padua, Italy. Abstract/Poster: "CRISPR-Cas9 mediated knockout of zebrafish *epg5* gene to study its functions during development and adult life".

2nd scientific retreat Department of Biology, Università degli studi di Padova, February 13-14 2017, Padua, Italy. Poster: "The *epg5* knockout zebrafish line: a model to study Vici syndrome".

63rd Italian Embryological Group (GEI) Congress. 12-15 June 2017, Rome, Italy. Abstract: "The *ambra1a, ambra1b* and *epg5* knock out lines: Three zebrafish models to study autophagy".

10th European ZebraFish Meeting, 3-7 July 2017, Budapest, Hungary. Abstract/Poster: "The *epg5* knockout transgenic line: a model to study Vici syndrome".